Alma Mater Studiorum – Università di Bologna

DOTTORATO DI RICERCA IN

IL FUTURO DELLA TERRA, CAMBIAMENTI CLIMATICI E SFIDE SOCIALI

CICLO XXXV

Settore Concorsuale: 03/A1 - CHIMICA ANALITICA

Settore Scientifico Disciplinare: CHIM/12 - CHIMICA DELL'AMBIENTE E DEI BENI CULTURALI

TREES: Radiocarbon and Dendrochronology - together for the RESOLUTION project

Presentata da: Silvia Cercatillo

Coordinatore Dottorato

Prof.ssa Silvana Di Sabatino

Supervisore

Prof.ssa Sahra Talamo

Co-supervisore

Prof.ssa Cristina Chiavari

Esame Finale Anno 2023

Acknowledgment

This Ph. D. project is entirely funded by the European Research Council under the European Union's Horizon 2020 Research and Innovation Programme (grant agreement no. 803147 RESOLUTION, https://site.unibo.it/resolution-erc/en).

A special thanks go to my supervisors, for their commitment, sustain and constructive feedbacks at each step of this path, and to Bernd for his availability and contagious enthusiasm.

A special acknowledgment goes to my colleagues Dragana, Laura and Enrico for their availability and for practical and moral support.

To my family.

Abstract

The year 14,226 BP marks an important border in the actual radiocarbon (^{14}C) calibration curve: the high resolution and precision characterising the first part (0 – 14,226 BP) of the curve are due to the potential represented by tree-ring datasets, which directly provide the atmospheric ^{14}C content at the time of tree-rings formation with high resolution. They systematically decrease going back in time, where only a few floating tree-ring chronologies alternate to other low-resolution records.

The lack of resolution in the dating procedure before 14,226 years BP leads to significant issues in the interpretation and untangling of tricky facts of our past, in the field of Human Evolution.

Research on sub-fossil trees and the construction of new Glacial tree-ring chronologies can significantly improve the radiocarbon dating in terms of temporal resolution and precision until 55,000 years BP to clear puzzles in the Human Evolution history.

In this thesis, the dendrochronological study, the radiocarbon dating and the extrapolation of environmental and climate information from sub-fossil trees found on the Portugal foreshore, remnants of a Glacial lagoonal forest, are presented.

The careful sampling, the dendrochronological measurements and cross-dating, the application of the most suitable cellulose extraction protocol and the most advanced technologies of the MICADAS system at ETH-Zurich, led to the construction of a new 220-years long tree-ring site chronology and to high resolution, highly reliable and with a tight error range radiocarbon ages.

At the moment, it results impossible to absolutely date this radiocarbon sequence by the comparison of $\Delta^{14}C$ of the trees and ^{10}Be fluctuations from the ice-cores. For this reason, tree growth analysis, comparisons with a living pine stand and forest-fires history reconstruction have made it possible to hypothesize site and climate characteristics useful to constrain the positioning in time of the obtained radiocarbon sequence.

Contents

CHAPTER 1

Introduction

1.1 Radiocarbon

The chemist and physicist Frank Libby was awarded the Nobel prize in chemistry in 1960 thanks to the first radiocarbon dating based on the ^{14}C isotope performed in 1949. This dating technique establishes the time of the organism's death when the radiocarbon intake ceases, and the radiometric clock starts. From that moment, the quantity of ^{14}C decreases turning into ^{14}N atoms as a result of β-decays since the organism no longer absorbs carbon from the surrounding environment, thus becoming a closed system. Its half-life, the time required to have the initial quantity of ^{14}C reduced by half, is around 5730 years.[1, 2]

The stable carbon isotopes ^{12}C and ^{13}C are the most abundant in nature (98,9% and 1,1%, respectively), whereas the concentration of the unstable ^{14}C is only in trace amounts (10^{-12} for a living organism). Radiocarbon is largely produced in the upper atmosphere by the incoming cosmic rays, which interact with atmospheric particles producing ^{14}C atoms, which are spread toward the earth lowest reservoirs and mixed with O and H atoms, forming compounds like $^{14}CO_2$ and $^{14}CH_4$. They enter the carbon cycle, and plants capture carbon dioxide through the photosynthesis process acquiring almost the same carbon isotopic signature of the atmosphere, i.e., tree rings faithfully record directly in the cellulose chains the carbon isotopic ratio of the atmosphere year by year. Animals absorb radiocarbon from the food chain and the living environment, as in the case of marine fauna (Fig. 1).

However, the ^{14}C production was not constant over time, and this is mainly due to changes in the magnetic shielding of the earth against cosmic rays caused by solar activity and the strength of the geomagnetic field. Moreover, factors such as the atmosphere-ocean exchange of CO_2, ocean circulation, winds, and biosphere dynamics determine variations in the radiocarbon distribution.[3-7] Consequently, this situation produces offsets both within reservoirs (ocean) and between North and

South hemispheres,[8] as highlighted in Hogg et al. 2002,[9] where the comparison of ^{14}C data series of tree samples from New Zealand and British Isles spanning the same time range shows an offset of 40 ± 13 years.

Because of these fluctuations of radiocarbon concentration over time, a univocal correlation of ^{14}C amount versus true age is not allowed. Indeed, the use of a calibration curve to convert radiocarbon ages into calendar ages referred to as IntCal is required. In this respect, two different calibration curves, one for the Northern[10] and one for the Southern[8] hemisphere, are built, and a third one is specific for the marine environment.[11]

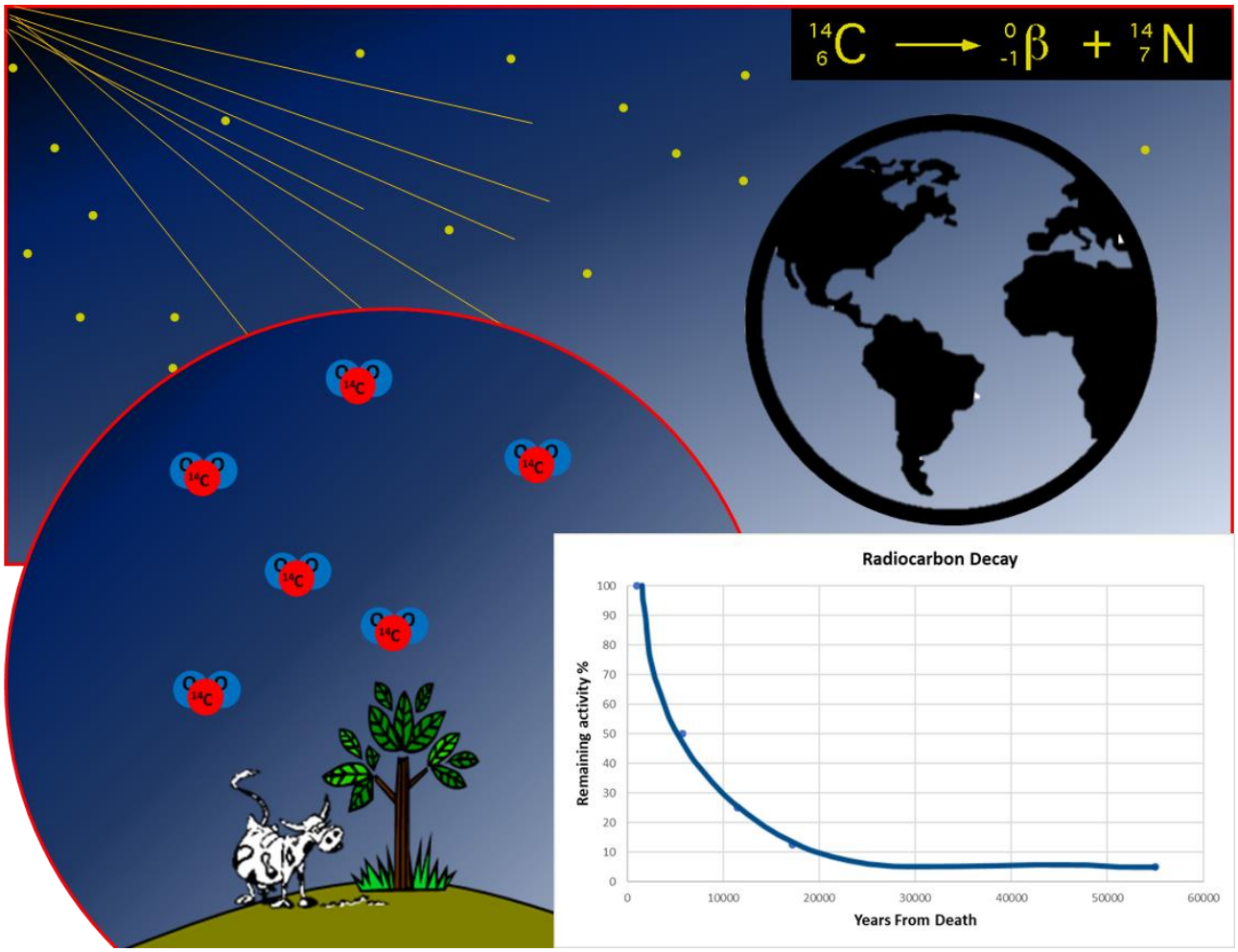

Fig. 1 *Illustration of radiocarbon production, distribution and decay*

1.2 Radiocarbon Calibration

The radiocarbon calibration curve tries to describe the natural fluctuations that occurred in the atmospheric ^{14}C concentration based on data series coming from several terrestrial and non-terrestrial radiocarbon archives, which incorporated ^{14}C directly from the surrounding environments and which are possible to absolutely date through different and independent dating methods, such as U/Th dating or counting annual layers such as laminated sediments or tree-rings. These datasets of known age and ^{14}C content allow defining correlations between ^{14}C concentration and calendar date.

The calibration curve provides the best calendar age estimation within the actual radiocarbon age range, which spans the time period from the present to 55,000 years in IntCal20,[10] when ^{14}C reaches its detection limit. The resolution and precision of calendar dates (denoted 'cal BP', which stands for 'calendar years before present, 1950 AD) are not the same for the entire length of the calibration curve. They are strictly correlated with the currently available ^{14}C data on which the curve is based (Fig. 2a and 2b).

Intcal20 is built on accurate and high-resolution tree-ring data back to ca. 14,226 cal BP.[10]

Tree rings are considered the best archive since they offer yearly values of the carbon isotope ratio directly recorded from the atmosphere, while other archives are characterised by the indirect link to the atmosphere and usually are of much lower resolution (some hundreds of years).

The actual tree-ring based portion of the calibration curve covers a time window of the Holocene and the Late Glacial, and it is composed of several matched chronologies: Holocene Oak Chronologies (HOC) of Germany, Ireland and Douglas Fir of the Oregon coast and the Preboreal Pine Chronology (PPC) of pines found in Germany and Switzerland.[12-16] These data sets span the entire Holocene back to 12,314 cal BP within the Younger Dryas, the start of the absolute dendrochronology. More recently, floating combined Late Glacial Pine chronologies[12,13,14,17-20] from Switzerland and central Germany were linked to extend the absolute tree-ring chronology by ^{14}C wiggle-match by ca. 2000 years to reach the actual limit of the dendrochronological based calibration back to 14,226 cal BP (±8 years 2σ).[21]

The extension of the absolute chronology requires time, work, and synergy of experts from different parts of the globe. Older floating chronologies (not dendro-matched to the absolutely dated chronology) already exist. They are considered to be the fundamental segments that will be hopefully dendro-matched and linked to the actual absolute dated chronology to prolong it. The current several existing floating chronologies testify not only the existence of forests during the Würm glaciation in

areas referred to as refugia, where special geographical and environmental characteristics buffered the severe climate conditions during the glaciation and allow the conservation of biodiversity,[22] but they also contribute to narrowing and refining the radiocarbon dating through wiggle-match. Some examples of floating chronologies of the Last Glacial period come from Italy where sub-fossil tree finds described in Corona et al. (1984)[23] and in Friedrich et al. (1999)[13] cover the range of 15,200 – 14,300 BP (Revine, TV) and other spanning the time range of 14,700-14,000 cal BP published in Friedrich et al. (2001, 2009)[17,24] and in Adolphi et al. 2017[25] (Palughetto, BL and Avigliana, TO) with ^{14}C-series (Fig. 3). Other examples of chronologies come from the Southern Hemisphere from New Zealand, around 30,000 cal BP published in Hogg et al. 2016b[26] and from Chile dated back to approximately 50,000 BP.[27]

Prior to 14,226 cal BP the datasets used in IntCal20 come mainly from speleothems, lake sediments, and marine cores, e.g., speleothems from Hulu cave to 53,900 cal BP[28] and Bahamas stalagmites between 28,000 and 44,000 cal BP[29] absolutely dated through U–Th. Varves, annually laminated sediments in lakes and marine environments from Cariaco Basin[30] and Lake Suigetsu form a significant part of the curve.[31] Marine foraminifera from Iberian[32] and Pakistan margins[33] matched by ^{18}O signature to Hulu Cave, and corals from Pacific and the Atlantic Ocean dated via U-Th[34-36] add to the dataset.

Except for tree rings and terrestrial macrofossil remains, which are perfect recorders of past atmospheric radiocarbon activity, the marine archives and speleothems are subject to reservoir effects. Because of internal ocean mixing over several centuries and millennia, the ocean reservoir is not in equilibrium with the atmosphere even though gas exchange occurs between ocean surface and atmosphere. Ocean currents and temperatures play an important role in the stratification and mixing of waters. For this reason, the marine reservoir effect is not constant in space and time.[37]

Another reservoir effect is observable for speleothems, calcite cave formations formed by the precipitation of minerals from water seeping into the soil and the cave. This water has firstly a ^{14}C content resulting from the atmosphere and soil interactions, and then it picks up fractions of "dead-carbon" (^{14}C-free) from carbonates in the soil above the cave. As a consequence, the speleothem age is affected by these contributions, and to use them for calibration, it is necessary to calculate the offset between the ^{14}C level of the atmosphere and that of the carbonate entering the cave, called Dead Carbon Fraction (DCF) which is between several hundred years and two millennia. In general, the DCF can be determined by comparing the ^{14}C content of samples of known age and tree rings or terrestrial macro remains of the same period.[38]

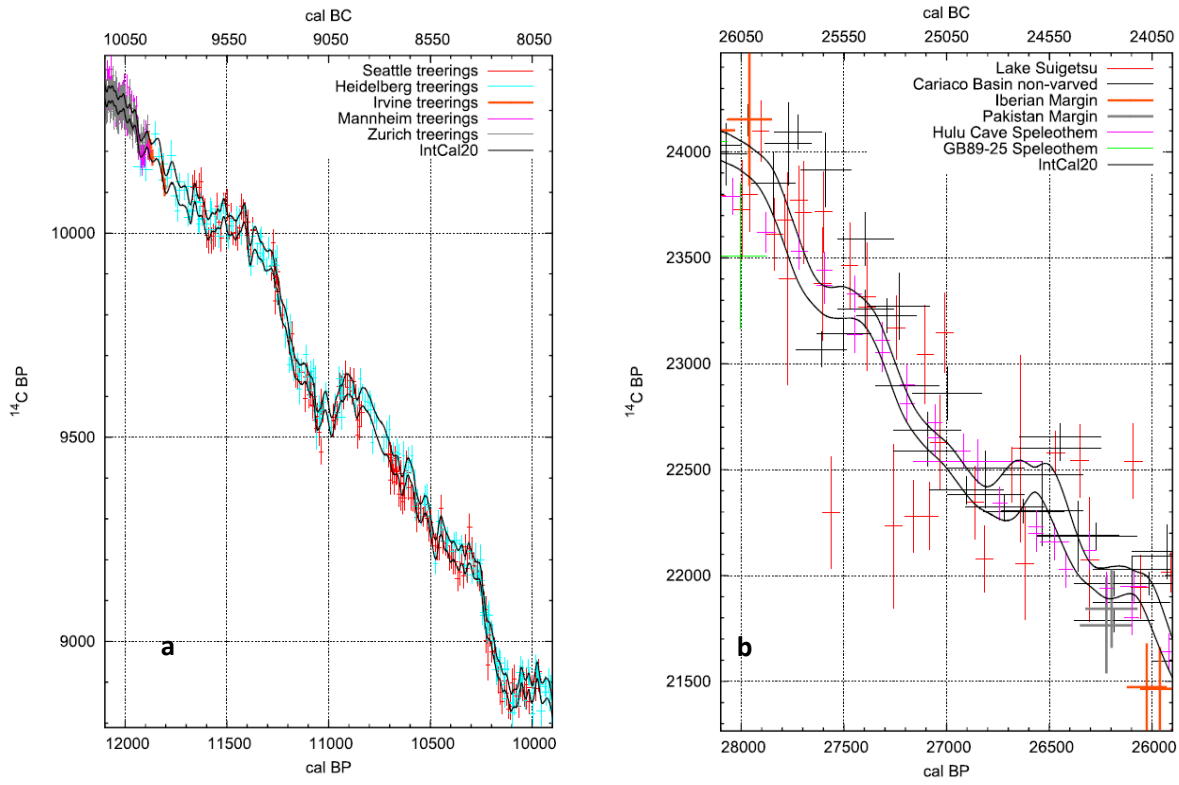

Fig. 2a *and* ***b*** *Intcal20 segments from 10,000 to 12,000 and 26,000 to 28,000 cal BP, respectively. For both pictures the employed datasets are listed in the graphs.*[10]

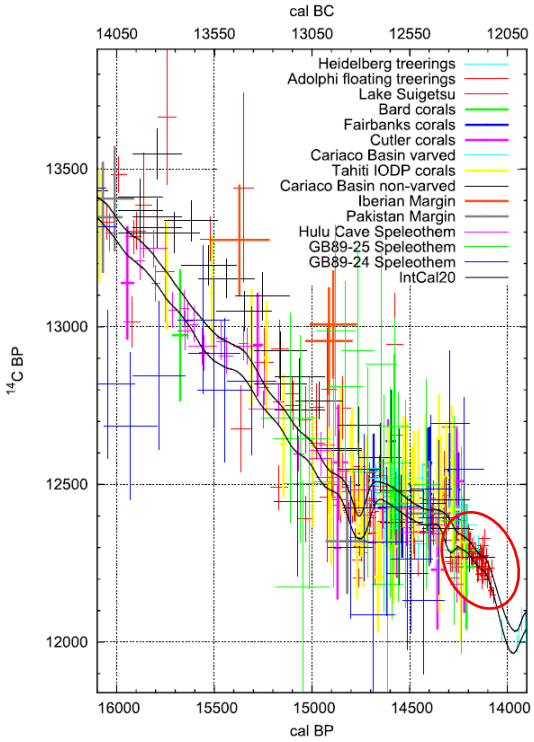

Fig. 3 *Intcal20 segments from 14,000 to 16,000 cal BP.*[10] *Circled in red the floating chronology published in Adolphi et al.* 2017.[25]

1.3 Dendrochronology

Dendrochronology is the science dealing with the study of tree-rings and tree-ring sequences, which can provide chronometric, environmental and climatic information.

Using tree cores or cross-sections of logs, the dendrochronologist measures and plots the widths of each ring, tracing a curve which proceeds from the innermost, respectively older (pith) toward the outermost, respectively younger part (bark), that span the entire tree life, or just a part of it: this very much depends on the characteristics of the sample and its state of preservation.

The ring width variation in a tree-ring curve is an expression of the tree growth that results from the incidence of different factors such as physiology, genetics, climate, characteristics of living environment, and occurrence of occasional or systematic external influences that happened during tree's life. Temperature, precipitation, nutrient availability, insect infestations, forest-fires are just some of the major influencing tree-growth factors that can imply variations in the number, size, and order of rings' cells and thus in the tree-ring characteristics such as ring width, wood density or wood anatomical features.[39]

Characteristic sequences of particularly narrow and wide annual rings may be referred to as signatures, which can provide environmental or climatic information and can be used as applicable "markers" for cross-matching between trees. The high similarity of tree ring curves of simultaneously growing trees of the same species and the same region with similar growing conditions allows for cross-matching of overlapping portions of tree-ring curves. This dendrochronological procedure allows to combine different synchronized tree-ring series to create longer and thus more extended tree-ring series, called tree-ring chronologies (Fig. 4). To this purpose, tree samples of the same species and belonging to the same climatic zone are typically used since their response to external factors is similar and comparable.[40]

Starting from chronologies of still living trees, for which the age of the outermost (youngest) ring is known, it is possible, by cross-dating of increasingly older trees, to go further back in time in order to assign a calendar year to each ring. Using dendrochronological cross-dating this reference series can then be used to synchronise tree ring series of wood of unknown age of the same species and growing region by their distinctive tree ring pattern and thus determine the years in which the tree lived. Cross-dating is thus a dating technique based on a cross-matching procedure to synchronize undated tree-ring sequences using already dated chronologies and therefore fix them in time.

To build chronologies, spanning thousands of years, it is necessary to find suitable old living trees and well-preserved trunks from archaeological and geological sites, such as gravel pits, clay pits or

bogs. The wood samples from those pre-historic sites are known as “sub-fossil” trees, which means that the wood fossilisation (chemical replacement of organic compounds with inorganic ones) and biological and chemical degradation took place only partially preserving the shape and a quantity of original organic matter to the present (Fig. 5 and Fig. 6a and 6b).

Conditions that are particularly favourable for wood preservation are: water saturation, low temperatures and anoxic storage conditions, which mainly influence biological degradation from fungi, bacteria and insects. Wood remnants completely buried in fine sediments, embedded in permafrost or ice, or submerged in water are typical examples[40, 41]of suitable environments for preservation. Nonetheless, the preservation of subfossil wood very much depends on the wood durability specific to each species.[42, 43]

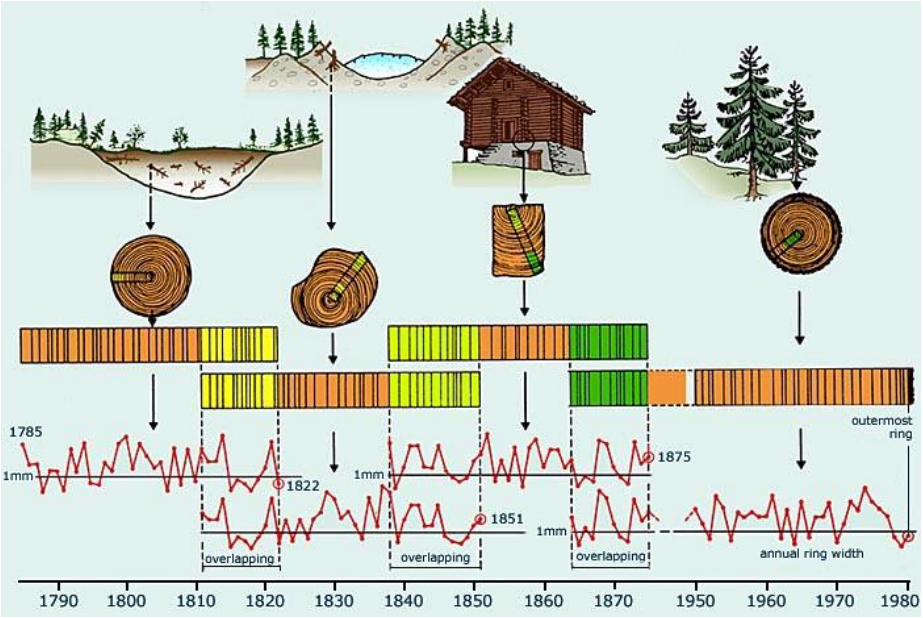

Fig. 4 *Cross-dating concept (from Tree Rings - Basics and Applications of Dendrochronology)* [40]

Fig.5 *Sub-fossil oak tree, Cava Rossini (CR), Italy*

Fig 6a *and* ***b*** *Sub-fossil larch trees, Revine (TV), Italy*

1.4 Problems in the absolute dating in Glacial times

The absolute tree-ring chronology and, therefore the tree-ring based radiocarbon calibration curve today extends back to 14,226 cal BP into the Glacial period.[10] For the older part of the timescale, IntCal20 comprises statistically integrated evidence from floating tree-ring chronologies, lacustrine and marine sediments, speleothems, and corals with continuously decreasing resolution and precision and which diverge very strongly over long periods.

In addition, the influence of contamination becomes more significant with increasing age. As a result, the calibrated ^{14}C ages in Glacial times are characterised by continuously decreasing resolution and precision with high error ranges that result in significant uncertainties of the calibrated ages.

The high uncertainties and the lack of precision in radiocarbon dating is challenging, and leads to significant issues in the field of archaeology in the interpretation and untangling of tricky facts linked to Human Evolution, that need precise dating.

In this respect, one of the most regarded debates that very much relies on precise data is the arrival of *Homo sapiens* in Europe, its time and way of interaction with Neanderthals, and its spread across the world.[44, 45] Moreover, the appearance of Art in the Palaeolithic time is still one of the most intriguing challenges for archaeologists. The new discovery and the secure directly date of a decorated Ivory pendant from Stajnia Cave in Poland at 41,500 years cal BP reveal the importance of the direct date of an object of Palaeolithic art to understand the origin of communication, celebration and expression of *Homo sapiens* in Europe.[46]

To improve the calibration precision of this period, the progressive update of the calibration curve with new, absolutely dated, high-resolution tree-ring based segments is needed that introduce higher resolution, narrow the calibrated age ranges and increase the calendar age precision.

In addition, improvements in high-precision radiocarbon age measurement dating techniques using MICADAS system (Mini Carbon Dating System)[47] and improved contamination removal procedures can significantly increase dating quality.

The importance of these two latter aspects is illustrated by Fewlass et al. (2020)[48], where the authors demonstrate that it is possible to produce very high precision ^{14}C ages of bone samples coming from the archaeological sequence of Bacho Kiro cave (Bulgaria) spanning the Middle and Upper Palaeolithic transition using new carbon contamination removing protocols during the collagen extraction procedure and dating through the high-precision MICADAS system. Despite this much improved measurements, the precise calibration is still hampered by the limitations of the existing calibration curve Intcal20.

1.5 Radiocarbon wiggle-match

Radiocarbon wiggle-match refers to the use of wiggles in the calibration curve, characteristic "up and down" or "wave" shapes of ^{14}C age vs calendar age due to variations in ^{14}C production, to match temporally overlapping age intervals. This technique is mainly applied to date tree-ring sequences when it is not possible to cross-date them through dendrochronology. Tree-rings are ideal for wiggle-matching because of the ordered ^{14}C age dataset with the annual resolution, which provides to fix them in time and to narrow the calibrated age range with a precision of some decades.[49]

Quarta et al. 2010[50] show the application of wiggle-match to tree-ring sequences from northern Italy dating back to the Iron Age (chronostratigraphic dating), which cannot be dendro-matched with the absolute dated chronology. This can happen both when the considered tree species are different from the ones forming the absolute dated chronology, mainly composed of data from pine (*Pinus sylvestris) and* oak (*Quercus robur)*, and when trees experienced quite different living environments. Wiggle-match is thus used to reduce the uncertainty of the age range obtained by radiocarbon calibration.

1.6 Project aim

The overall purpose of this thesis is to combine the potential of dendrochronology and the radiocarbon dating technique to develop new floating tree-ring width chronologies and high-resolution ^{14}C-data sequences from sub-fossil trees grown during the most recent Glacial, this means beyond the existing absolutely dated tree-ring chronologies, i.e., the tree-ring-based radiocarbon calibration at 14,226 cal BP.[10]

We use these series to create new tree-ring based ^{14}C-series, fix them in time using paleoclimate information from the tree-rings and compare to existing paleoclimate records. Moreover, the comparison of the ^{14}C-series from the tree-rings to the isotope ^{10}Be from ice-cores is used to link ^{14}C sections from floating tree-ring series to the independently dated Arctic and Antarctic ice core scale, and therefore, to define the position of the developed chronologies on the calibration curve to improve the resolution within segments of the radiocarbon calibration curve.

To achieve these goals, we searched for preserved sub-fossil trees from the Glacial period in their respective Glacial refuge areas, constructed floating tree-ring chronologies, extracted paleoclimate information and once linked to the ice core calendar, use the high-resolution and high-precision ^{14}C series chronologies to have a more accurate calibration of ^{14}C data.

The cellulose extraction - Exploring different methods of cellulose extraction for ^{14}C dating (Chapter 2)

In the radiocarbon dating method, contamination is an important aspect to consider because it could lead to younger or older age results. The efficiency of an extraction protocol is centrally focused on contamination removal.

In this regard, three already known different wood pretreatment protocols were tested and evaluated in order to obtain high-reliable radiocarbon dates. Starting from samples of known age spanning the entire radiocarbon age range, the % cellulose yield and the ^{14}C age have guided to the choice of a suitable pretreatment protocol. This study was published in the *New Journal of Chemistry*.[51]

Dendrochronology and Radiocarbon of glacial trees from Furadouro, Portugal (Chapter 3)

The core goal is to construct Glacial tree-ring based radiocarbon series. Therefore, new sub-fossil pine trees collected in Portugal were studied. The tree-ring series were used to create a new tree-ring width chronology and a high-resolution ^{14}C data series dated around 29,000 ^{14}C BP. From the annual rings of the subfossil trees, information on growth conditions and climate at the time of the trees' growth could be obtained, which, together with the radiocarbon data, could also be very helpful for fixing the trees in time. Trees' growth analysis and wood anatomical features provided palaeo-ecological information i.e., forest fires, and the comparison with living trees provided information on palaeo-climate and -ecology.

Conclusions and future outlook (Chapter 4)

This new established radiocarbon sequence represents a good starting point for the construction of a new floating chronology, which in future could be incorporated into the radiocarbon calibration curve. Moreover, floating glacial chronologies testify the presence of forests during the last glaciation and may provide paleoclimate and palaeoecological information, such as forest fire history and some climate characteristics.

References

1 M. S. a. H. A. Polach, *Radiocarbon*, 1977, 19, 355-63.

2 H. Godwin, *Nature*, 1962, 195, 984-.

3 E. C. Anderson, W. F. Libby, *Physical Review*, 1951, 81, 64-9.

4 M. Stuiver, T. F. Braziunas, *Geophysical Research Letters*, 1998, 25, 329-32.

5 K. Hughen, S. Lehman, J. Southon, J. Overpeck, O. Marchal, C. Herring, J. Turnbull, *Science*, 2004, 303, 202-7.

6 T.-C. Chiu, R. G. Fairbanks, L. Cao, R. A. Mortlock, *Quaternary Science Reviews*, 2007, 26, 18-36.

7 K. B. Rodgers, S. E. Mikaloff-Fletcher, D. Bianchi, C. Beaulieu, E. D. Galbraith, A. Gnanadesikan, A. G. Hogg, D. Iudicone, B. R. Lintner, T. Naegler, P. J. Reimer, J. L. Sarmiento, R. D. Slater, *Clim. Past*, 2011, 7, 1123-38.

8 A. G. Hogg, T. J. Heaton, Q. Hua, J. G. Palmer, C. S. M. Turney, J. Southon, A. Bayliss, P. G. Blackwell, G. Boswijk, C. Bronk Ramsey, C. Pearson, F. Petchey, P. Reimer, R. Reimer, L. Wacker, *Radiocarbon*, 2020, 62, 759-78.

9 A. G. Hogg, F. G. McCormac, T. F. G. Higham, P. J. Reimer, M. G. L. Baillie, J. G. Palmer, *Radiocarbon*, 2002, 44, 633-40.

10 P. J. Reimer, W. E. N. Austin, E. Bard, A. Bayliss, P. G. Blackwell, C. Bronk Ramsey, M. Butzin, H. Cheng, R. L. Edwards, M. Friedrich, P. M. Grootes, T. P. Guilderson, I. Hajdas, T. J. Heaton, A. G. Hogg, K. A. Hughen, B. Kromer, S. W. Manning, R. Muscheler, J. G. Palmer, C. Pearson, J. van der Plicht, R. W. Reimer, D. A. Richards, E. M. Scott, J. R. Southon, C. S. M. Turney, L. Wacker, F. Adolphi, U. Büntgen, M. Capano, S. M. Fahrni, A. Fogtmann-Schulz, R. Friedrich, P. Köhler, S. Kudsk, F. Miyake, J. Olsen, F. Reinig, M. Sakamoto, A. Sookdeo, S. Talamo, *Radiocarbon*, 2020, 62, 725-57.

11 T. J. Heaton, P. Köhler, M. Butzin, E. Bard, R. W. Reimer, W. E. N. Austin, C. Bronk Ramsey, P. M. Grootes, K. A. Hughen, B. Kromer, P. J. Reimer, J. Adkins, A. Burke, M. S. Cook, J. Olsen, L. C. Skinner, *Radiocarbon*, 2020, 62, 779-820.

12 M. Friedrich, S. Remmele, B. Kromer, J. Hofmann, M. Spurk, K. Felix Kaiser, C. Orcel, M. Küppers, *Radiocarbon*, 2004, 46, 1111-22.

13 M. Friedrich, B. Kromer, M. Spurk, J. Hofmann, K. F. Kaiser, *Quaternary International*, 1999, 61, 27-39.

14 K. F. Kaiser, M. Friedrich, C. Miramont, B. Kromer, M. Sgier, M. Schaub, I. Boeren, S. Remmele, S. Talamo, F. Guibal, O. Sivan, *Quaternary Science Reviews*, 2012, 36, 78-90.

15 J. R. Pilcher, M. G. L. Baillie, B. Schmidt and B. Becker, *Letters to Nature*, 1984, 312, 150-152.

16 F. Reinig, D. Nievergelt, J. Esper, M. Friedrich, G. Helle, L. Hellmann, B. Kromer, S. Morganti, M. Pauly, A. Sookdeo, W. Tegel, K. Treydte, A. Verstege, L. Wacker, U. Büntgen, *Quaternary Science Reviews*, 2018, 186, 215-24.

17 M. Friedrich, B. Kromer, K. F. Kaiser, M. Spurk, K. A. Hughen, S. J. Johnsen, *Quaternary Science Reviews*, 2001, 20, 1223-1232.

18 M. Schaub, K. F. Kaiser, D. C. Frank, U. Buentgen, B. Kromer, S. Talamo, 2008a, *Boreas*, 37, 74-86

19 M. Schaub, U. Büntgen, K. F. Kaiser, B. Kromer, S. Talamo, K. K. Andersen, S. O. Rasmussen, *Quaternary Science Reviews*, 2008b, 27, 29-41.

20 F. Reinig, A. Sookdeo, J. Esper, M. Friedrich, G. Guidobaldi, G. Helle, B. Kromer, D. Nievergelt, M. Pauly, W. Tegel, K. Treydte, L. Wacker, U. Büntgen, *Radiocarbon*, 2020, 62, 883-9.

21 A. Sookdeo, B. Kromer, F. Adolphi, J. Beer, N. Brehm, U. Büntgen, M. Christl, T. Eglinton, M. Friedrich, G. Guidobaldi, G. Helle, R. Muscheler, D. Nievergelt, M. Pauly, F. Reinig, W. Tegel, K. Treydte, C. Turney, H. Synal and L. Wacker, *EGU General Assembly 2020, Online*, 2020.

22 F. Médail, K. Diadema, *Journal of Biogeography*, 2009, 36, 1333-45.

23 G. Casadoro, G. B. Castiglioni, E. Corona, F. Massari, M. G. Moretto, A. Paganelli, F. Terenziani and V. Toniello, *Bollettino Comitato Glaciologico Italiano*, 1984, 24, 22-63.

24 M. Friedrich, B. Kromer, D. Reichle, S. Remmele, M. Peresani, *Dendrocronologie del Tardoglaciale dal Palughetto. In: Peresani, M., Ravazzi, C. (Eds.), Le foreste dei cacciatori paleolitici. Ambiente e popolamento umano in Cansiglio tra tardoglaciale e postglaciale.* 2009. 97-120.

25 F. Adolphi, R. Muscheler, M. Friedrich, D. Güttler, L. Wacker, S. Talamo, B. Kromer, *Quaternary Science Reviews*, 2017, 170, 98-108.

26 A. Hogg, J. Southon, C. Turney, J. Palmer, C. B. Ramsey, P. Fenwick, G. Boswijk, U. Büntgen, M. Friedrich, G. Helle, K. Hughen, R. Jones, B. Kromer, A. Noronha, F. Reinig, L. Reynard, R. Staff, L. Wacker, *Radiocarbon*, 2016, 58, 709-33.

27 F. A. Roig, C. Le-Quesne, J. A. Boninsegna, K. R. Briffa, A. Lara, H. Gruddk, P. D. Jones and C. Villagràn, *Letters to Nature*, 2001, 410, 567-570

28 H. Cheng, R. L. Edwards, J. Southon, K. Matsumoto, M. Feinberg Joshua, A. Sinha, W. Zhou, H. Li, X. Li, Y. Xu, S. Chen, M. Tan, Q. Wang, Y. Wang, Y. Ning, *Science*, 2018, 362, 1293-7.

29 D. L. Hoffmann, J. W. Beck, D. A. Richards, P. L. Smart, J. S. Singarayer, T. Ketchmark, C. J. Hawkesworth, *Earth and Planetary Science Letters*, 2010, 289, 1-10.

30 K. Hughen, J. Southon, S. Lehman, C. Bertrand, J. Turnbull, *Quaternary Science Reviews*, 2006, 25, 3216-27.

31 C. Bronk Ramsey, T. J. Heaton, G. Schlolaut, R. A. Staff, C. L. Bryant, A. Brauer, H. F. Lamb, M. H. Marshall, T. Nakagawa, *Radiocarbon*, 2020, 62, 989-99.

32 E. Bard, F. Rostek, G. Ménot-Combes, *Quaternary Research*, 2004, 61, 204-14.

33 E. Bard, G. Ménot, F. Rostek, L. Licari, P. Böning, R. L. Edwards, H. Cheng, Y. Wang, T. J. Heaton, *Radiocarbon*, 2013, 55, 1999-2019.

34 E. Bard, M. Arnold, B. Hamelin, N. Tisnerat-Laborde, G. Cabioch, *Radiocarbon*, 1998, 40, 1085-92.

35 R. G. Fairbanks, R. A. Mortlock, T.-C. Chiu, L. Cao, A. Kaplan, T. P. Guilderson, T. W. Fairbanks, A. L. Bloom, P. M. Grootes, M.-J. Nadeau, *Quaternary Science Reviews*, 2005, 24, 1781-96.

36 N. Durand, P. Deschamps, E. Bard, B. Hamelin, G. Camoin, A. L. Thomas, G. M. Henderson, Y. Yokoyama, H. Matsuzaki, *Radiocarbon*, 2013, 55, 1947-74.

37 E. Q. Alves, K. D. Macario, F. P. Urrutia, R. P. Cardoso, C. Bronk Ramsey, *Quaternary Science Reviews*, 2019, 209, 129-38.

38 J. Southon, A. Noronha, H. Cheng, R. Edwards, Y. Wang, *Quaternary Science Reviews*, 2012, 33, 32-41.

39 U. Büntgen, A. Crivellaro, D. Arseneault, G.L. Baillie, D. J. Barclay, M. Bernabei, J. Bontadi, G. Boswijk, D. Brown, D. Christie, O.V. Churakova, E.R. Cook, R. D'Arrigo, N. Davi, J. Esper, P. Fonti, C. Greaves, R. M. Hantemirov, M. K. Hughes, A.V. Kirdyanov, P. J. Krusic, C. Le Quesne, F. C. Ljungqvist, M. McCormick, V. S. Myglan, K. Nicolussi, C. Oppenheimer, J. Palmer, C. Qin, F. Reinig, M. Salzer, M. Stoffel, M. Torbenson, M. Trnka, R. Villalba, N. Wiesenberg, G. Wiles, B. Yang, A. Piermattei, 2022. *Science Bulletin*, 67, 2336-2344.

40 F. H. Schweingruber, *Tree Rings - Basics and Applications of Dendrochronology*, Springer Dordrecht, 1988.

41 R. Shmulsky, P. D. Jones, *Forest products and wood science: an introduction*, Wiley-Blackwell, Chichester, West Sussex, U.K. ; Ames, Iowa, 2011.

42 J. Baar, Z. Paschová, T. Hofmann, T. Kolář, G. Koch, B. Saake, P. Rademacher, *Holzforschung*, 2019, 74, 47-59.

43 M. Fejfer, M. Zborowska, O. Adamek, D. Dzieduszyńska, P. Kittel, J. Petera-Zganiacz, J. Twardy, *Drewno*, 2014, 57, 81-95.

44 J.-J. Hublin, N. Sirakov, V. Aldeias, S. Bailey, E. Bard, V. Delvigne, E. Endarova, Y. Fagault, H. Fewlass, M. Hajdinjak, B. Kromer, I. Krumov, J. Marreiros, N. L. Martisius, L. Paskulin, V. Sinet-Mathiot, M. Meyer, S. Pääbo, V. Popov, Z. Rezek, S. Sirakova, M. M. Skinner, G. M. Smith, R.

Spasov, S. Talamo, T. Tuna, L. Wacker, F. Welker, A. Wilcke, N. Zahariev, S. P. McPherron, T. Tsanova, *Nature*, 2020, 581, 299-302.

45 A. Haws Jonathan, M. Benedetti Michael, S. Talamo, N. Bicho, J. Cascalheira, M. G. Ellis, M. Carvalho Milena, L. Friedl, T. Pereira, K. Zinsious Brandon, *Proceedings of the National Academy of Sciences*, 2020, 117, 25414-22.

46 S. Talamo, W. Nowaczewska, A. Picin, A. Vazzana, M. Binkowski, M. D. Bosch, S. Cercatillo, M. Diakowski, H. Fewlass, A. Marciszak, D. Paleček, M. P. Richards, C. M. Ryder, V. Sinet-Mathiot, G. M. Smith, P. Socha, M. Sponheimer, K. Stefaniak, F. Welker, H. Winter, A. Wiśniewski, M. Żarski, S. Benazzi, A. Nadachowski, J.-J. Hublin, *Scientific Reports*, 2021, 11, 22078.

47 L. Wacker, G. Bonani, M. Friedrich, I. Hajdas, B. Kromer, M. Němec, M. Ruff, M. Suter, H. A. Synal, C. Vockenhuber, *Radiocarbon*, 2010, 52, 252-62.

48 H. Fewlass, T. Tuna, Y. Fagault, J.-J. Hublin, B. Kromer, E. Bard, S. Talamo, *Scientific Reports*, 2019, 9.

49 B. Kromer, *Dendrochronologia*, 2009, 27, 15-9.

50 G. Quarta, M. I. Pezzo, S. Marconi, U. Tecchiati, M. D'Elia, *Radiocarbon*, 2010, 52, 915-23.

51 S. Cercatillo, M. Friedrich, B. Kromer, D. Paleček, S. Talamo, *New Journal of Chemistry*, 2021, 45, 8936-8941

CHAPTER 2

2.1 Introduction to cellulose extraction

The determination of radiocarbon content in wood samples starts from chemical extractions of uncontaminated and pure cellulose. Cellulose is isolated to detect the atmospheric carbon content. Wood is mainly composed of cellulose (40 – 60%), lignin (16 – 33%), and other components such as resins and waxes.

Cellulose is the fraction of choice for dating trees since it is a long polymer, which is considered to be stable.[1,2] To obtain reliable ^{14}C ages, any contamination by extraneous carbon in the sub-fossil wood must be removed.

For woods of Glacial time, humic acids and carbonates are the most common source of modern carbon and "dead" (^{14}C-free) carbon contamination, respectively. Humic acids are fractions of organic matter soluble in alkaline environment introduced from groundwater supply,[3] and carbonates are transported and deposited by water in the sediment within wood embedded during the burial time, but their amount very much depends on the soil type.

During the extraction procedure, acid and basic steps have to ensure to obtain pure and uncontaminated datable material.

For radiocarbon dating of Upper Pleistocene samples, contamination by young carbon is more problematic than contamination by fossil carbon, e.g., 1% of modern carbon contamination added to a sample of 37,000 ^{14}C BP will reduce its radiocarbon age by 5,500 years, whereas 1% ^{14}C-free carbon will increase the radiocarbon age by only 80 years. Therefore, when assessing the effectiveness of pretreatment procedures, older ages are generally considered more reliable.

For my thesis project, I wanted to identify the most effective pretreatment procedure, to be applied to ancient sub-fossil trees of the Glacial period (Upper Pleistocene) in order to extract cellulose and efficiently remove the exogenous contamination.

To this aim, I chose to compare three different protocols, which, according to the literature, can be applied, with good results, also to old wood. Results were mainly evaluated on the basis of the cellulose yield (% of cellulose) and reliable ^{14}C age.

2.2 Samples preparation and tested extraction methods at the BRAVHO laboratory

In order to establish the most efficient and reliable cellulose extraction protocol for Glacial time sub-fossil trees, three different extraction protocols are tested in the radiocarbon BRAVHO laboratory at Bologna University.

The pretreatment procedures for cellulose extraction involve the use of a variable quantity of wood between 20 and 200 mg. It significantly depends on cellulose content, i.e., the preservation state.

Wood samples are chopped into small pieces to facilitate and speed up chemical reactions. The best are small sticks or thin rectangulars of no more than 1 or 2 cm size. Powder is workable, but better to avoid for the difficulties linked to the pipetting procedures.

Chemical steps generally involved in cellulose extraction use HCl solution to remove contamination by carbonate and to prevent CO_2 absorption from the air.

The use of a strong base as NaOH serves to remove humic acids and start the disruption of lignin structure.

Lastly, an oxidation step (bleaching) follows to remove lignin, hemicellulose and other extractives.

Here the 3 protocols considered the most suitable for the purposes are briefly described:

- ABA-B (Acid-Base-Acid-Bleaching) described in Capano et al. (2018)[4] involves the basic steps of pretreatment (ABA) (Fig. 7a and 7b) and final bleaching (Fig. 7c) with a solution of 5% $NaClO_2$ and some drops of HCl is added to get pure cellulose;
- BABAB (Base-Acid-Base-Acid-Bleaching) shown in Němec et al. (2010)[1] includes an initial long (overnight) bath in 5% NaOH, which cleans the sample from humic acids and makes cellulose more accessible to the following chemical steps. This step is effective as well as aggressive and causes a considerable loss of mass;
- 2ChlorOx (two oxidation steps performed with chlorine) is applied in Gillespie (2019)[5], who performed two oxidative steps, one carried out in an alkaline environment and the other in an acidic one.

2.3 Graphitisation and ^{14}C determination

The just extracted cellulose is dried (Fig. 8a and 8b and Fig. 9) and an aliquot of it equal to 2,5 – 3 mg is weighted into 4 x 4 x 11 mm aluminium cups (Fig. 10a) suitable to the graphitisation step. The cups were previously cleaned with dichloromethane and dried at ca. 300 ° C in the oven. The quantity of cellulose weighted is suitable for samples containing ca. 40% of carbon (C).

Once filled up with cellulose, the cups are folded and rolled up as shown in Fig. 10b.

To proceed with the graphitisation procedure, they are combusted in the elemental analyser of AGE 3 (Automated Graphitization Equipment) to produce CO_2 (Fig. 10c). This gas is then reduced with H_2 injection and using 3,5 mg of iron powder as a catalyst to produce graphite. The graphite is then pressed into a target, ready to be measured by an Accelerator Mass Spectrometer (AMS).

During the extraction procedure, a background sample is always pretreated, together with the samples. This is especially used to check if modern contamination occurs during the extraction steps since background samples have a radiocarbon age near or beyond the radiocarbon dating limit (ca. 55,000 years).

Aluminium cups with Oxalic acid II (OxII) and Phtalic acid anhydride are also prepared, combusted in the elemental analyser and then analysed in the AMS machine. The first is the Radiocarbon Standard of known activity, which refers to the atmospheric activity in 1950 corrected for human activities.[6] The second one is a chemical blank and thus ^{14}C-free.

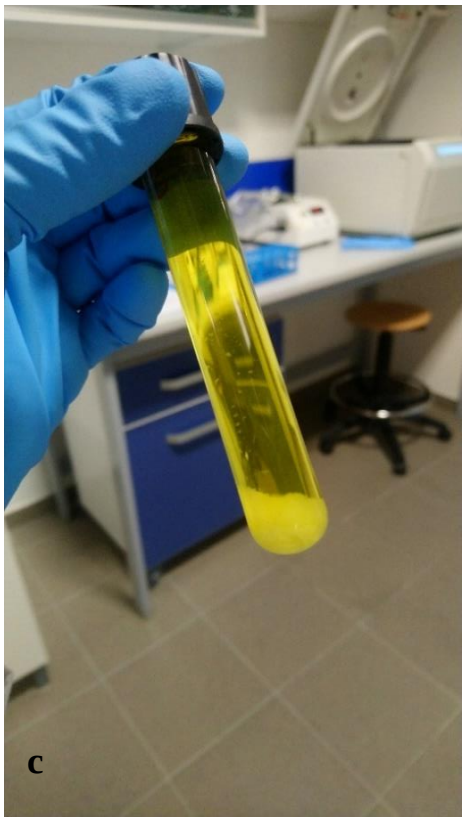

Fig. 7a *and* ***b*** *Acid (HCl) and base (NaOH),*
7c *Bleaching ($NaClO_2$)*

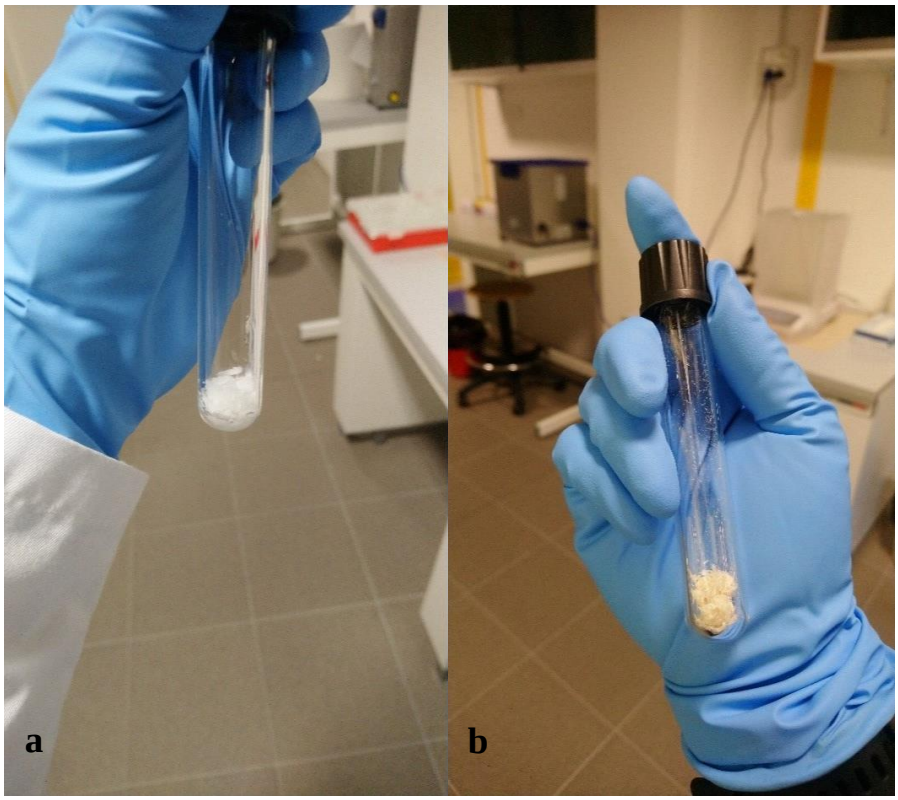

Fig. 8a *Cellulose at the end of the extraction protocol;* ***8b*** *Cellulose after drying*

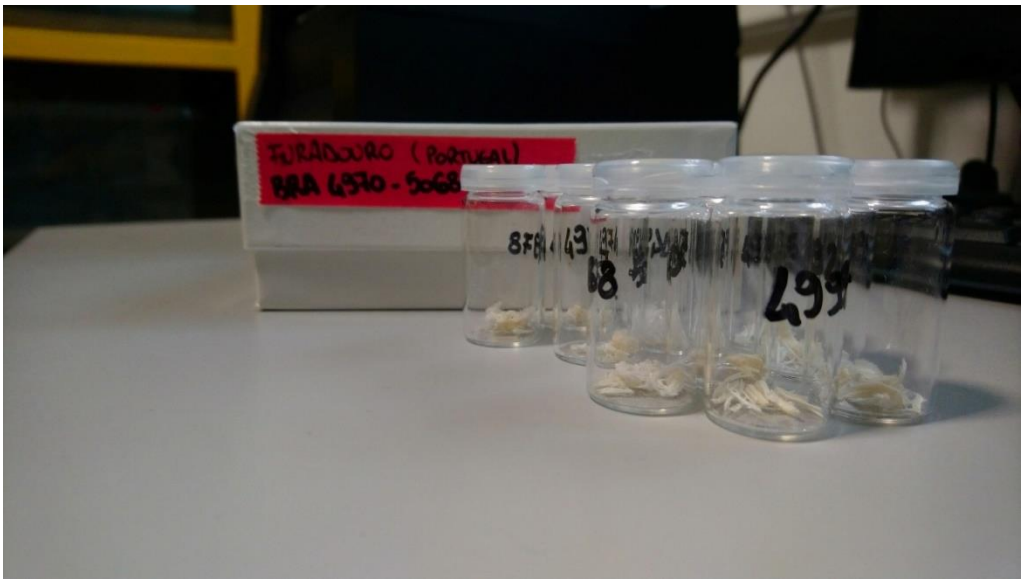

Fig. 9 *Dried cellulose samples stored in glass vials*

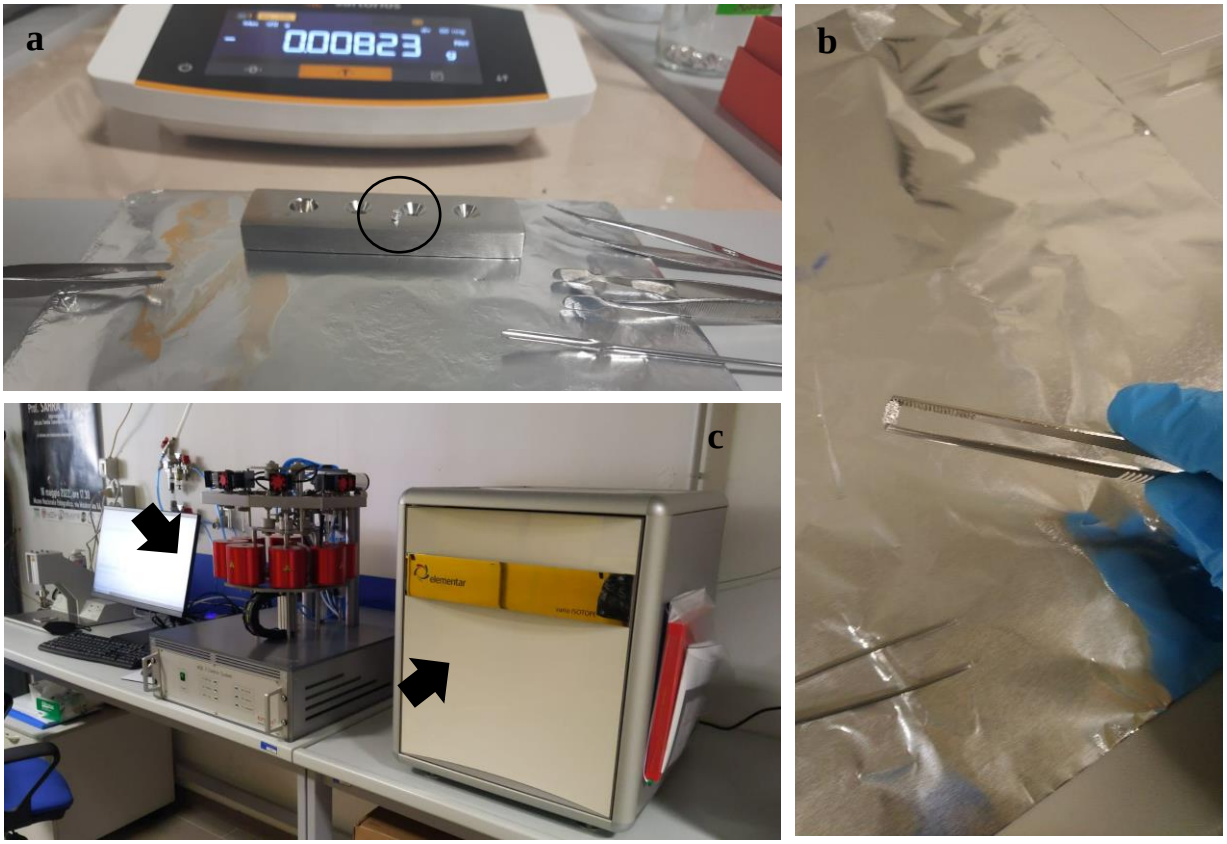

Fig. 10a *and* ***b*** *Aluminium cups preparation;* ***10c*** *Age 3 (combustion reactors) on the left and the analyser on the right*

2.4 Exploring different methods for cellulose extraction for ^{14}C dating

S. Cercatillo, M. Friedrich, B. Kromer, D. Paleček and S. Talamo

Published in *New Journal of Chemistry*, 2021

DOI: 10.1039/d1nj00290b

NJC

PAPER

View Article Online
View Journal | View Issue

Cite this: *New J. Chem.*, 2021, **45**, 8936

Exploring different methods of cellulose extraction for ^{14}C dating

Silvia Cercatillo, [a] Michael Friedrich, [b] Bernd Kromer, [c] Dragana Paleček [a] and Sahra Talamo [a]

In this study we aim to identify the optimal cellulose extraction protocol for ^{14}C dating of wood, with a focus on glacial trees. To achieve this, we compare three cellulose extraction methods on the basis of cellulose yield and ^{14}C age. The study is conducted on 12 wood samples of different species, in varying states of preservation with ages covering the full ^{14}C age range. Cellulose is extracted from each sample following three different protocols selected from the literature: ABA-B, BABAB and 2Chlorox. The extracted cellulose was graphitised and dated with the MICADAS (Mini Carbon Dating System) at the ETH AMS laboratory. Although all three methods are considered efficient, the BABAB protocol, despite being a more aggressive procedure, allows the extraction of a sufficient amount of cellulose to be ^{14}C dated and leads to the most reliable results, particularly for very old and background samples (samples with ^{14}C content of zero).

Received 18th January 2021,
Accepted 23rd March 2021

DOI: 10.1039/d1nj00290b

rsc.li/njc

Introduction

Cellulose ($C_6H_{10}O_5$) is an abundant biopolymer. The use of this compound is spreading in many fields, including the biomedical, packaging and environmental sectors, thanks not only to its chemical and physical properties, but also as a renewable, sustainable and biodegradable material.[4–6] In this study we chemically isolate cellulose from wood to exploit another of its unique qualities: its record of atmospheric carbon content.[7,8] Through the photosynthesis process, atmospheric CO_2 is stored as carbon in plants. During growth, the ratio of carbon isotopes in the plant tissues is in equilibrium with the atmosphere. After active growth has ceased, the radioactive carbon isotope (^{14}C) concentration starts to decrease. The concentration of ^{14}C can be measured with annual resolution from the cellulose extracted from tree rings.[8] Radiocarbon is the most precise and universal tool for dating events of the last 55 000 years,[9] the limit of the radiocarbon method. Here we study sub-fossil tree remnants (wood fragments in which the organic component is not fully decomposed and is only partially fossilized) grown in the glacial period. We intend to improve the resolution of the radiocarbon calibration curve (used to convert ^{14}C ages into calendar ages) beyond the current extent of the unbroken dendrochronological curve (back to 14 226 years cal BP†) to allow more precise age determinations.[9] Cellulose is the fraction of choice for dating trees.[2,7,8,10] To obtain reliable ^{14}C ages any contamination by extraneous carbon in the sub-fossil wood must be removed. Contamination can occur by young carbon, *e.g.* humic acid introduced from groundwater supply, or from ^{14}C-free carbonates. For radiocarbon dating of Upper Pleistocene samples, contamination by young carbon is more problematic than contamination by fossil carbon: 1% of modern carbon contamination added to a sample of 37 000 ^{14}C BP will reduce its age by 5500 years, whereas 1% ^{14}C-free carbon will increase the age by only 80 years. Therefore, when assessing the effectiveness of pretreatment procedures, older ages are generally considered more reliable. Several studies report cellulose extraction protocols for young Holocene trees as well as wood near/beyond the limit of ^{14}C dating (>55 000 years BP).[1,3,11] We want to identify the most effective pretreatment procedure to extract cellulose and efficiently remove exogenous contamination from sub-fossil trees spanning the glacial period. We compare three different protocols, including a novel technique which has been recently published. We selected subfossil trees of different species from different time periods to identify the limits and capabilities of each extraction method. For most of the samples the age is already known, either from dendrochronology or from radiocarbon dating. The results are evaluated on the basis of the cellulose yield and the ^{14}C age.

[a] *Department of Chemistry G. Ciamician, BRAVHO Radiocarbon Laboratory, Alma Mater Studiorum, University of Bologna, Via Selmi 2, Bologna 40126, Italy*
[b] *Hohenheim Gardens, University of Hohenheim, Emil-Wolff-Strasse 38, Stuttgart D-70599, Germany*
[c] *Institute of Environmental Physics, Heidelberg University, Heidelberg D-69120, Germany*

† Conventional term for radiocarbon calibrated dates corresponding to calendar years considering 1950 as present. Cal – (calibrated) BP – before present (1950).

Experimental

Materials and methods

Twelve wood samples within the age range of ^{14}C dating were selected from our archive (Table 1). Samples (*Pinus sylvestris* L.) from Furadouro were found in an ancient forest bed under the sandy shore of the northern Atlantic coast of Portugal, near the city of Ovar, accessible only during rare events of minimum low tide.[12] In this study, three sub-samples of the same tree section were dated. The sample from Revine (*Larix decidua*) was found in a larch forest preserved in colluvial and lacustrine deposits near the lake of Revine (Treviso) in the Italian Pre-Alps.[13] Cairo Montenotte (*Pinus sylvestris* L.) is part of a sub-fossil pine tree stump sampled from glacial sediments in Savona (Italy) in 2018. The conifer wood sample from Reichwalde is a background sample,[14] which was found in Miocene layers in the lignite mining area in Saxony, Germany.[15] Wood samples from Győrújfalu (*Fraxinus spec.*) and Győrzámoly (*Ulmus spec.*) were found in Hungary, near the city of Győr, in Quaternary gravel sediments in a tributary of the Danube River. The Győrzámoly sample was previously dated at the Heidelberg radiocarbon laboratory to beyond the ^{14}C dating limit (> 55 000 years BP). Recently, samples from Győrújfalu were unsuccessfully pretreated (cellulose was not obtained) at Mannheim radiocarbon laboratory. To verify their preservation state, they were tested again. The sample from Illegio is a larch stump (*Larix decidua*) found in sediments dating to the LGM (Last Glacial Maximum) in the basin of the Tagliamento River in the Carnic alps of the Friuli-Venezia-Giulia region (Italy), as described in Monegato *et al.*[16] The sample analysed here was found *in situ* together with another larch trunk, dated by Hajdas *et al.*[17] The Late Glacial pine (*Pinus sylvestris* L.) from Breitenthal was found in a gravel pit in southern Germany near the Günz River, together with other pines. They were dendrochronologically analysed by Friedrich *et al.*[18] Samples from Ebensfeld and Freising are Holocene oak (*Quercus spec.*) and pine (*Pinus sylvestris* L.) found in Quaternary deposits of the rivers Isar and Main in southern Germany. They were remnants of old riparian forests buried by river activity and found in gravel pits. They are parts of the Holocene oak and pine chronologies of central Europe.[18,19]

Pretreatment methods

Three sub-samples were taken from each of the 12 trees, one for each protocol. Nine sub-samples weighed ~200 mg, and 3 samples ~40 mg to ensure that all methods could be applied in cases of limited material. All samples were chopped into small pieces and were put into 10 mL glass tubes and processed according to the three different protocols: ABA-B,[1] BABAB[2] and 2ChlorOx.[3] The classic ABA method[1,8,23] was tested with the addition of a final bleaching step (ABA-B).[1] The BABAB method adds an initial overnight bath in alkaline solution to the ABA method followed by a final oxidative bleaching step.[2] The recently published 2ChlorOx method involves an alkaline hypochlorite and an acidic chlorite oxidation bleaching step, repeated two times.[3]

ABA-B[1]. Samples were treated with 4% HCl to remove contamination from carbonates, then washed with MilliQ water, followed by a 4% NaOH bath, and a second 4% HCl step to remove any absorbed atmospheric CO_2. Each step was carried out for ~1 hour. A bleaching solution (5% $NaClO_2$ and some drops of 4% HCl) to remove lignin and other contaminants was applied for ~1 hour,[24,25] then renewed to increase efficiency, as suggested by Capano *et al.*,[1] and left for another hour. All procedures are carried out in a heater-block at 75 °C. The final extract was dried in an oven at 80 °C.

Table 1 Sample information. Samples are ordered by age (from youngest to oldest)

Bologna lab code BRA-	Site	Species	Ref.	Dendro-date or ^{14}C age (if floating)
3275	Ebensfeld, Germany	Oak (*Quercus spec.*)	Friedrich *et al.*;[19] Friedrich *et al.*[18]	Ring 60–85 (72): 5569 BP (3620 BC)
3276	Freising, Germany	Pine (*Pinus sylvestris* L.)	Friedrich *et al.*;[19] Friedrich *et al.*[18]	Ring 20–40 (30): 10.872 BP (8923 BC)
3272	Breitenthal, Germany	Pine (*Pinus sylvestris* L.)	Friedrich *et al.*[19]	Ring 50–80 (65): 11.840 BP (9891 BC)
3274	Revine, Italy	Larch (*Larix decidua*)	Kromer *et al.*;[20] Friedrich *et al.*;[19] Kaiser *et al.*[21]	~15 000 ^{14}C BP
3271	Furadouro, Portugal	Pine (*Pinus sylvestris* L.)	This study	~27 000 ^{14}C BP (untreated)
3282	Furadouro, Portugal	Pine (*Pinus sylvestris* L.)	This study	~27 000 ^{14}C BP (untreated)
3283	Furadouro, Portugal	Pine (*Pinus sylvestris* L.)	This study	~27 000 ^{14}C BP (untreated)
3277	Illegio, Italy	Larch (*Larix decidua*)	This study	Not dated
3278	Cairo Montenotte, Italy	Pine (*Pinus sylvestris* L.)	This study	Not dated
3279	Győrújfalu, Hungary	Ash (*Fraxinus spec.*)	This study	Background (probably Eemian)
3281	Győrzámoly, Hungary	Elm (*Ulmus spec.*)	This study	Background (probably Eemian)
3273	Reichwalde, Germany	Conifer (*c.f.* Chamaecyparis)	Sookdeo *et al.*;[14] Scott *et al.*[22]	Background (Miocene)

BABAB[2]. Samples were left in a 4% NaOH bath at 75 °C overnight to dissolve the lignin (making the cellulose more accessible to reagents)[2] and the humic acid (soluble at high pH) from the soil.[26,27] The following day, the acid–base–acid steps (as described above for the ABA-B protocol) were performed. The final bleaching step to remove lignin, hemicellulose and other extractives[24,25] was carried out for 2 hours at 75 °C, followed by 15 minutes in an ultrasonic bath at room temperature in the same bleach solution. Samples were then washed several times with MilliQ water to reach pH 5 and dried in an oven at 80 °C.

2ChlorOx[3]. Two oxidative steps were applied. The first was performed in an alkaline environment at room temperature with NaClO and NaOH for 2 hours, followed by an acidic wash with HCl, and a second oxidative reaction with $NaClO_2$ and HCl started at 70 °C for another 2 hours. These steps were then repeated. Following this procedure, samples were washed to neutrality and dried in an oven at 80 °C. This is in contrast to Gillespie's procedure,[3] where the final product was freeze-dried.

After each step, samples were rinsed thoroughly with MilliQ water until the required pH was reached: ≤pH 10 before acid steps and ≥pH 4 before alkaline steps. To help solid–liquid separation samples were centrifuged and decanted. The weight of the initial dried sample and the weight of the dried final product were considered to calculate the cellulose yield % of each pretreated sample.

Graphitisation and ^{14}C dating

At the Ionplus laboratory, 2.5–3.0 mg dried cellulose was weighed into aluminium cups, compressed and then combusted in an elemental analyser coupled to an AGE 3. The resulting CO_2 was converted into graphite in the reactors using H_2 and 3.5 mg iron powder as a catalyst. Graphite was pressed into a target (sample holders) ready for AMS analyses at the ETH laboratory in Zurich. Samples of phthalic acid anhydride (chemical blank) and oxalic acid II (radiocarbon standard), kindly provided by the Ionplus laboratory, were graphitised and measured together with our samples in the ETH MICADAS (Mini Radiocarbon Dating System).[28]

Results and discussion

The final cellulose yield of all pretreated samples is shown in Fig. 1. For two thirds of the triple tests, ABA-B and 2ChloOx resulted in a similar yield (within 5%). In contrast, for most samples, BABAB reduced the sample mass to lower than 35% of the initial weight. In general, all the pretreatment methods used in this study resulted in a substantial loss of the initial sample mass as only cellulose was targeted, which constitutes 40–44% of the dry weight of both soft- and hardwood trees[25] and it is tightly connected to the state of wood preservation. 2ChlorOx was the most conservative among the considered protocols, together with ABA-B. Nevertheless, 50% of samples had a final yield between 20 and 40%, and the other half between 0 and 20%. In the BABAB procedure, in addition to the final bleaching stage, samples were first soaked in an alkaline bath of sodium hydroxide to dissolve humic acid and the polymeric molecules constituting lignin. The dissolution of lignin leads to a significant mass loss, as highlighted in Table 2: after the alkaline bath, 75% of our samples lost more than 30% of their initial weight. It is interesting to note the different behaviours of the background samples (BRA-3273, BRA-3279, BRA-3281) that show a significant loss of mass of 73% for BRA-3281, 50% for BRA-3279 and 46% for BRA-3273. At the end of the BABAB procedure, only BRA-3273 yielded sufficient cellulose to be radiocarbon dated. It is obvious that the

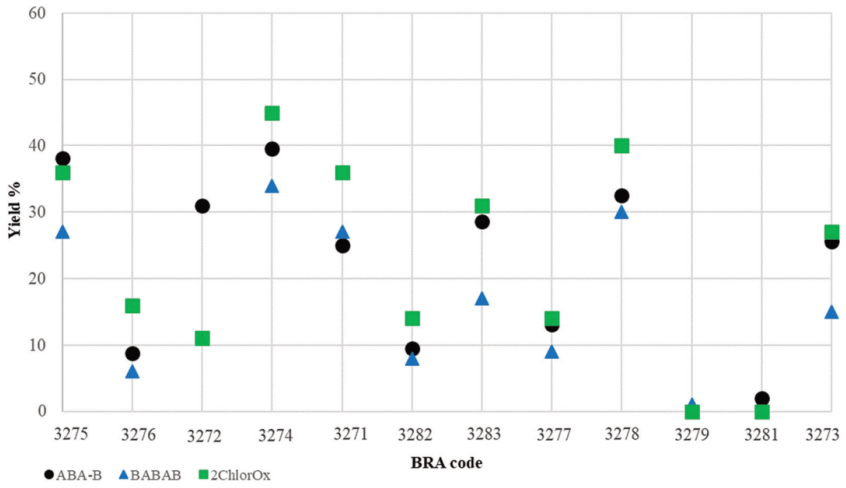

Fig. 1 Comparison of sample cellulose yields (%) following pretreatment with the different methods (2ChlorOx, ABA-B, BABAB). Samples are ordered by age (from youngest to oldest).

Table 2 Mass loss (%) for each sample after a 4% NaOH overnight bath at 75 °C in the BABAB procedure

Bologna lab code BRA-	Mass loss (%)
BRA-3275	39
BRA-3276	32
BRA-3272	30
BRA-3274	22
BRA-3271	51
BRA-3282	58
BRA-3283	27
BRA-3277	41
BRA-3278	39
BRA-3279	50
BRA-3281	73
BRA-3273	46

pretreatment protocol adopted plays an important role in the isolation of cellulose and the quantity of datable material obtained. However, it is also true that the state of preservation, which is an intrinsic property of the sample, has to be taken into consideration when choosing the pretreatment method since it defines the available amount of cellulose. Samples BRA-3276, BRA-3279 and BRA-3281 are examples of this: for the last two samples (both background samples) the state of preservation was very low, and we could only extract 0–3% cellulose, which was not a sufficient amount to be ^{14}C dated. Similarly, from the relatively young Holocene sample BRA-3276 only a small cellulose yield of $<$20% was obtained after the 2ChlorOx procedure, and $<$10% after the ABA-B and BABAB procedures. In contrast to the background samples, BRA-3276 is a relatively young (Holocene) pine wood which is poorly preserved. In general, we observed very different cellulose yields in both young (Holocene) and old (Upper Pleistocene) samples. There was no clear trend observable with burial time. Preservation depends on a combination of site-specific bedding conditions, burial time, and the durability of wood of different tree-species. In this respect, species such as oak, elm, pine and larch form heartwood in the inner part of the stem which contains phenolic compounds such as tannins, or other substances (*i.e.* resins), which make it much more resistant to decay than other types of wood, *i.e.* ash.[29,30] The absence of residual cellulose from the background sample BRA-3279 may be due to a species-specific low resistance of ash, as a non-heartwood. Regarding the influence of burial conditions on the preservation of the trunk, we observe a similar situation between our sites, which enables good preservation of wood, even though the preservation status of individual trees from the different sites depends on the combination of all preservation factors. The subfossil trees from Hungary were found in Interglacial fluvial gravels which were part of the aquifer of the Danube River valley.[15] As the trees were submerged in groundwater for most of the glacial period, they were predominantly exposed to anoxic bacterial decay. Trees from Furadouro were remnants of a pine forest in a lagoon close to the sea between 29 100–20 700 years BP, when the Atlantic ocean was below the present level.[12] The site was covered by fluvial sandy sediments during the Pleniglacial phase of the last ice age. Due to sea-level rise in the post-glacial period, the trees were submerged after that time, which explains the low level of bacterial destruction (*i.e.* good cellulose preservation). The larch trees from Illegio[17] (BRA-3277) and Revine[13] (BRA-3274) and the pine from Cairo Montenotte (BRA-3278) were found in glaciofluvial and colluvial sediments which kept the wood permanently under anoxic conditions and lead to remarkably good cellulose preservation, particularly at Revine and Cairo Montenotte. In comparison, the lower level of preservation at Illegio (BRA-3277) may be the result of local bedding conditions at that site. For the Holocene trees (BRA-3275; BRA-3276; BRA-3272) found in fluvial sediments,[18,19] the permanently water-saturated conditions below the groundwater table was the crucial factor for high levels of preservation. The variation in preservation may be due to the local situation. The good preservation of the oak (BRA-3275) is due to the natural durability of this species due to the high content of tannins in oak heartwood.[30]

The efficiency of contamination removal was evaluated through the ^{14}C dating shown in Table 3 and Fig. 2. For the three dendro-dated samples (top row of Fig. 2) the calibrated ranges of the ^{14}C ages cover the known calendar date. The measured ages of the sample pairs/triplets do not show significant variations. The results of the different pretreatment methods fall within the 2σ error range for 7 out of the 9 samples dated (background sample BRA-3273 excluded). The most significant difference is observed for sample BRA-3278: the ABA-B and BABAB extracts date to the background age level, whereas the 2ChlorOx extract is significantly younger. For BRA-3282, the BABAB extract is 2.7σ younger than the mean of the ABA-B and 2ChlorOx extracts. For the background sample BRA-3273, the F ^{14}C (Fraction Modern, defined as the ratio of ^{14}C specific activity of the sample and of the radiocarbon standard OxII, normalised to δ^{13}C, as described by Stenström *et al.*[31]) values of the ABA-B and BABAB extracts (shown in

Table 3 Carbon amount (%) following combustion and AMS ^{14}C results of samples pretreated following the ABA-B, BABAB and 2ChlorOx protocols

Bologna lab code BRA-	Method	Carbon content (%)	F^{14}C	±1σ	Age (^{14}C BP)	±1σ
3275	BABAB	44.0	0.54978	0.00145	4806	21
	2ChlorOx	34.9	0.55050	0.00141	4795	21
3276	BABAB	42.4	0.30513	0.00097	9535	25
	2ChlorOx	40.3	0.30510	0.00097	9536	26
3272	BABAB	44.7	0.28228	0.00094	10 160	27
	2ChlorOx	44.2	0.28292	0.00093	10 142	26
3274	BABAB	42.2	0.15275	0.00068	15 093	36
	2ChlorOx	40.9	0.15584	0.00068	14 932	35
3271	ABA-B	42.4	0.02589	0.00035	29 352	109
	BABAB	41.6	0.02666	0.00035	29 115	107
	2ChlorOx	44.7	0.02636	0.00035	29 207	108
3282	ABA-B	43.5	0.02592	0.00035	29 343	110
	BABAB	40.4	0.02740	0.00036	28 897	106
	2ChlorOx	47.0	0.02606	0.00035	29 297	109
3283	BABAB	45.3	0.02603	0.00036	29 309	110
	2ChlorOx	51.4	0.02631	0.00036	29 223	105
3277	ABA-B	39.9	0.01820	0.00033	32 183	144
	BABAB	40.8	0.01748	0.00032	32 505	149
	2ChlorOx	31.6	0.01802	0.00032	32 261	145
3278	ABA-B	42.2	0.00169	0.00025	51 285	1 207
	BABAB	41.3	0.00112	0.00025	54 613	1 807
	2ChlorOx	43.2	0.00316	0.00026	46 254	661

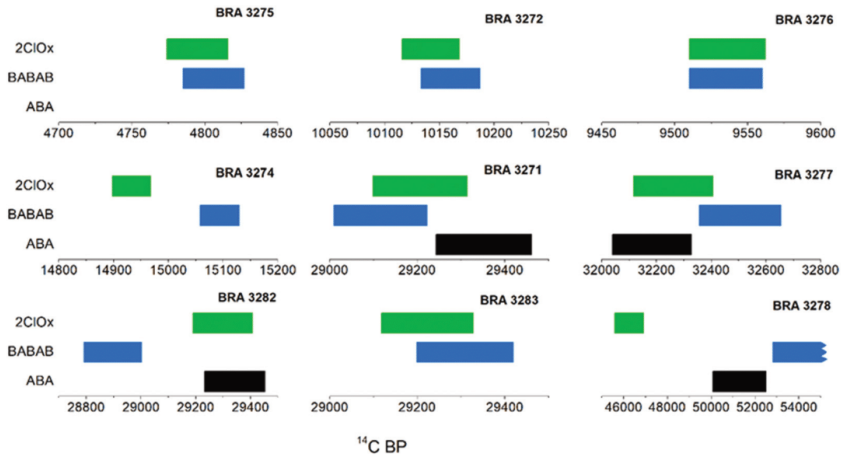

Fig. 2 Comparison of ^{14}C age ranges (1σ) of the pretreatment methods. 7 out of 9 samples (background sample BRA-3273 excluded) are within 2σ error range. BRA-3278 and BRA-3282 show the most significant differences.

Table 4 Background F^{14}C values measured in this study

Bologna lab code BRA-	Method	F^{14}C	±1σ
3273	ABA-B	0.00264	0.00008
	BABAB	0.00265	0.00009
	2ChlorOx	0.00290	0.00009

Table 4) are essentially identical (0.00265), whereas the 2ChlorOx extract is higher (0.00290) by 2σ compared to the other two methods. It is also interesting to compare the age results obtained for sample BRA-3271 which was previously speed-dated (*i.e.* AMS dating of CO_2 gas of untreated sample)[32] and dated again in this study after the application of different pretreatment procedures. The result obtained from the untreated sample is younger by 2200 ^{14}C years than the ages obtained from cellulose after pretreatment in this study. Contamination by 0.9% modern carbon in the untreated sample would account for this discrepancy.

Conclusions

The extraction and dating of cellulose from glacial sub-fossil wood are a key tool for improving the resolution of the radiocarbon calibration curve beyond the Holocene period. Cellulose extraction is fundamental to ensure correct dating. We aimed to determine the most effective extraction procedure on the basis of cellulose yield and ^{14}C age, particularly focussing on trees grown in the glacial period (older than 14 226 years cal BP). In light of the obtained results, the ABA-B method was sufficiently conservative in term of cellulose yield and efficiently removed contamination even from samples older than 30 000 years cal BP. The 2ChlorOx method led to almost the same final yield of cellulose compared to ABA-B, but appeared slightly less capable of removing young contamination in very old and background samples. The BABAB method is the harshest pretreatment method to apply in the case of poorly preserved trees, and it led to the highest loss of material during pretreatment but the results were the most reliable. Therefore, the pretreatment procedure must be chosen according to the preservation state of the wood sample. Based on this study, we have adopted BABAB as our standard pretreatment protocol since it is the most adequate method and guarantees high ^{14}C-dating quality. From our data and other studies referred to here, we can confirm that ABA-B pretreatment protocol represents a suitable alternative, especially for smaller sample quantities and wood samples with lower preservation status.

Conflicts of interest

There are no conflicts to declare.

Acknowledgements

This project is funded by the European Research Council under the European Union's Horizon 2020 Research and Innovation Programme (grant agreement no. 803147 RESOLUTION, https://site.unibo.it/resolution-erc/en). We thank Prof. Nuno Bicho and the Ph.D. candidate Pedro Horta of the University of Algarve, Portugal, for the work done and the suggestions given to us during the RESOLUTION fieldwork in Portugal. We thank Dr. Giovanni Monegato and Prof. Alessandro Fontana for providing the Illegio sample and Prof. Alessandro Michetti for providing Cairo Montenotte sample. We are grateful to Joël Bourquin, Dr. Simon Fahrni and Dr. David Ramrath of the Ionplus laboratory of Zurich who made available to us the graphitisation equipment (AGE 3) and the pneumatic sample press (PSP), in addition to their personal availability and

technical support. We acknowledge Dr. Lukas Wacker of the Laboratory of Ion Beam Physics of ETH for providing the AMS dates and for his personal availability. We thank Dr. Helmut Dalitz for technical and administrative support. We thank Prof. Luca Prodi, whose advice helped to improve this manuscript. We are very grateful to Dr. Helen Fewlass for her fundamental input and a British colleague who edited the English and considerably improved the manuscript. We acknowledge the Editor, Prof. P. Junk, and two anonymous reviewers for their constructive and helpful comments.

References

1 M. Capano, C. Miramont, F. Guibal, B. Kromer, T. Tuna, Y. Fagault and E. Bard, *Radiocarbon*, 2018, **60**, 51–74.
2 M. Němec, L. Wacker, I. Hajdas and H. Gäggeler, *Radiocarbon*, 2010, **52**, 1358–1370.
3 R. Gillespie, *Radiocarbon*, 2019, **61**, 131–139.
4 O. Nechyporchuk, M. N. Belgacem and J. Bras, *Ind. Crops Prod.*, 2016, **93**, 2–25.
5 M. Prakash Menon, R. Selvakumar, P. Suresh kumar and S. Ramakrishna, *RSC Adv.*, 2017, **7**, 42750–42773.
6 W. H. Danial, R. M. Taib, M. A. A. Samah, R. M. Salim and Z. A. Majid, *RSC Adv.*, 2020, 42400–42407.
7 K. J. Anchukaitis, M. N. Evans, T. Lange, D. R. Smith, S. W. Leavitt and D. P. Schrag, *Anal. Chem.*, 2008, **80**, 2035–2041.
8 J. B. Gaudinski, T. E. Dawson, S. Quideau, E. A. G. Schuur, J. S. Roden, S. E. Trumbore, D. R. Sandquist, S.-W. Oh and R. E. Wasylishen, *Anal. Chem.*, 2005, **77**, 7212–7224.
9 P. J. Reimer, W. E. N. Austin, E. Bard, A. Bayliss, P. G. Blackwell, C. Bronk Ramsey, M. Butzin, H. Cheng, R. L. Edwards, M. Friedrich, P. M. Grootes, T. P. Guilderson, I. Hajdas, T. J. Heaton, A. G. Hogg, K. A. Hughen, B. Kromer, S. W. Manning, R. Muscheler, J. G. Palmer, C. Pearson, J. van der Plicht, R. W. Reimer, D. A. Richards, E. M. Scott, J. R. Southon, C. S. M. Turney, L. Wacker, F. Adolphi, U. Büntgen, M. Capano, S. M. Fahrni, A. Fogtmann-Schulz, R. Friedrich, P. Köhler, S. Kudsk, F. Miyake, J. Olsen, F. Reinig, M. Sakamoto, A. Sookdeo and S. Talamo, *Radiocarbon*, 2020, **62**, 725–757.
10 K. Schollaen, H. Baschek, I. Heinrich, F. Slotta, M. Pauly and G. Helle, *Dendrochronologia*, 2017, **44**, 133–145.
11 A. Hogg, J. Southon, C. Turney, J. Palmer, C. B. Ramsey, P. Fenwick, G. Boswijk, U. Büntgen, M. Friedrich, G. Helle, K. Hughen, R. Jones, B. Kromer, A. Noronha, F. Reinig, L. Reynard, R. Staff and L. Wacker, *Radiocarbon*, 2016, **58**, 709–733.
12 H. M. Granja, T. A. M. Dte Groot and A. L. Costa, *Sedimentology*, 2008, **55**, 1203–1226.
13 G. Casadoro, E. Corona, F. Massari, M. G. Moretto, A. Paganelli, F. Terenziani and V. Toniello, *Bollettino del Comitato Glaciologico Italiano*, 1976, 22–63.
14 A. Sookdeo, B. Kromer, U. Büntgen, M. Friedrich, R. Friedrich, G. Helle, M. Pauly, D. Nievergelt, F. Reinig, K. Treydte, H.-A. Synal and L. Wacker, *Radiocarbon*, 2019, **62**, 891–899.
15 M. Friedrich, M. Knipping, P. Kroft, A. Renno, S. Schmidt, O. Ullrich and J. Vollbrecht, *Arbeits- und Forschungsberichte zur sächsischen Bodendenkmalpflege*, 2001, **43**, 21–94.
16 G. Monegato, C. Ravazzi, M. Culiberg, R. Pini, B. Miloš, G. Calderoni, J. Jež and R. Perego, *Palaeogeogr., Palaeoclimatol., Palaeoecol.*, 2015, **436**, 23–40.
17 I. Hajdas, L. Hendriks, A. Fontana and G. Monegato, *Radiocarbon*, 2017, **59**, 727–737.
18 M. Friedrich, S. Remmele, B. Kromer, J. Hofmann, M. Spurk, K. Felix Kaiser, C. Orcel and M. Küppers, *Radiocarbon*, 2004, **46**, 1111–1122.
19 M. Friedrich, B. Kromer, M. Spurk, J. Hofmann and K. Felix Kaiser, *Quaternary International*, 1999, **61**, 27–39.
20 B. Kromer, M. Spurk, S. Remmele, M. Barbetti and V. Joniello, *Radiocarbon*, 1997, **40**, 351–358.
21 K. F. Kaiser, M. Friedrich, C. Miramont, B. Kromer, M. Sgier, M. Schaub, I. Boeren, S. Remmele, S. Talamo, F. Guibal and O. Sivan, *Quat. Sci. Rev.*, 2012, **36**, 78–90.
22 E. M. Scott, G. T. Cook and P. Naysmith, *Radiocarbon*, 2016, **52**, 859–865.
23 J. R. Southon and A. L. Magana, *Radiocarbon*, 2010, **52**, 1371–1379.
24 J. Grumo, L. j. Jabber, J. Patricio, M. R. Magdadaro, A. Lubguban and A. Alguno, *J. Appl. Fundam. Sci.*, 2017, **9**, 124–133.
25 R. Shmulsky and P. D. Jones, *Forest products and wood science: an introduction*, Wiley-Blackwell, Chichester, West Sussex, UK, Ames, Iowa, 2011.
26 A. Baglieri, A. Ioppolo, M. Nègre and M. Gennari, *Org. Geochem.*, 2007, **38**, 140–150.
27 S. Khatami, Y. Deng, M. Tien and P. G. Hatcher, *J. Environ. Qual.*, 2019, **48**, 1565–1570.
28 L. Wacker, G. Bonani, M. Friedrich, I. Hajdas, B. Kromer, M. Němec, M. Ruff, M. Suter, H. A. Synal and C. Vockenhuber, *Radiocarbon*, 2010, **52**, 252–262.
29 A. Taylor, B. Gartner and J. Morrell, *Wood Fiber Sci.*, 2002, **34**, 587–611.
30 J. Baar, Z. Paschová, T. Hofmann, T. Kolář, G. Koch, B. Saake and P. Rademacher, *Holzforschung*, 2019, **74**, 47–59.
31 K. E. Stenström, G. Skog, E. Georgiadou, J. Genberg and A. Johansson, *Nuclear Physics*, Lund University, 2011, pp. 1–17.
32 A. Sookdeo, L. Wacker, S. Fahrni, C. P. McIntyre, M. Friedrich, F. Reinig, D. Nievergelt, W. Tegel, B. Kromer and U. Büntgen, *Radiocarbon*, 2017, **59**, 933–939.

References

1 M. Němec, L. Wacker, I. Hajdas, H. Gäggeler, *Radiocarbon*, 2010, 52, 1358-70.

2 J. B. Gaudinski, T. E. Dawson, S. Quideau, E. A. G. Schuur, J. S. Roden, S. E. Trumbore, D. R. Sandquist, S.-W. Oh, R. E. Wasylishen, *Analytical Chemistry*, 2005, 77, 7212-24.

3 S. Khatami, Y. Deng, M. Tien, P. G. Hatcher, *Journal of Environmental Quality*, 2019, 48, 1565-70.

4 M. Capano, C. Miramont, F. Guibal, B. Kromer, T. Tuna, Y. Fagault, E. Bard, *Radiocarbon*, 2018, 60, 51-74.

5 R. Gillespie, *Radiocarbon*, 2019, 61, 131-9.

6 K. E. Stenström, G. Skog, E. Georgiadou, J. Genberg, A. Johansson, *Lund University, Nuclear Physics*, 2011, 1-17.

CHAPTER 3

Dendrochronology and radiocarbon of glacial trees from Furadouro, Portugal

3.1 Dendrochronology of Furadouro

Following earlier reports,[1,2] we found glacial sub-fossil pine trunks in various spots on the Furadouro coastal area (Portugal). They were collected during two different campaigns in 2020 and 2021; their study led to the build of a new tree-ring chronology.

Fig. 11 *Furadouro, Portugal (Google Maps)*

3.1.1 Field work: Furadouro site and sub-fossil trees collection

Furadouro is located on the north coast of Portugal, near the city of Ovar, 30 km south of Porto (Fig. 11).

The coastal area is nowadays characterised by wide sandy beaches (ca. 100 m wide) interrupted by steep cliffs vegetated at the top, where the lithological Holocene and late Pleistocene sequence is exposed (Fig. 12). The outcropped layers witness the past alternation of lagoonal, beach and aeolian environments and moreover, horizons of paleo-soil (Podzol) are present.[1, 2]

Fig. 12 *Exposed depositional sequence, Furadouro (2020)*

Tectonics and sea-level changes were and still are the fundamental driving forces which determined the main environmental variations i.e., transitions between continental, marine and transitional *facies* during Holocene and late Pleistocene.[1] The trees were found *in situ* on the Furadouro foreshore during minima of low tide. They are remnants of a Glacial lagoonal forest that rooted in a soil that was covered by organic and sandy sediments. The preservation of the tree stumps implies close coincidence between the event that caused the soil to subside and the surge of water that covered the soil with sand. Such coincidence would i.e., be expected of an earthquake that caused a drop of the coastal area and the generation of a tsunami.[3]

The two sampling campaigns were held in March 2020 (11th, 12th and 13th) and October 2021 (7th, 8th and 9th) during times of minima of low tide (niptide) when larger areas of the beach, usually underwater, are exposed for some hours. During that brief time window, the sub-fossil trunks were found: some of them stuck out of the sand only a few centimetres, others were clearly visible (Fig. 13).

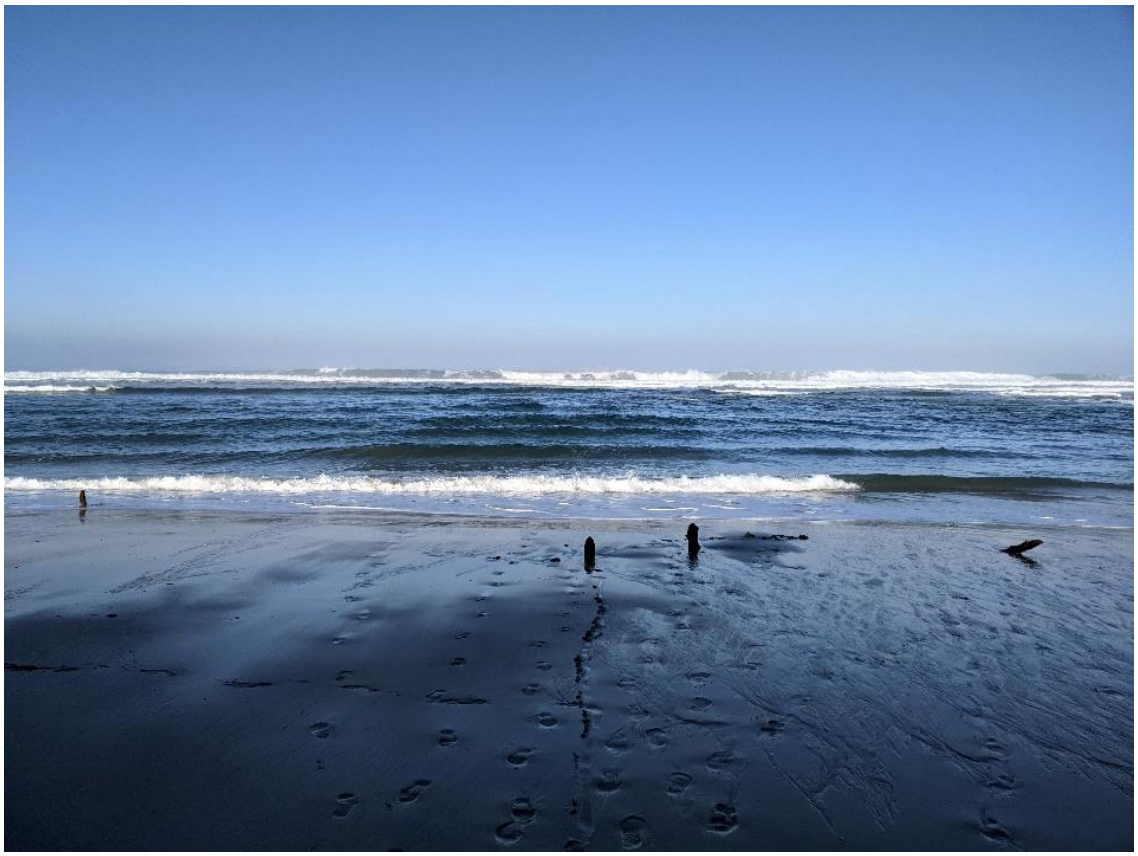

Fig. 13 *Sub-fossil trunks sticking out of the sand, Furadouro (2021)*

Once the trunks were pinpointed, the sand around was rapidly dug to make a larger portion of the sample visible (Fig. 14a and 14b).

These are remains of tree stumps, *in situ* position, which are still rooted in the original paleo soil and whose trunk was preserved up to a maximum height of ca. 1 m. The wood of the trunks was partly eroded on one side due to multiple exposures to the waves. Due to the high-water level in the sediment, it was only occasionally possible to excavate the stumps down to the root level. However, in all cases the root level could be determined by palpation; thus, the preserved stem height could be determined and documented.

A tree disc was taken from the trunks as deep as possible, but at least 20-30 cm above the root level, using a chainsaw (Fig. 14c and 14d). Only in one case, the sample was found not *in situ* on the beach at the foot of the slope. It was a rounded piece of wood reworked by sand and water. Each sample was photographed, labelled, and wrapped in plastic foil to keep it wet (Fig. 14e).

Eleven trees during the first campaign and six trees during the second one were sampled in six different spots (1-6) organised as shown in the map (Fig. 15), spot n. 6 is the location, where the only sample not *in situ* was found.

Fig.14a *and* ***b*** *Digging out the sand around the trunks;* ***14c*** *Sample cutting;* ***14d*** *Cross-section;* ***14e*** *Sample wrapping*

Fig. 15 *Spots at the Furadouro foreshore (Google Earth)*

3.1.2 Samples preparation

The tree discs cut on the beach and wrapped in plastic were transported to the University of Hohenheim, Stuttgart, Germany. There, the samples were cut into thinner (3-6 cm) discs, washed and gently brushed to remove sand from the surface and the sides, and then re-labelled.

The discs were frozen both to keep them wet, making the surface suitable for razor blade cut (Fig. 16a and 16b), and to prevent biological degradation, especially from fungi. The wood of the trunks was very soft because parts of the cellulose degraded through time.

In order to be able to examine the annual rings under a light microscope, the frozen cross-sections were cut manually over the entire cross-sectional area using razor blades. After the slices were thawed and dried for some time, chalk was rubbed into the surface to increase the contrast and make the annual rings and finest wood anatomical features clearly visible.

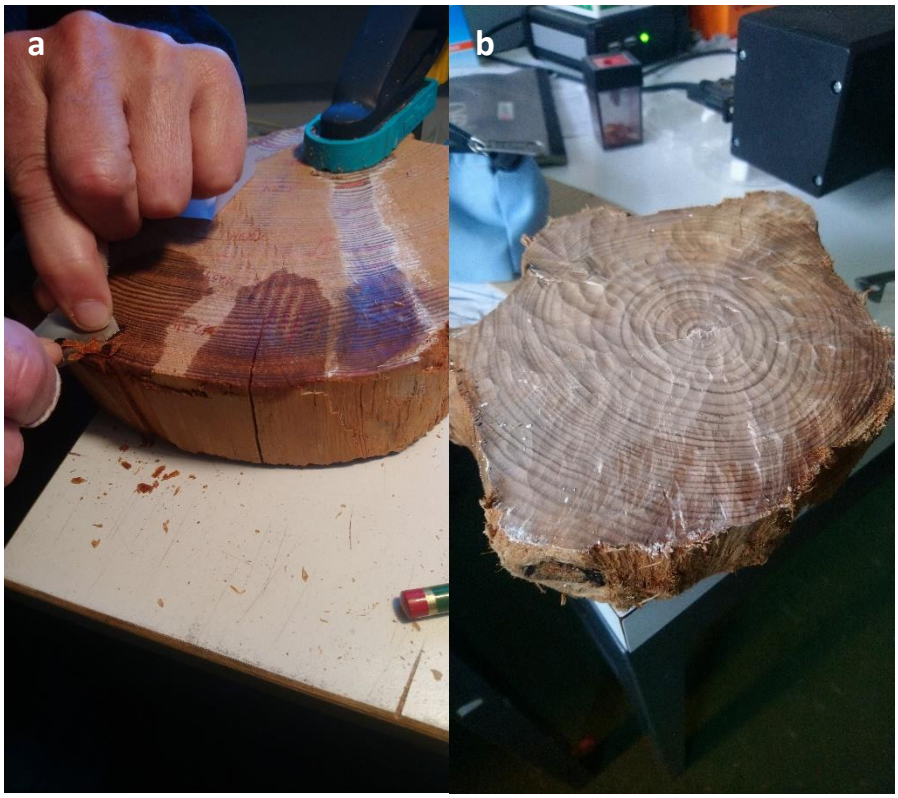

Fig. 16a *Surface planing;* ***16b*** *Surfaced sample*

3.1.3 Wood identification

Through macroscopic characteristics, such as wood structure and resin ducts, a pre-identification of conifer species could be done already in the field.

A more precise determination of the species was based on microsections (cross-, tangential and radial sections) using a transmitted light microscope and using identification keys,[4] and reference specimens.

Therefore, all trees were sub-sampled and kept in water.

Here the essential anatomical wood characteristics are the type of pitting in rays, the presence of transversal tracheids and the cell wall formation of the transversal tracheids with tooth shaped walls, which allow the assignment to the genus *Pinus* and the delimitation of the specific pine species.

Tracheids are the most common wood cell type in conifer wood and have both structural and water-transport functions in a longitudinal direction from the roots to the crown of the tree. Rays (Fig. 17a) consist mainly of rows of parenchymatic cells in radial direction going from the cambium, where wood cells are produced, toward the pith ensuring the water and nutrients transport in horizontal direction. The type of connection (pits) between tracheids and medullary ray cells and the typical shape of the transverse tracheids (marginal medullary ray cells) are important diagnostic characteristics here. The existence of rays with transversal tracheids with tooth-shaped walls and ray parenchyma cells with large open pits in all wood samples indicate the *Pinus sylvestris*-type (Fig. 17b). As the two pine species *Pinus sylvestris* L. and *Pinus nigra* cannot be reliably distinguished from each other in terms of wood anatomy, we call the species Pinus sylvestris nigra cf.

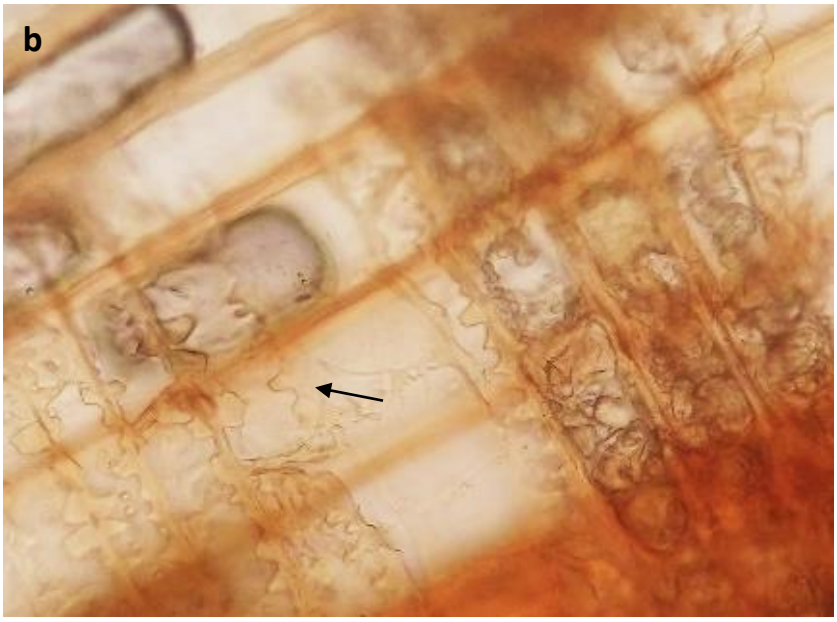

Fig. 17a *Rays on the radial section (circle);* ***17b*** *Distinctive toothed-edge intersection area in the tangential section of samples of Furadouro (arrow)*

3.1.4 Tree-ring measurements and tree curves

Once the samples are surfaced by razor blades, the tree-rings are well visible. Superficial rubbing of chalk enhances the contrast significantly and generally helps to identify rings and other wood anatomical features such as density bands, resin ducts and frost-rings.

Two radii are the minimum number selected to measure the tree-ring width of the sample both, to avoid counting errors and calculate a mean curve that better represents the wood increment.

Radii are generally tracked from the pith to the bark in the directions offering a higher number of rings and avoiding areas of growth disturbances, such as reaction wood, a response to mechanical, non-climatic stresses.

First, tree-rings were counted, and for every tenth, the ring was marked with a pencil (Fig. 18). This operation allows control of the subsequent annual ring measurement and helps avoid mistakes. An automatic tree-ring measurement device linked to software (TSAP Win scientific 4.81c) together with a binocular (10 – 40 fold magnification) was used to measure the annual tree-ring width.

Fig. 18 *Red pencil marks every 10 rings help counting and avoiding mistakes*

Each tree-ring is composed of earlywood, produced during spring and characterised by wood cells with thin cell walls and a big lumen that is adapted to good water

transportation, and latewood, produced during summer formed by cells with thick cell walls and small lumen which provide strength and elasticity to the wood.
For this reason, latewood appears less porous and darker than earlywood. The transition between latewood and the following earlywood is abrupt and marks the tree-ring boundary very clearly (Fig.19).

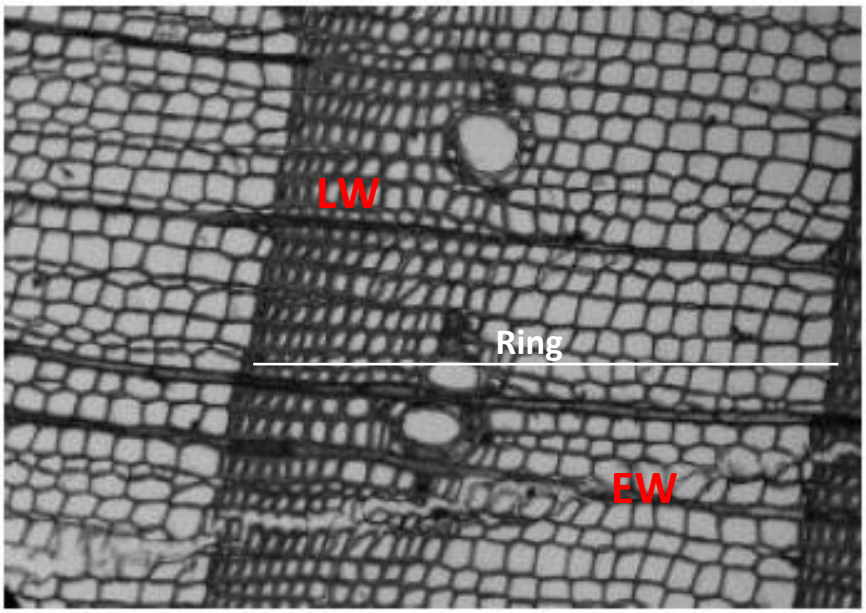

Fig. 19 *Tree ring EW (earlywood) and LW (latewood)* (Speer, 2010)[11]

The ring boundary as the starting point is identified via a crosshair in the binocular, the sample is then moved with the measuring stage to the following ring boundary, the measurement is triggered manually, and the measured distance is then transferred via the software as a value to a data set (Fig.20).

Fig. 20 *Measurement device*

This results in a series of annual ring widths of each radius, which can be plotted as a tree-ring curve (ring width against ring number). The curves of the different radii are then synchronised and brought into alignment, the position is fixed, and the mean curve of all radius curves of a sample is calculated (Fig. 21). In the case of non-synchronous curves, e.g., due to locally absent rings in a radius, the radii are again examined on the wood under the binoculars, absent rings are identified, and radii are re-measured if necessary.

In all samples examined, only occasional cases of locally absent rings (absent rings on individual radii) occurred, which could be identified with certainty by crosschecking between the radii. However, no case of total absent rings (annual ring absent on all radii) was observed.

From all 17 Furadouro samples, a tree-ring mean curve was obtained.

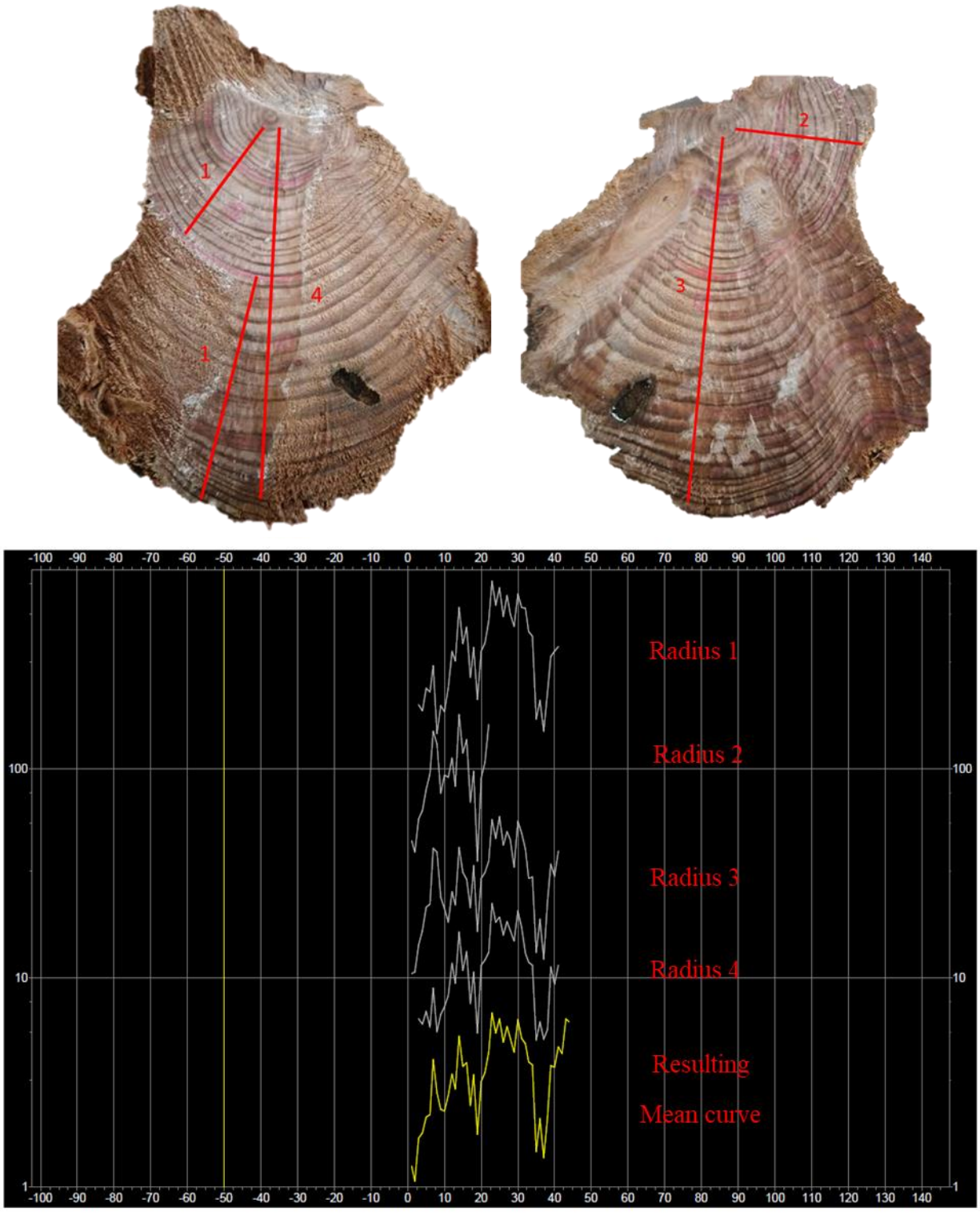

Fig. 21 *Corresponding radii in synchronous position. For better visibility, the curves were shifted in y-direction. The yellow curve marks the resulting mean tree-ring curve*

3.1.5 Dendrochronological cross-match and chronology building

The tree-ring curves of the individual trees from Furadouro were then compared mathematically and visually and examined for possible synchronous positions. We used the TSAP program (TSAP Win scientific 4.81c) for this purpose.

The visual comparison is facilitated by so-called signatures. These are particularly distinctive narrow or wide rings that are similarly formed in all trees in the same year. Fig. 22 shows an example: all curves have the same signature. A characteristic sequence of three narrow rings, which corresponds to a minimum in all series.

Fig. 22 *Four tree-ring curves in synchronous position with distinctive signature rings (red circled) pronounced in all trees in a similar way*

The degree of correspondence between different tree series can be calculated using different statistical parameters. These can also be used to calculate the significance, i.e., the statistical confidence of the corresponding synchronous position. When comparing the tree-ring curves, they are shifted against each other year by year and the similarity is determined visually and mathematically for each year. Clear significant similarity with synchronous signatures and high statistically significant correlation values determine a secure synchronous position.

Regarding the statistical comparison, there are parameters used to express the degree of correspondence of different tree series, and in particular, these statistical parameters were used here:

Gleichlaeufigkeit (Glk): the Gleichlaeufigkeit is an interval sign test that estimates the year-to-year agreement between the interval trends of two tree-ring series and expresses how strong the agreement is between the series.[5]

It is expressed as a percentage of compared values (%). A value of 0 means full anti-correlation, 50% means no similarity (random distribution) and 100% means a full agreement. In studies of living pines of the same stand, values of about 70-85 % are observed. Synchronous pines of one region show values of 60-80 %.[6]

The statistical significance of the Gleichlaeufigkeit depends not only on the value, but also on the number of pairs compared, i.e., on the length of the overlapping interval.

$$glk(x,y) = 1 - \frac{1}{n-1}\sum_{i=1}^{n-1}|G_{ix} - G_{iy}|$$

where, x and y are two data series.[5,7]

- T-value: the T-value is another test of agreement. It combines the correlation coefficient (in this case, Pearson correlation coefficient, r) with a student test (T-test). It is expressed as a dimensionless value. T=0 means no correlation and T=100 means identical curves.

In contrast to the sign test (Gleichlaeufigkeit), the T-value takes into account the absolute annual ring width values and therefore, the series fluctuations.

T-values > 5 can be seen as a threshold value for significant correlation, i.e., as a secure cross-match of two tree-ring series.

$$t = \frac{r\sqrt{N-2}}{\sqrt{1-r^2}}$$

where, r is the Pearson correlation coefficient and N is the number of pairs. [8,9,10]
The Pearson correlation coefficient (r) describes the strength and the direction of a linear correlation and takes on a value between -1 and +1, where values of -1 and +1 express perfectly negative and positive correlation of two variables, respectively. A value of zero means that there is no correlation between the two series.

When the mean tree-ring curves of the single trees from Furadouro were compared mathematically and visually and examined for possible synchronous positions, the visual comparison remains a fundamental step since it allows to detect possible missing or false rings. Missing, or locally absent rings occur when the tree does not form a growth ring in years with extremely poor growing conditions, or only in certain areas of the stem.[11]
False rings are additional, apparently complete growth zones formed within one growing season. They occur when during the growing period tree-growth is interrupted temporarily due to severe conditions and the tree starts forming terminal tissue (latewood), but with better conditions of growth it starts again in the same period, producing a renewed series of earlywood and latewood. The result is density fluctuations (false rings) that often look like two complete annual rings. As in our case the terminal tissue of false rings is mostly incomplete, they can be morphologically distinguished from true tree rings under the microscope, or they can be identified by cross-match with different radii or trees of the same site.
The use of the computer programme Cofecha (Holmes, 1999) to identify missing rings was not necessary due to the short length of the series and the high similarity.
The comparisons and cross-match procedures then allow building a tree-ring width site chronology by calculating means of all synchronized tree-ring series.
The variations of tree-ring chronologies express the mean growth of the trees, which is the response to local site growth factors i.e., local climate. Their analysis, as in this case, aims to extrapolate ecological and climate information. For this purpose, it is necessary to remove individual non-climatic biological disturbance signals from the tree-ring series, such as the individual, biological tree age trend, i.e., the physiological ring-width variations due to the specific biological growth phase. In the growth of young trees, increments of height and thickness of the wooden stem dominate, therefore the juvenile phase of tree-ring series is characterized by wide rings. With

increasing age, rings become narrower, as more assimilates are used for fructification.[12-14]

This results in a biological, non-climatic induced growth trend of the tree-ring width. The removal of this biological trend due to age or any other bio-ecological factor can be operated by fitting a trend curve to the raw tree-ring width data (*detrending* or *standardization*). The resulting series (ring width indices) from the division between each ring width and the corresponding value of the fitting curve form a new indexed and smoother data-series that better expresses the external growth conditions of the tree in the respective years. This procedure is referred to as *indexation*.[5,12]

3.1.6 Sampling for radiocarbon dating and radiocarbon age determination

In order to obtain high-resolution radiocarbon data, we have sampled blocks of three tree-rings from individual trees for the entire period of the Furadouro pine chronology. The tree discs were prepared accordingly, and the annual rings were carefully separated under the binocular with the help of a scalpel. About 40 - 70 mg of dry wood was sampled and brought to Eppendorf tubes.

To obtain an almost decadal resolution, as a first step every third block (i.e., every 9 years) was selected for cellulose extraction and ^{14}C analysis. The sub-samples were pretreated in the BRAVHO laboratory following both BABAB and ABA-B protocols, according to the state of preservation and the available quantity of wood, as discussed in chapter 2.[15]

The samples, together with 5 backgrounds, were sent to the ETH laboratory in Zurich for graphitisation and dating.

3.2 Results and discussion

3.2.1 Tree-ring chronology from Furadouro

The Furadouro tree-ring chronology spans 220 years and consists of 14 out of 17 pine trees recovered during both fieldtrips (Table 1) (Fig. 23). All 14 tree-ring mean curves could be cross-dated by statistical analysis and visual comparisons, with the exception of 3 trees (FURA0- 607, 657 and 658), for which statistically significant cross-dating failed.

The high similarity and agreement between the series and between the series and the chronology are shown in Table 2, where the t-value with Baillie-Pilcher standardization (TBP),[8] the Gleichlaeufigkeit (Glk) and the Pearson correlation coefficients (r) are reported.

In general, most trees show statistically significant correlations to each other and to the chronology. In cases when individual series showed weaker correlations to other single series due to individual growth variations, their cross-match could be proven reliably by visual comparisons. The chronology shows clear statistically significant values of Pearson correlation, Gleichlaeufigkeit and T-Value (BP) with all single tree series (Table 2 and 3). The mean correlation values ($\bar{X}$) indicate homogeneity among the tree-ring series of the site. The resulting chronology, therefore, is robust.

Dendro code	BRA n.	Spot	N. Radii	N.Rings	Pith	Waney edge	Pos. Start	Pos. End
FURA0600	600	1	7	72	Yes	No	32	103
FURA0601	601	2	11	146	Yes	No	1	146
FURA0602	602	2	8	168	Yes	No	32	199
FURA0603	603	2	4	65	Yes	No	18	82
FURA0604	604	2	6	104	Yes	No	39	142
FURA0605	605	2	5	91	Yes	No	32	122
FURA0606	606	2	4	105	Yes	No	6	110
FURA0607	607	3	7	106	Yes	No		
FURA0608	608	4	22	143	Yes	No	78	220
FURA0609	609	2	7	125	Yes	No	29	153
FURA0610	610	2	14	155	Yes	No	17	171
FURA0653	653	5	6	49	Yes	No	58	106
FURA0654	654	5	9	32	No	No	47	78
FURA0655	655	5	8	44	Yes	No	36	79
FURA0656	656	5	11	43	Yes	No	52	94
FURA0657	657	5	9	51	Yes	No		
FURA0658	658	6	8	87	No	No		

Table 1 *Samples overview. The spots refer to the map of Fig. 15. The presence or absence of the pith and of the waney edge is indicated by "yes" or "no". Start and End refer to the position of the tree on the chronology. The samples 607, 657, 658 do not cross-match to any other tree of the chronology, therefore they were not integrated into the Furadouro chronology.*

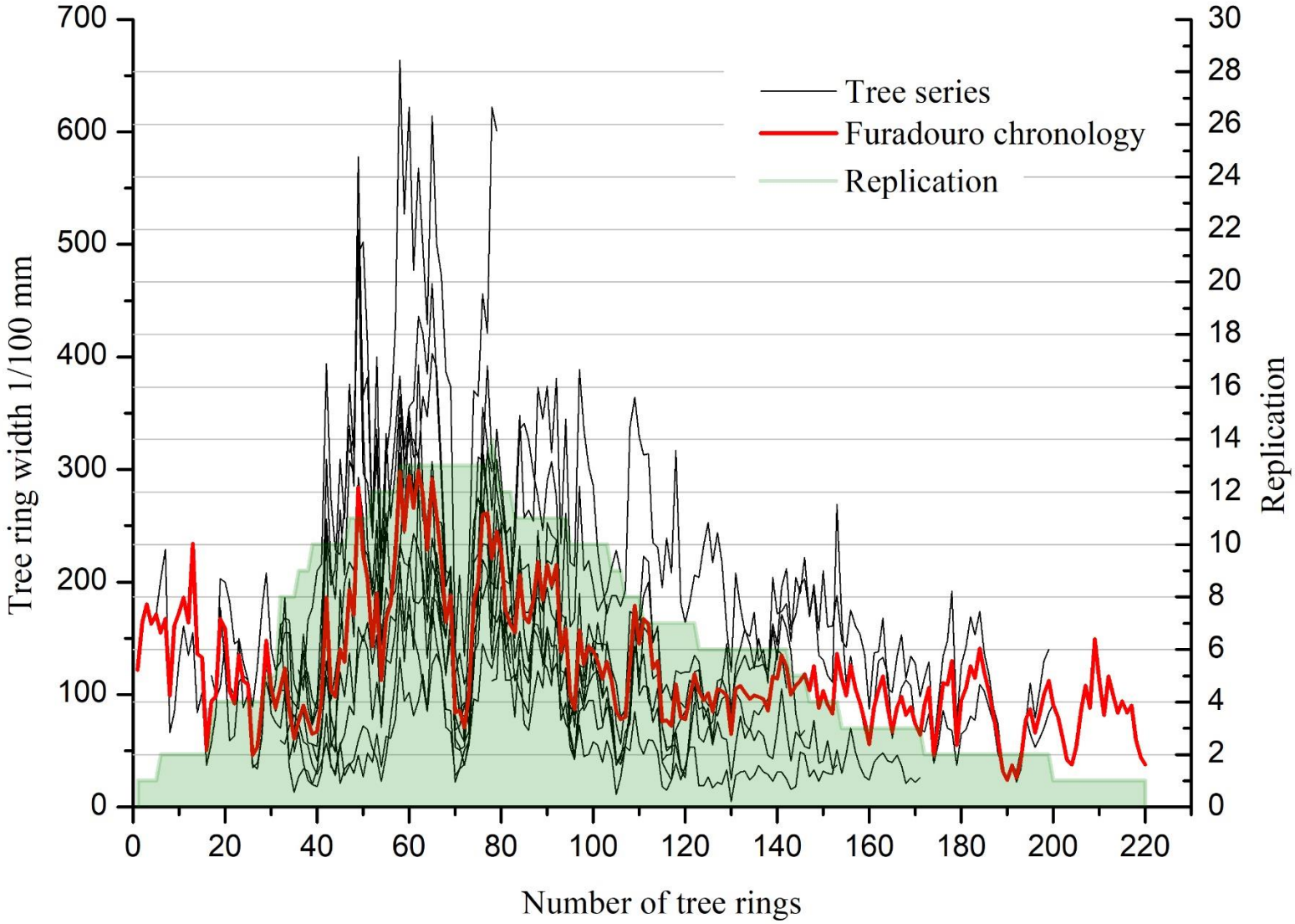

Fig. 23 *The Furadouro site chronology (red curve) and the raw ring width series of the 14 single trees (black curves). The green background area indicates the replication values of the chronology.*

	FURA0600/ 72	FURA0601/ 146	FURA0602/ 168	FURA0603/ 65	FURA0604/ 104	FURA0605/ 91	FURA0606/ 105	FURA0608/ 143	FURA0609/ 125	FURA0610/ 155	FURA0653/ 49	FURA0654/ 32	FURA0655/ 44	FURA0656/ 43
FURA0600/ 72	* 100,0/ 72	* 5,6/ 72	4,2/ 72	3,3/ 51	3,9/ 65	* 6,3/ 72	3,7/ 72	2,0/ 26	* 7,3/ 72	* 7,5/ 72	3,8/ 46	2,4/ 32	4,6/ 44	0,5/ 43
FURA0601/ 146	* 73,2/ 72	* 100,0/ 146	* 7,7/ 115	* 7,1/ 65	* 5,9/ 104	* 6,9/ 91	* 11,4/ 105	3,1/ 69	* 7,3/ 118	* 9,6/ 130	2,6/ 49	3,4/ 32	3,9/ 44	2,6/ 43
FURA0602/ 168	* 66,2/ 72	* 71,9/ 115	* 100,0/ 168	* 5,0/ 51	* 7,2/ 104	* 7,2/ 91	* 6,3/ 79	* 8,5/ 122	* 8,3/ 122	* 7,3/ 140	3,9/ 49	4,2/ 32	4,9/ 44	4,6/ 43
FURA0603/ 65	* 64,0/ 51	* 75,0/ 65	* 71,0/ 51	* 100,0/ 65	2,9/ 44	3,7/ 51	* 9,0/ 65	~~0,1/ 5~~	* 5,8/ 54	* 7,6/ 65	3,2/ 25	3,7/ 32	2,7/ 44	2,1/ 31
FURA0604/ 104	* 61,7/ 65	* 65,5/ 104	* 63,1/ 104	* 61,6/ 44	* 100,0/ 104	* 8,1/ 84	* 5,2/ 72	4,5/ 65	* 6,8/ 104	* 6,5/ 104	2,4/ 49	2,5/ 32	* 6,6/ 41	3,3/ 43
FURA0605/ 91	* 66,9/ 72	* 78,3/ 91	* 76,7/ 91	* 62,0/ 51	* 78,3/ 84	* 100,0/ 91	4,4/ 79	5,0/ 45	* 7,2/ 91	* 7,7/ 91	5,0/ 49	3,0/ 32	* 7,1/ 44	3,6/ 43
FURA0606/ 105	* 72,5/ 72	* 84,1/ 105	* 72,4/ 79	* 77,3/ 65	* 69,0/ 72	* 69,2/ 79	* 100,0/ 105	3,0/ 33	* 5,2/ 82	* 8,3/ 94	2,5/ 49	3,4/ 32	3,4/ 44	2,6/ 43
FURA0608/ 143	52,0/ 26	* 61,0/ 69	* 76,9/ 122	~~50,0/ 5~~	* 62,5/ 65	* 68,2/ 45	* 67,2/ 33	* 100,0/ 143	3,6/ 76	3,5/ 94	2,8/ 29	~~0,0/ 1~~	~~* 100,0/ 2~~	~~1,7/ 17~~
FURA0609/ 125	* 80,3/ 72	* 73,5/ 118	* 69,4/ 122	* 77,4/ 54	* 63,6/ 104	* 75,0/ 91	* 75,9/ 82	58,0/ 76	* 100,0/ 125	* 7,8/ 125	3,4/ 49	3,6/ 32	4,0/ 44	2,1/ 43
FURA0610/ 155	* 79,6/ 72	* 74,4/ 130	* 71,9/ 140	* 68,0/ 65	* 68,0/ 104	* 78,3/ 91	* 73,1/ 94	* 63,4/ 94	* 78,2/ 125	* 100,0/ 155	2,2/ 49	2,9/ 32	4,2/ 44	1,7/ 43
FURA0653/ 49	* 63,3/ 46	57,3/ 49	56,3/ 49	* 68,8/ 25	54,2/ 49	* 62,5/ 49	53,1/ 49	58,9/ 29	53,1/ 49	46,9/ 49	* 100,0/ 49	2,3/ 21	2,2/ 22	3,0/ 37
FURA0654/ 32	* 77,4/ 32	* 87,1/ 32	* 77,4/ 32	* 74,2/ 32	58,1/ 32	* 64,5/ 32	* 83,9/ 32	~~0,0/ 1~~	* 80,6/ 32	* 71,0/ 32	* 67,5/ 21	* 100,0/ 32	* 5,4/ 32	2,8/ 27
FURA0655/ 44	* 67,4/ 44	* 65,1/ 44	* 67,4/ 44	55,8/ 44	* 82,5/ 41	* 76,7/ 44	* 61,6/ 44	~~0,0/ 2~~	* 72,1/ 44	* 69,8/ 44	* 64,3/ 22	* 67,7/ 32	* 100,0/ 44	3,1/ 28
FURA0656/ 43	52,4/ 43	* 69,0/ 43	* 71,4/ 43	* 73,3/ 31	* 75,0/ 43	* 69,0/ 43	* 66,7/ 43	~~56,3/ 17~~	* 61,9/ 43	* 64,3/ 43	* 65,3/ 37	* 84,6/ 27	* 70,4/ 28	* 100,0/ 43
FURA_Chr/ 220	*** 77,5/ 72**	*** 83,4/ 146**	*** 83,8/ 168**	*** 81,3/ 65**	*** 71,4/ 104**	*** 80,6/ 91**	*** 83,2/ 105**	*** 83,5/ 143**	*** 78,2/ 125**	*** 79,2/ 155**	**65,6/ 49**	*** 83,9/ 32**	*** 74,4/ 44**	*** 73,8/ 43**
FURA_Chr/ 220	*** 8,9/ 72**	*** 18,3/ 146**	*** 18,4/ 168**	*** 9,0/ 65**	*** 10,3/ 104**	*** 10,3/ 91**	*** 12,9/ 105**	*** 17,1/ 143**	*** 11,6/ 125**	*** 13,1/ 155**	*** 5,8/ 49**	*** 5,6/ 32**	*** 6,5/ 44**	**3,8/ 43**

Table 2 *Gleichlaeufigkeit (black) and TBP (red) values of the tree-series and of the Furadouro chronology. Each series is identified as "Dendro-code/length". Values that refer to an overlap length of less than 20 rings are cancelled. Stars * indicate significant values of Glk > 60 % and TBP > 5,0*

	FURA0600/ 72	FURA0601/ 146	FURA0602/ 168	FURA0603/ 65	FURA0604/ 104	FURA0605/ 91	FURA0606/ 105	FURA0608/ 143	FURA0609/ 125	FURA0610/ 155	FURA0653/ 49	FURA0654/ 32	FURA0655/ 44	FURA0656/ 43
FURA0600/ 72	1,000/ 72													
FURA0601/ 146	* 0,532/ 72	1,000/ 146												
FURA0602/ 168	* 0,744/ 72	* 0,555/ 115	1,000/ 168											
FURA0603/ 65	* 0,434/ 51	* 0,713/ 65	* 0,531/ 51	1,000/ 65										
FURA0604/ 104	0,294/ 65	* 0,660/ 104	* 0,392/ 104	* 0,590/ 44	1,000/ 104									
FURA0605/ 91	* 0,629/ 72	* 0,694/ 91	* 0,771/ 91	* 0,615/ 51	* 0,555/ 84	1,000/ 91								
FURA0606/ 105	* 0,547/ 72	* 0,794/ 105	* 0,609/ 79	* 0,689/ 65	* 0,715/ 72	* 0,684/ 79	1,000/ 105							
FURA0608/ 143	-0,154/ 26	0,071/ 69	* 0,548/ 122	~~-0,364/ 5~~	0,302/ 65	* 0,393/ 45	0,290/ 33	1,000/ 143						
FURA0609/ 125	* 0,816/ 72	* 0,432/ 118	* 0,747/ 122	* 0,368/ 54	* 0,332/ 104	* 0,720/ 91	* 0,432/ 82	0,264/ 76	1,000/ 125					
FURA0610/ 155	* 0,780/ 72	* 0,547/ 130	* 0,653/ 140	* 0,518/ 65	* 0,473/ 104	* 0,729/ 91	* 0,649/ 94	0,262/ 94	* 0,701/ 125	1,000/ 155				
FURA0653/ 49	* 0,546/ 46	* 0,364/ 49	* 0,582/ 49	0,421/ 25	* 0,502/ 49	* 0,501/ 49	* 0,607/ 49	0,434/ 29	* 0,504/ 49	* 0,366/ 49	1,000/ 49			
FURA0654/ 32	* 0,731/ 32	* 0,654/ 32	* 0,750/ 32	* 0,603/ 32	* 0,609/ 32	* 0,655/ 32	* 0,788/ 32	~~0,000/ 1~~	* 0,586/ 32	* 0,743/ 32	* 0,808/ 21	1,000/ 32		
FURA0655/ 44	* 0,768/ 44	* 0,731/ 44	* 0,705/ 44	* 0,606/ 44	* 0,727/ 41	* 0,691/ 44	* 0,785/ 44	~~-1,000/ 2~~	* 0,653/ 44	* 0,779/ 44	* 0,727/ 22	* 0,817/ 32	1,000/ 44	
FURA0656/ 43	0,336/ 43	0,383/ 43	* 0,391/ 43	0,409/ 31	* 0,518/ 43	0,291/ 43	* 0,593/ 43	~~0,327/ 17~~	0,262/ 43	0,386/ 43	* 0,690/ 37	* 0,698/ 27	* 0,681/ 28	1,000/ 43
FURA_Chr/ 220	*** 0,785/ 72**	*** 0,801/ 146**	*** 0,854/ 168**	*** 0,700/ 65**	*** 0,703/ 104**	*** 0,848/ 91**	*** 0,875/ 105**	*** 0,740/ 143**	*** 0,718/ 125**	*** 0,812/ 155**	*** 0,655/ 49**	*** 0,889/ 32**	*** 0,904/ 44**	*** 0,616/ 43**

Table 3 *Pearson correlation coefficients of the indexed tree-series. Each series is identified as "Dendro-code/length". Values that refer to an overlap length of less than 20 rings are cancelled. Stars * indicate significant correlation coefficients with a level of significance of P>= 99%.*

To remove the age dependence of the ring-width variations from the tree-ring curves and to show up long-term fluctuations, we standardized the series using a 31-years moving average function. From the indexed tree series, the indexed chronology is calculated that lack the biological juvenile trend (Fig. 24).

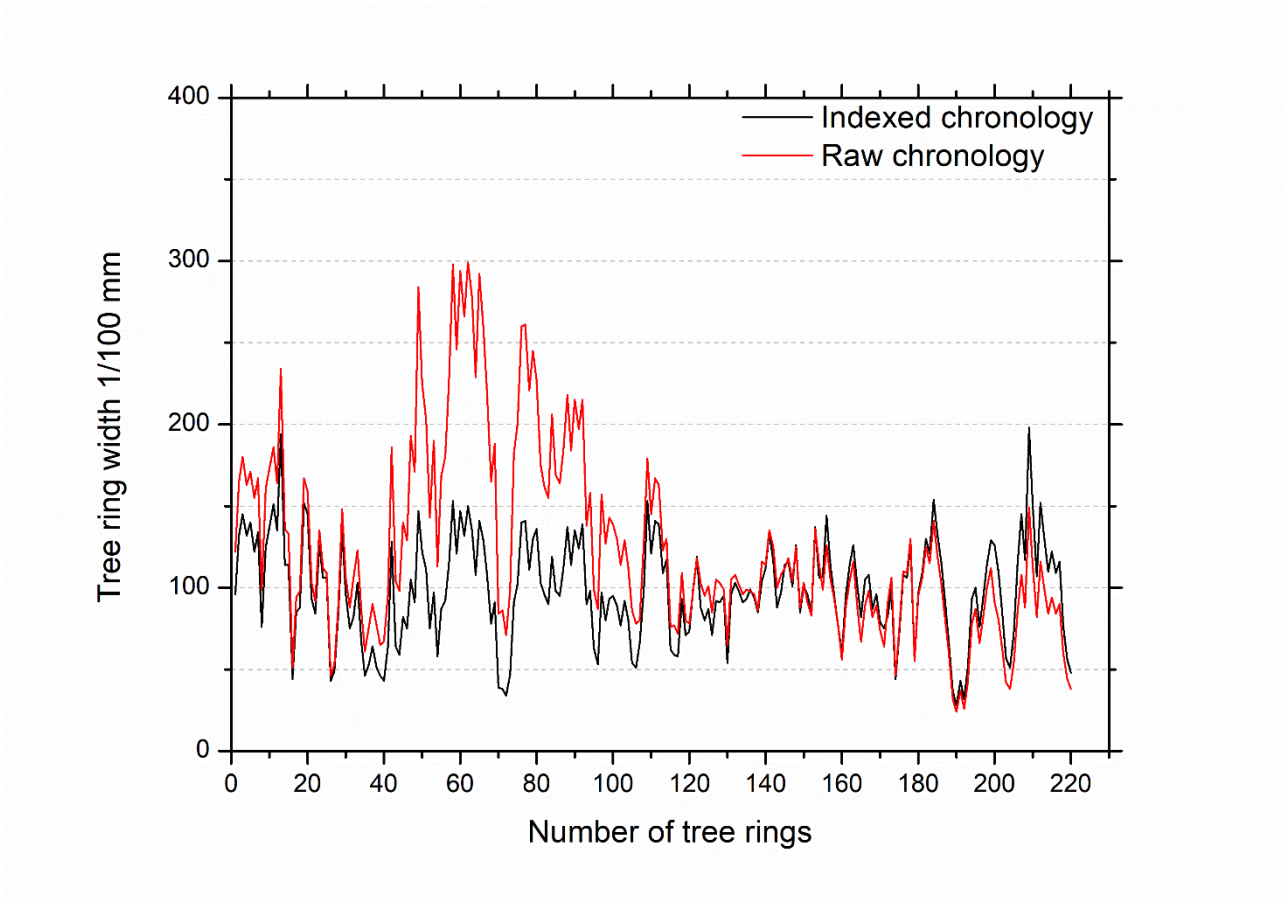

Fig. 24 *The Furadouro site chronology: raw data chronology (red) and indexed chronology (black)*

Additional statistics tree-ring parameters are given in Table 4. The mean ring width (MRW) was calculated using the raw ring width series and the resulting chronology. To avoid age-related bias of MRW we also calculated MRW of the first 50 rings ($MRW_{(50)}$) starting with the pith. All trees show surprising favourable growth with $MRW_{(50)}$ ~ 2-3mm and Max RW > 5mm, that clearly demonstrate good growth conditions in that period on the site.

The trees found in spot n. 5 (653, 654, 655 and 656) that represent a younger cohort of pines are characterized by wider rings (MRW ~ 2,86 mm; $MRW_{(50)}$ of 2,86 mm) compared to the other trees, which have a MRW of ~ 1,30 mm, $MRW_{(50)}$ of 1,52mm.

This demonstrates specific favourable growth conditions for the second cohort that starts growing ca. 40 years after the first.

The mean sensitivity (MS) (Mean MS: 27,6) is relatively low and in the range of Late Holocene pines.[16-20] The MS of the single tree series is in the same range like the MS of the chronology that demonstrates the high synchronicity of the series and the uniform fluctuations of the trees. Here, the ratio $\frac{\text{MS (tree series)}}{\text{MS (chronology)}}$ ~ 1 denotes the high agreement between all the series and the chronology (Table 5).

The autocorrelation (AC) parameter expresses the influence of the preceding years' conditions on the radial growth of the current ring. The higher the autocorrelation coefficient, the higher the influence.[5] Here the values of autocorrelation refer to the year before (lag = 1). The autocorrelation values of all trees show statistically significant correlation values ($r > 0,5$), that underline the high influence of the previous years' growth on the current growth, which can be explained i.e., by extensive carbon storage. Pines that growing under unfavourable site or climate conditions (extremely cold or dry conditions) are characterized by low AC.[12]

Similarly to the MS, the tendency change (TC) is a measure of the tree-ring width variation (increment or decrement). The absolute growth values are not taken into account. The tendency change indicates how often there are changing fluctuations in growth (wider or narrower than in the previous year) within a tree ring curve, and thus gives an indication of the climate sensitivity of a site.

Furadouro trees show TC-values of 50-68 % indicating favourable growth conditions with only moderate climate sensibility.[20]

Dendro code	MRW 1/100 mm	$MRW_{(50)}$ 1/100 mm	Min. Ring Width	Max. Ring Width	Autocorrelation (AC)	Mean Sensitivity % (MS)	Tendency Change % (TC)
FURA0600	205	220	67	578	0,61	26	68
FURA0601	118	87	13	355	0,65	34	54
FURA0602	140	159	20	287	0,71	23	58
FURA0603	146	134	53	311	0,46	27	56
FURA0604	89	85	21	175	0,58	27	53
FURA0605	101	108	22	230	0,64	32	56
FURA0606	106	89	3	314	0,64	47	53
FURA0608	156	158	24	389	0,54	22	58
FURA0609	149	252	24	499	0,56	26	61
FURA0610	94	220	5	346	0,53	33	63
FURA0653	244	244	109	403	0,71	17	50
FURA0654	304	304	58	502	0,74	24	52
FURA0655	358	358	104	664	0,62	27	67
FURA0656	238	238	95	549	0,79	22	62
FURA_Chrono	175	190			0,60	24	58

Table 4 *Additional statistics values of single tree series and the resulting Furadouro chronology. The autocorrelation values refer to a lag of 1, i.e., it refers to the previous year. The MRW is calculated on the raw tree series; MRW (50) is calculated on rings 1-50 of the series, AC, MS and TC are calculated on the indexed tree series*.

Dendro code	MS (tree series) / MS (chronology)
FURA0600	1,08
FURA0601	1,42
FURA0602	0,96
FURA0603	1,13
FURA0604	1,13
FURA0605	1,33
FURA0606	1,96
FURA0608	0,92
FURA0609	1,08
FURA0610	1,38
FURA0653	0,71
FURA0654	1,00
FURA0655	1,13
FURA0656	0,92

Table 5 *Mean sensitivity ratios between tree series and chronology.*

3.2.2 Radiocarbon age of Furadouro chronology

Twenty-four blocks of 3 rings each were taken from the entire length of the Furadouro chronology for radiocarbon age determination. The chronology falls in a ^{14}C age range between about 29,413 and 29,173 BP (Table 6).

To pretreat the samples, both ABA-B and BABAB protocols were used as tested in Cercatillo et al (2021)[15]. The choice was made on the basis of the available quantity of material and the status of preservation.

Tree n. 608 is the longest of the chronology, the only one which allows the extension until 220 years, and its preservation status is good in the innermost part and gets worse toward the outside, i.e., a light and brittle wood. Therefore, to save a sufficient quantity of datable material, those samples (BRA- 5180, 5181, 5186, 5188 and 5189) were pretreated with a mild pretreatment, ABA-B, which, however, did not completely remove the contamination as clearly evident from the systematically younger ^{14}C age results highlighted in Table 6: from 1,400 to 400 years younger than the previous age. In Cercatillo et al. (2021)[15] 3 samples from the Furadouro tree n. 607 (not belonging to this chronology) were successfully pretreated with both protocols, and the obtained results were comparable. It is reasonable to conclude that, although ABA-B can be a reliable and alternative pretreatment for well-preserved tiny samples in order to save cellulose for dating, in case of samples with a bad status of preservation ABA-B led to unreliable results.

Tree code	Sample code	Rings (start-end)	Pretreatment	^{14}C age	Error (1σ)
601	BRA 4974	1-3	BABAB	29,413	± 89
601	BRA 4972	7-8	BABAB	29,534	± 90
601	BRA 4070	12-13	BABAB	29,407	± 90
603	BRA 4995	18-21	BABAB	29,534	± 92
603	BRA 4992	28-30	BABAB	29,496	± 90
603	BRA 4988	40-42	BABAB	29,490	± 90
603	BRA 4985	49-51	BABAB	29,368	± 88
603	BRA 4982	58-60	BABAB	29,373	± 88
603	BRA 4978	70-72	BABAB	29,524	± 89
603	BRA 4975	79-81	BABAB	29,470	± 90
608	BRA 4999	90-92	BABAB	29,175	± 86
608	BRA 5002	99-101	BABAB	29,323	± 88
608	BRA 5005	108-110	BABAB	29,293	± 88
608	BRA 5008	117-119	BABAB	29,157	± 87
608	BRA 5012	129-131	BABAB	29,109	± 87
608	BRA 5015	138-140	BABAB	29,167	± 88
608	BRA 5019	150-152	BABAB	29,119	± 87
608	BRA 5180	159-161	ABAB	27,682	± 78
608	BRA 5181	168-170	ABAB	28,487	± 82
608	BRA 5029	180-182	BABAB	29,129	± 86
608	BRA 5031	186-192	BABAB	29,173	± 88
608	BRA 5186	204-207	ABAB	28,699	± 85
608	BRA 5188	208-212	ABAB	28,425	± 81
608	BRA 5189	213-217	ABAB	28,930	± 85

Table 6 *Radiocarbon age results. The samples highlighted in red are those removed from the radiocarbon sequence, because systematically younge*

3.2.3 Trees growth analysis: germination and dying phases study

Growth dynamic can be described by determining germination and dying years of the trees of a site using the waney edge (the last ring before the bark, i.e., the youngest) and the pith (the innermost ring, i.e., the oldest) (Table 7).

Almost at all pine trees collected in Furadouro the pith is preserved, with the exception of tree 654, for which the putative position of the pith and the number of missing inner tree-rings could be estimated by determining the original position of the pith on the basis of the rounding of the tree-rings and the course of the medulla rays (no more than 2 to 4 rings were missing from the corresponding innermost ring).

On the other hand, at none of the trees the outermost ring, i.e., the waney edge, and the bark was preserved. But based on the rounding of the trunk and the preserved sapwood area, it can be assumed, that for most trees only a very few rings are missing up to the waney edge. Therefore, the year of death roughly corresponds to the outermost ring.

It is in any case necessary to consider the original height of the disc in the standing trunk to evaluate the time respectively to the number of missing rings the tree needed to reach the height where the disc was taken. Hence, to estimate the true germination year and taking into account that cuts were made at 20-50 cm from the root system, i.e., the former soil surface, we estimate that 10 ± 5 years must be added to reach the germination year of the trees. Accordingly, we add 5 years to the actual position of the pith of all our trees, as reported in the Table 7 in the "Estimated Start Position" column.

In the bar plot graph of Fig. 25 two main germination-phases are distinguishable. A first group of trees (n=9) started the growth within the first 30-40 years and a second one (n=4) 10-20 years later.

The pines of spot I and II belong to the first germination phase, while the ones of spot V belong to the second phase, as visible in the bar plot graph of Fig. 26 and as shown in Table 7. It is noteworthy, that all the trees found in spot V have a shorter lifespan than the ones belonging to the other spots. The mean individual age of the first tree group is about 114,5 years, while the mean age of the second group is around 42 years. Therefore, spot V represent a young cohort of pines.

According to the germination dates of our sub-fossil trees, sprouting of new trees was fairly constant and uniform in a time window of almost 60 years with only two main

germination-phases within a short period. This indicates that the growth conditions at the site got favourable before the pines start growing and allowed more new trees to establish and thus the successive re-forestation of the studied lagoonal area. Given the fact that we identified 14 pines of the same period on 5 different spots, it is likely to conclude, that the lagoonal forest was not composed by trees much older than those found. Moreover, the short time window of germination and the absence of sprouted trees after 100 years suggests that the favourable germination conditions which allowed the successive forestation of the area during the first period of 100 years, probably got worse in the second century that suppressed new tree's germination and establishment and led to the progressive dieback of the trees on that site.

As any of the trees preserved the outermost ring, that would allow to date the precise year of death, the study of the dying-phase can be done only roughly. Nevertheless, for all trees we could define the year of the death as a *terminus post quem*, that means that the tree died in a period after a certain year plus a few years only.

Considering bar graph of Fig. 27 and considering that just few rings miss to the waney edge, we can conclude that the trigger of the general dieback of the trees was not a single event, instead it is more likely that multiple individual events that involved some of the pine trees had caused their dieback.

For example, the trees 654, 655 and 603, that died in the same time interval could have been involved in the same destructive event. Their positions, far apart from each other (spot V and spot II, see Fig. 28) suggest that the event was not closely localized, but affect the entire lagoonal forest. As clearly visible from the chronology shown in the background of each graph, the rings' widths have the major fluctuations and the greater amplitudes with maxima peaks in the first 80 years, reaching more than 6 mm that is in correspondence with the juvenile phases of the trees. During this juvenile phase of about 20-30 years during which the tree especially aims to a fast growth to increase the mechanical functions of the trunk, get enough light, nutrients and win the ecological competition toward other individuals.[21]

Dendro code	Spot	N. Radii	N. Rings	Pith	Waney edge	Start Pos.	Estimated Start Pos.	End Pos.
FURA0600	I	7	72	Yes	No	32	27	103
FURA0601	II	11	146	Yes	No	1	-4	146
FURA0602	II	8	168	Yes	No	32	27	199
FURA0603	II	4	65	Yes	No	18	13	82
FURA0604	II	6	104	Yes	No	39	34	142
FURA0605	II	5	91	Yes	No	32	27	122
FURA0606	II	4	105	Yes	No	6	1	110
FURA0608	IV	22	143	Yes	No	78	73	220
FURA0609	II	7	125	Yes	No	29	24	153
FURA0610	II	14	155	Yes	No	17	12	171
FURA0653	V	6	49	Yes	No	58	53	106
FURA0654	V	9	32	No	No	47	42	78
FURA0655	V	8	44	Yes	No	36	31	79
FURA0656	V	11	43	Yes	No	52	47	94

Table 7 *Trees belonging to the first germination phase (green) and trees belonging to the second germination phase (red).*

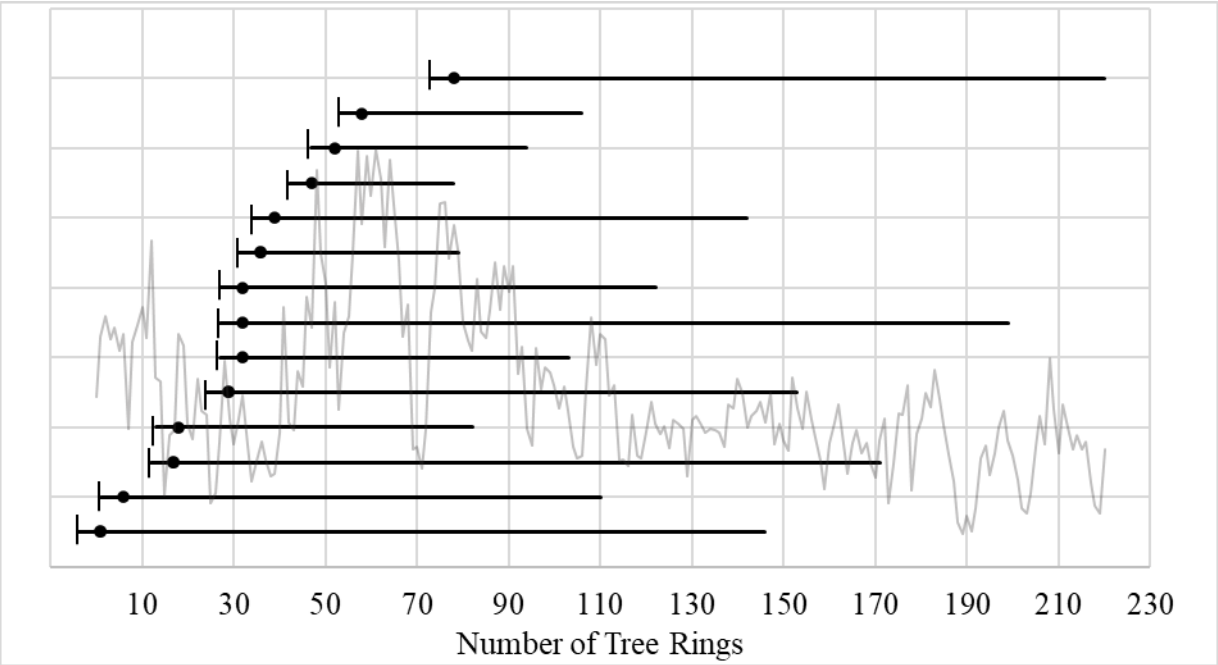

Fig. 25 *Trees sorted by germination year. The length of each horizontal line corresponds to the individual age of the trees. The dots indicate the piths and the vertical lines indicate the estimation of the real year of germination. In the background the raw ring width chronology.is shown.*

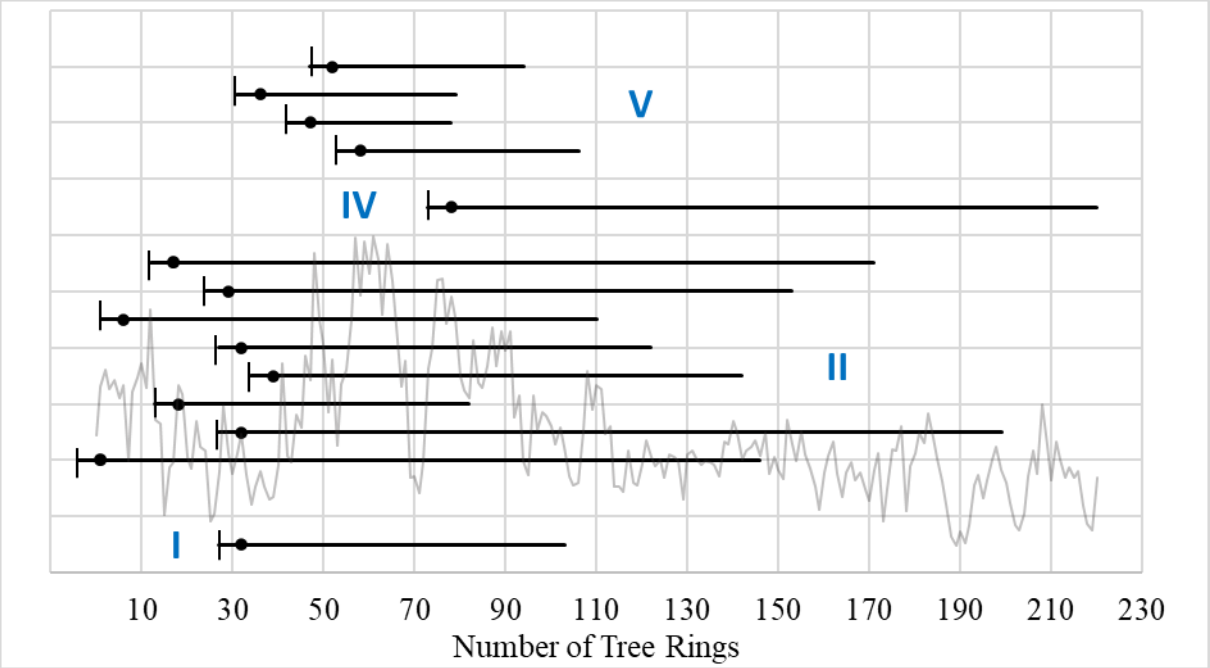

Fig. 26 *Trees sorted by spots: I, II, IV and V. The length of each horizontal line corresponds to the individual age of the trees, the dots indicate the piths and the lines indicate the estimation of the real year of germination. In the background the raw ring width chronology is shown.*

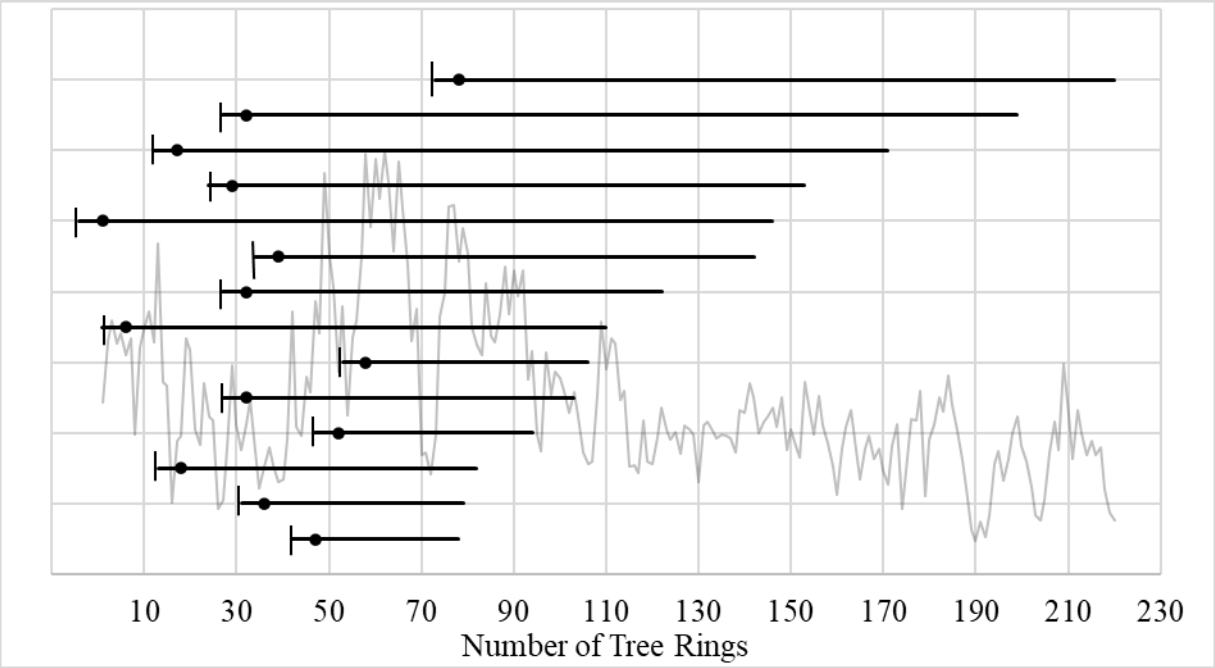

Fig. 27 *Trees sorted by death year. The length of each horizontal line corresponds to the individual age of the trees, the dots indicate the piths and the lines indicate the estimation of the real year of germination. In the background the raw ring width chronology is shown.*

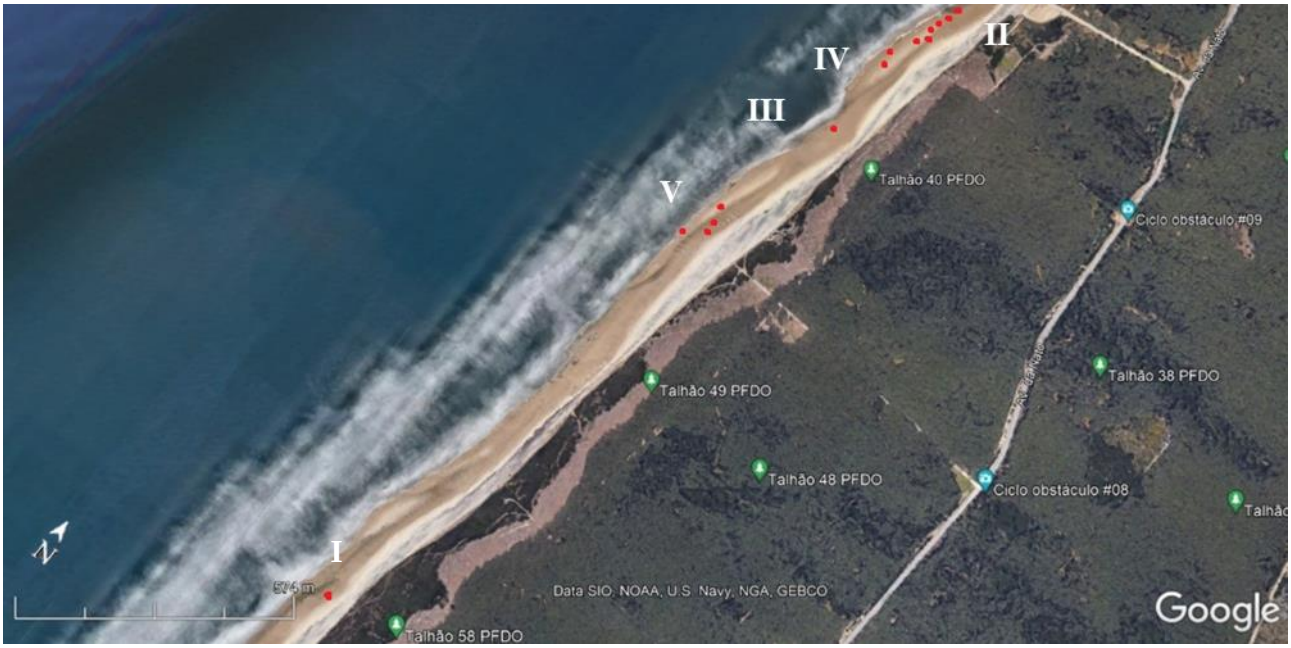

Fig. 28 *Map of the Furadouro site. The red dots indicate where the trees were sampled and the relative spot number (Google Earth).*

3.2.4 Paleo-ecology: fire history

Fires can be an important driver in the forests' stability and dynamic and especially low-intensity fires (surface or ground fires) can bring benefits to the ecosystem cleaning the understory from leaves, dry twigs, low vegetation contributing to prevent more destructive high-intensity fires. Low and medium-intensity fires promote the nutrients enrichment of the soil thanks to the ash and the renewal of the species, for example of those whose seeds' spread is promoted by fire events.[22-24]

Some pine species, including Scots pines (*Pinus sylvestris*), are fire-tolerater. Their characteristics make them less vulnerable to fire, as the height which minimizes the crown's involvement in moderate fires, the thick and insulating bark to protect the cambium, deep root-system hardly affected by fire for water and nutrients and the releasing of the seeds from cones favoured by extreme heat. Moreover, during fires it is likely that species less fire-adapted are burnt, leading to a decrease in the forest's ecological competition and to an increase of water, nutrients and light availability promoting pioneer and light-demanding trees, like pines.[22,24-26]

In the samples undisputed fire trails (scars, charcoals, discolorations and black resin ducts) have been found. Clear evidence of the occurrence of fires are visible on the outermost area and on the cross-section of almost all trees. In the graph of Fig. 32 the blue dots and arrows identify those samples having clear burned areas on the outside, which suggest that a fire event surely occurred subsequent to that year (ring) defining a *terminus post quem*. Traces of charcoals and discolorations (Fig. 29) can occur even after trees' death, this is the case of Fig. 29a and 29b, where innermost burned areas on the cross-section clearly result from fires in the year when the tree died or *post-mortem*, since they are not associated with reaction wood. On the other hand, fire scars clearly recorded fire damages and the respective reaction of the tree and therefore are indisputable and direct proof that a fire hit the tree, damaged part of the cambium, but the tree survived and continued growing. Fire scars, which are injuries of the tree cambium, have a distinctive curl pattern due to the growth of new wood to cover the wound, as clearly visible in Fig. 30.

Their study can help to reconstruct forest fires' history, since they can provide an exact date (year) of the fire event, and, in some cases, even the season in which the fire occurred.[27,28] Among the pine trees, three of them (602, 608 and 656) show three temporally distinct fire scars, which clearly proof the occurrence of forest fires at years

64, 70 and 94 of the common chronology. At the first two events the scars are clearly located after latewood formation, dating the fire event into the late summer or winter season. For the third event the scar's position was not clearly determinable. Thus, here the season of the fire cannot be defined.

The number of fire scars that could be detected in the samples of our trees is certainly to be seen as a minimum number, as we just sampled a small part of the tree stem. It is likely that more fires occurred and more fire trails were present in the logs that we missed due to the sampling of a small portion of the stem and the erosion of the trunks. In the graph of Fig. 32, the fire scars are highlighted by yellow rhombuses drawn on the interested tree and from the same graph it is likely that the fire events testified by the fire scars were of low or moderate intensity and not dramatic and destructive, since all studied trees survived the fires of years 64 and 70 respectively. In contrast to that the last of the three fire events that occurred in year 94 killed trees 654, 655 and 656, which show clear burning proofs. Considering that the outermost 15 and 16 rings of tree 654 and 655 are eroded while the outermost available ring of tree 656 corresponds to the same year of the fire, these three trees most probably died in the same fire event in year 94 that is characterized by a marked ring width drop in the following years 95 and 96 as seen in the chronology.

In correspondence of the fires in years 64 and 70 in almost all trees, marked growth depressions followed the year of the fire event (see graph 33) which can be explained by the damage to branches and needles of the tree by the fire. The typical tree-ring pattern of a significantly drop in the annual ring widths followed by an increase above average for a few years that follows a fire event testifies that for most of the trees the fire events implied a short-term growth reduction of some years (around 4-5), which coincide with the years needed to regenerate its needles followed by a recovery due to the positive effects of forest fires on this species. Moreover, this characteristic sequence of tree-ring widths in almost all trees suggests that the entire local forest or at least a significant part of the lagoonal forest was affected by these fire events, as the big distances between the spots of the examined trees demonstrate (Fig. 28). As this specific growth pattern is very characteristic, it can be used to identify other possible forest fires in the single tree-ring sequences, which hit the forest during the 220 years and of which there is any record in the samples.

In the graph 33 we mark positions of assumed additional fires at years 16, 26, 35, 43, 85, 105, 115 and 187 by dashed lines. They were identified based on distinctive

sequences of tree-ring width, similarly to the ring width signatures seen in connection with the identified forest fires by fire scares in the wood.

The capacity of Scots pines to take advantage and regenerate from low and medium-intensity fires is known in different kind of forest and climate not only in the short-term, i.e., some years from the fire event, but also in the long-term the upward growth is promoted.[29,30]

According to the direct detected fire evidence combined with the hypothesized fires we recognize a minimum fire recurrence time of ca. 10 years in the first 100 years, while a lower frequency is detected in the following period. In comparison, in the late Holocene boreal coniferous forests in Eurasia and North America are affected by forest fires only every (50) 80-300 years.[31] The surprisingly high fire frequency at Furadouro Glacial pine forest can be caused by seasonal dry climate conditions (especially during summer), which cause flammable material to accumulate in the understorey in combination with frequent thunderstorms with lightning, that can trigger the fires. A comparably high fire frequency in modern time is found at the sparse, grass-rich ponderosa pine ecosystem in Colorado, North America, where the observed average fire recurrence time is about 6-12 years.[32] There, the grass-rich herb layer, which accumulates a large amount of combustible material in a short time, and the dry summers combined with summer thunderstorms lead to frequent but less destructive ground fires, a scenario that could also be imagined for the Glacial forest of Furadouro.

Fig. 29 *Discolorations and charcoals on the cross-section and on the outermost area*

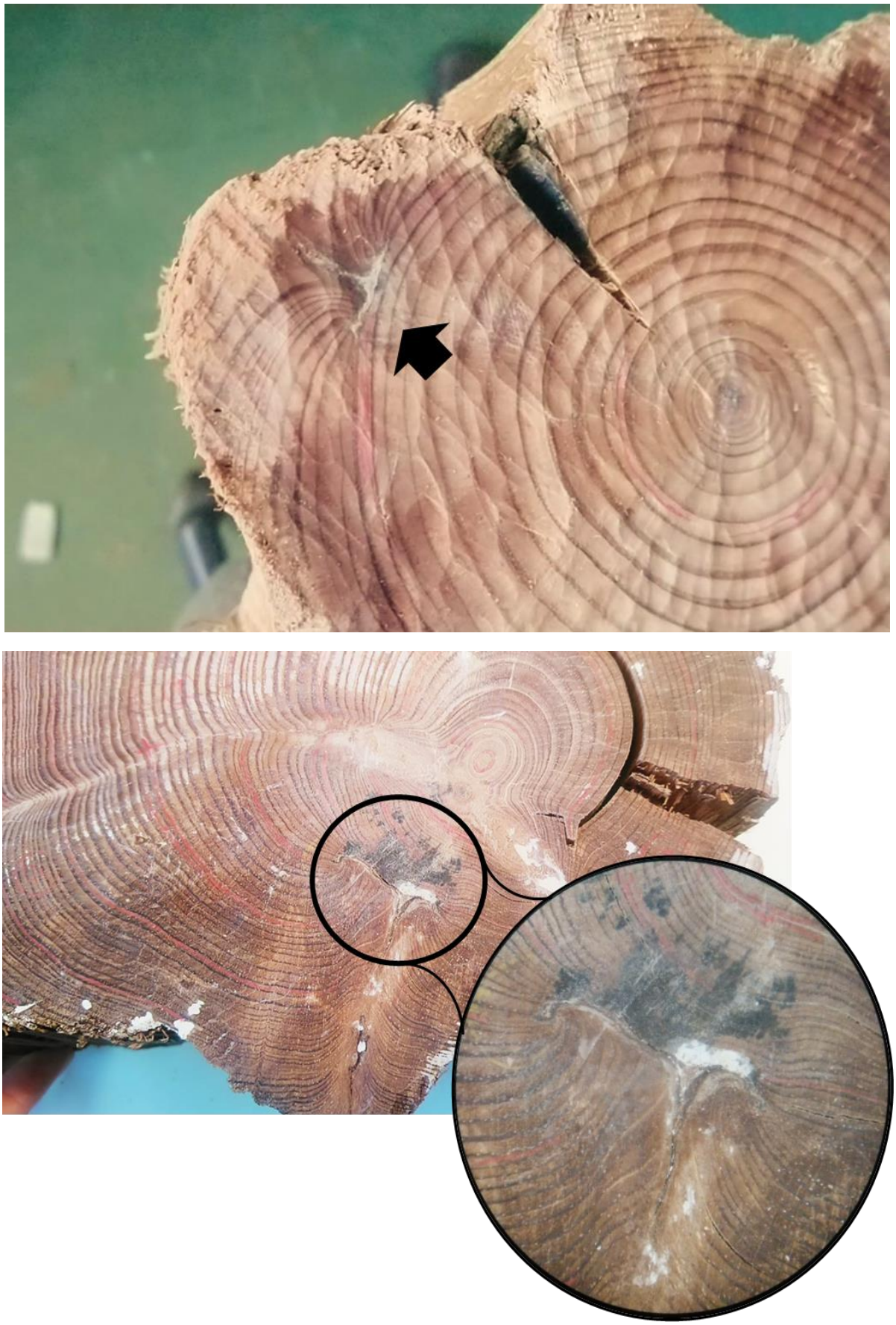

Fig. 30 *Fire scars and charcoals on the cross-section*

Traumatic resin ducts are wood anatomical anomalies that can be observed in some of the sub-fossil pine samples found in Furadouro. They are resin containing structures which unlike the common resin ducts, are more densely distributed in certain areas which are located near a wound (for example, a fire scar) or they can simply be the tree response to a stressful condition of biotic and/or abiotic origin, which triggers massive resin production for a fundamental protective role.[33,34]

The high temperatures reached during fire events can cause the explosion of the ducts containing flammable resin and volatile compounds[26] resulting in black exploded resin ducts, as the ones documented in the microscopy picture of Fig.31.

Their presence in the tree-rings do not provide an absolute date for a fire event, but it is certain that the fire occurred subsequent to the year (ring), where the last black resin ducts were detected (*terminus post quem*).

In the graph of Fig. 32 rings in which the black resin ducts are recognized are marked with orange dots. It is important to mention, that the resin ducts are not uniformly distributed within the tree-ring and along the stem. For this reason, their absence does not prove that the tree was subjected to any stress, but the sampled discs could not contain their evidence. Considering this, the black resin ducts detected in tree 655 might be attributable to fire at year 64, while the ones of trees 656 and 609 maybe be due to the fire event of year 70 or to another unidentified fire event that occurred later.

Fig. 31 *Traumatic black resin ducts*

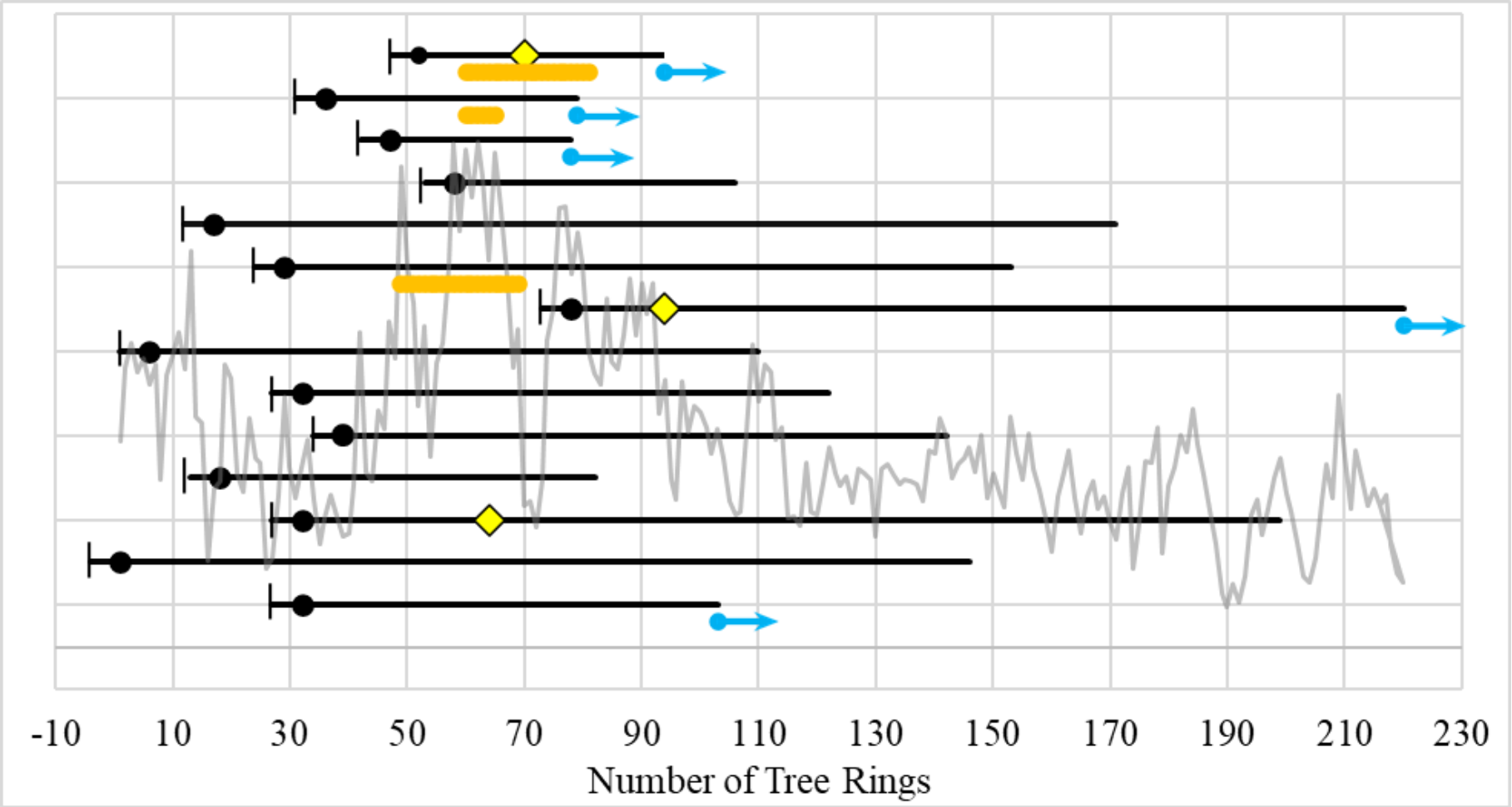

Graph 32 *Forest fire history (I). The horizontal lines represent the trees, the length corresponds to the individual age of the trees, the dots indicate the piths and the lines indicate the estimation of the real year of germination. Trees are ordered from FURA0600 to FURA0656 from the bottom to the top. The yellow rhombuses indicate the rings with fire scars; the orange lines indicate the rings with black resin ducts; the blue dots and arrows represent the outermost rings with clear evidence of charred wood. In the background in grey is the Furadouro raw ring-width chronology.*

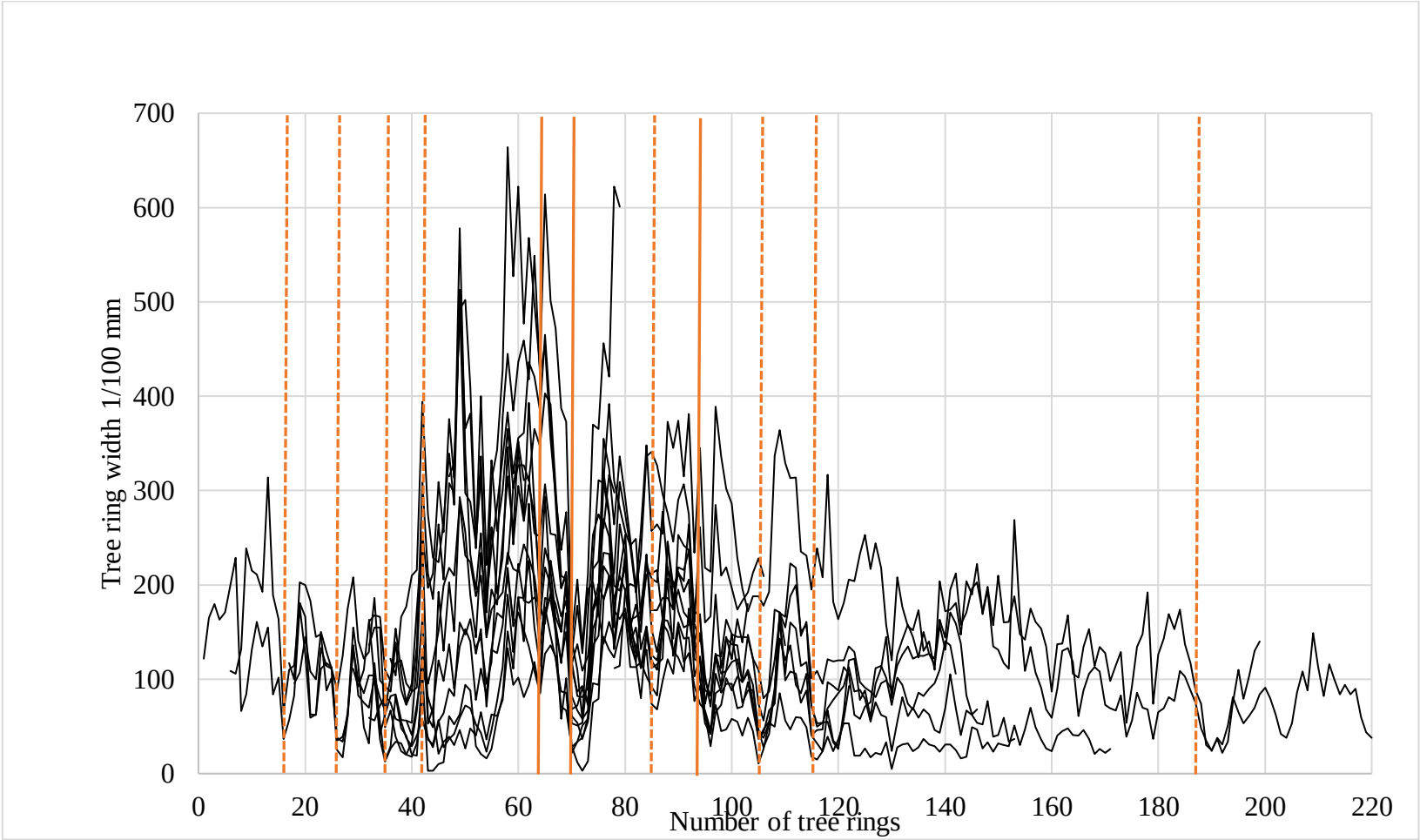

Graph 33 *Forest fire history (II). Local fire history of the Glacial pine forest of Furadouro from 14 synchronised pines. Fire years, identified by fire scars in the wood are marked by solid lines. Dashed lines indicate estimated fire events by characteristic ring-width features.*

3.2.5 Pine forest positioning in space and time

The Pinus sylvestris-nigra trunks collected during the two sampling campaigns are not the only plant macro-remains found in the present Portuguese foreshore. Indeed, other tree remnants and charcoals of pines and other broadleaves species as oak and ash (*Quercus robur-petraea* and *Fraxinus* sp., respectively), with similar radiocarbon ages, have been widely found in the low tide areas of the NW Iberian Peninsula adjacent to Furadouro in the localities of Esmoriz and San Pedro de Maceda, 5 and 14 kilometres away, respectively.[1,2,35]

These remnants, together with the ancient forest soil on which the pine trees were rooted that is similar to the one intermittently outcropping at the beach full of well visible rests of roots and wood (Fig. 34), testify the existence of a well-developed environment for vegetation growth. It confirms that the coastal area on the westerly Iberian Peninsula may have acted as refugee area for different forest tree species during the Pleistocene Würm glaciation.

Around 30,000 years ago, the estimated mean global sea-level was 70 - 80 m below the current one[36, 37] and the area near Ovar was characterised by the alternation of different paleoenvironments, due to advances and retreats of the shoreline (sea-level fluctuations), as testified by the stratigraphy (Fig. 35) studied in Granja & Carvalho (1995),[1] Granja (1998)[38] and Amorena et al. (2007)[35]. The driving forces, that have mainly caused the changes among lagoonal, beach and aeolian facies, have been the tectonic, still active today, and the sea-level fluctuations. The main tectonic movements are related to the Iberian microplate and the Atlantic passive margin, which induce moderate level of seismicity and occasional larger earthquakes, as the famous Lisbon earthquake in 1755.[39] From the late Quaternary the west Portugal coast is subject to a general uplift,[1, 39] which is probably bringing to light the pine trunks, objects of this study.

A gradually rise of see level, maybe also favoured by tectonic movements, could be taken into consideration for the disappearance of the forest, which could have been killed because of the burial from sand and sea-water, which, at the same time, preserved it until now. A similar case is reported in Roig et al. (2001)[40], where a glacial

forest in Pelluco, Chile, was buried in sediment, probably because of a single and strong seismic event, and preserved.

It is also important to consider, that a tsunami, caused by a particularly strong seismic event, as the one in 1755, could have killed coastal lagoonal forests, even if the return period of 1000 - 2000 years of such big events makes it unlikely. However, the fact that the coastline at 32 ka BP was 20-50 km outside the modern coastline due to the as much as 70-80 m lower sea level speaks against this.[2, 37] Additionally we may also consider that the study of the dying phase of the trees (see chapter 3.2.3) mainly suggests that their final death did not occur simultaneously. Assuming a single seismic-induced tsunami event as the cause of the final die-off is therefore not very likely.

Fig. 34 *Paleosol outcropping at the Furadouro foreshore (2020)*

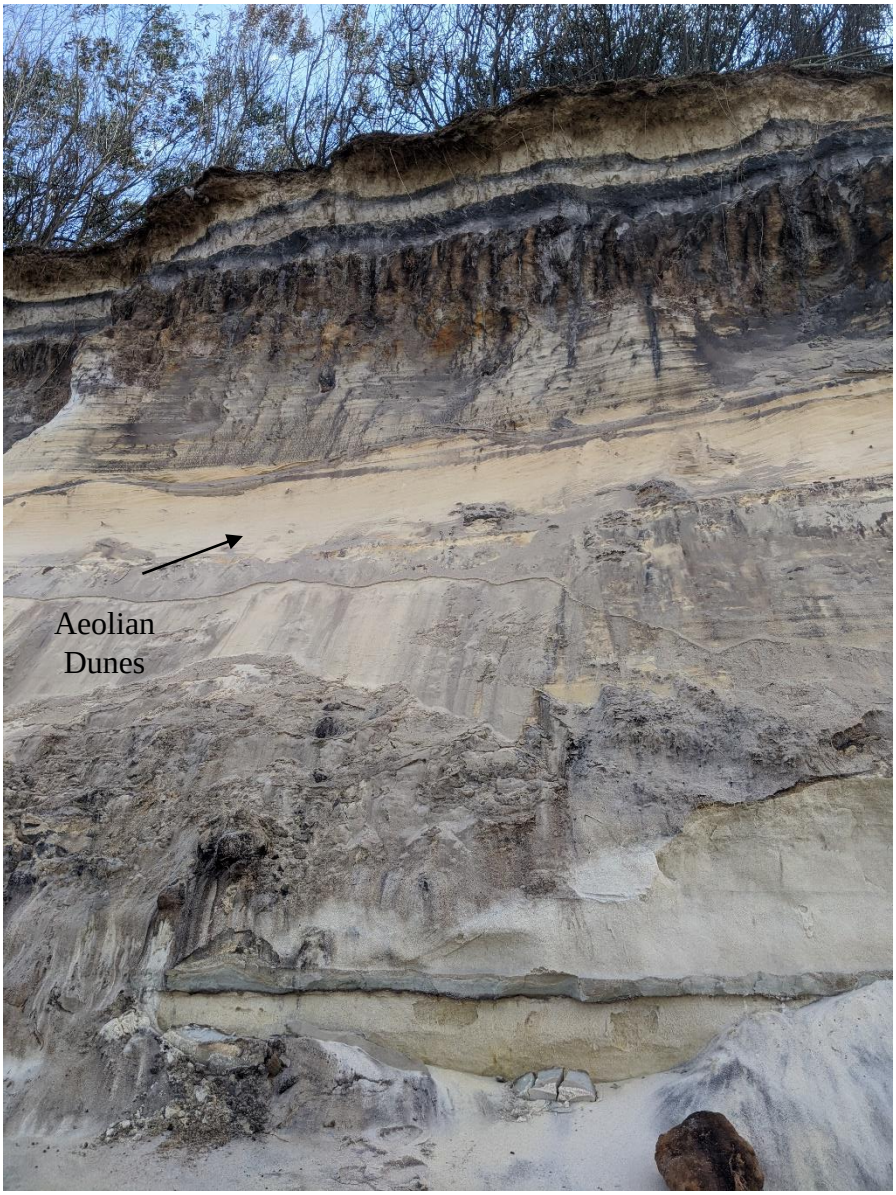

Fig. 35 *Sedimentary section at the back of the Furadouro foreshore (2020)*

The entire site tree-ring chronology was radiocarbon dated with nearly decadal resolution and with a tight error range (mean error = ±88 years) resulting in a high-resolution and high-precision radiocarbon sequence (see Table 6).

The ^{14}C age values, with the exception of those obtained from samples pretreated with ABA-B protocol, as explained in chapter 3.2.3, are shown in the graph of Fig 36.

The radiocarbon results date the samples to ~ 29,000 BP that is within the last ice age (Würm, ~ 110,000 - 10,000 years ago) in the upper Pleistocene.

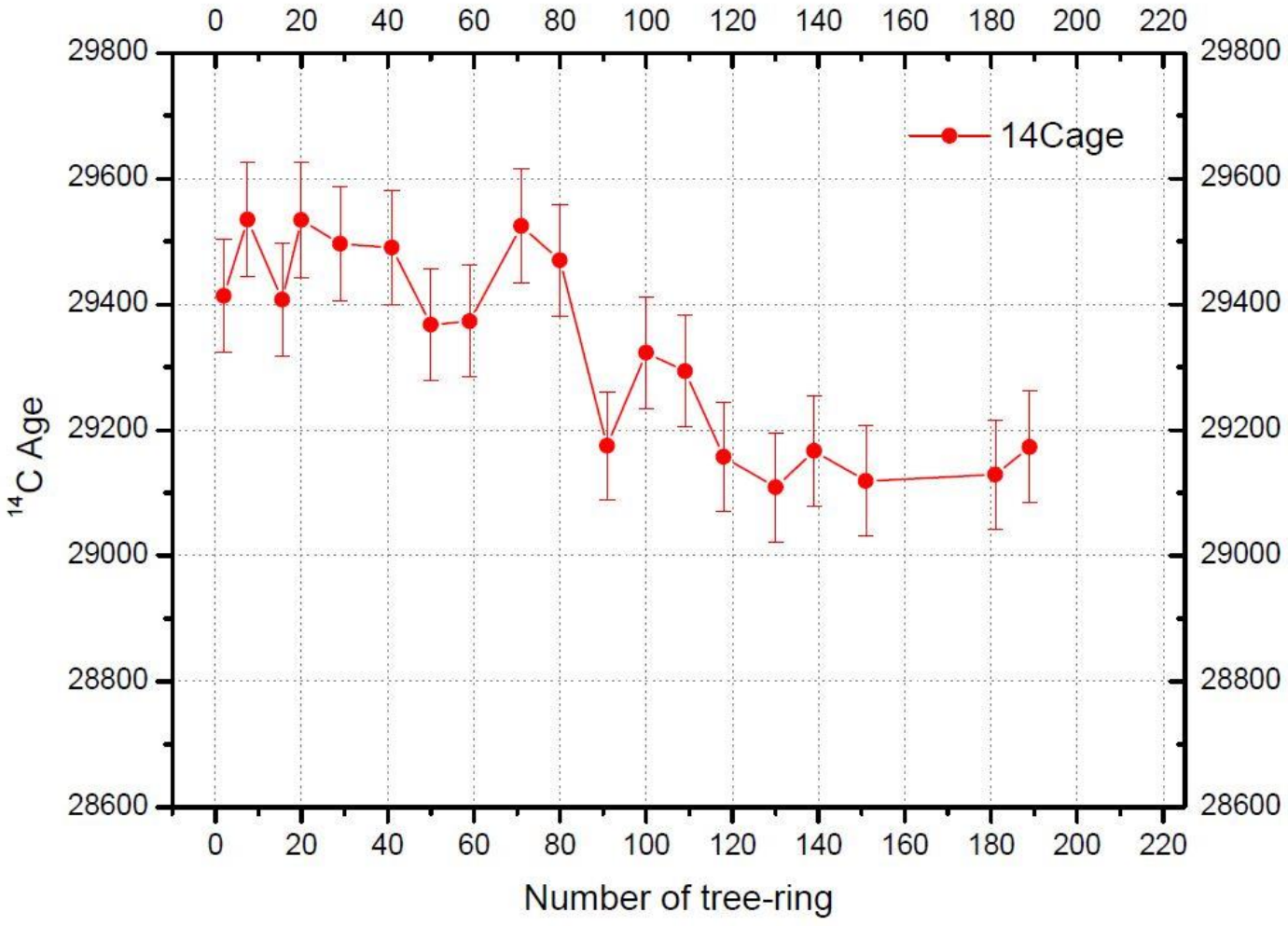

Fig. 36 *High-resolution and high-precision ^{14}C sequence of the Furadouro site chronology*

In this time period, Intcal20,[41] the current radiocarbon calibration curve relies on terrestrial and marine datasets, as varves, foraminifera and speleothems, which due to their low precision (the error can exceed ± 400 years) and resolution, give to Intcal20 a smooth structure, which does not completely reflect the real radiocarbon fluctuations at that time, preventing an ideal dating of the sequence.[42]

The calibration with Intcal20 of the radiocarbon sequence obtained from Oxcal 4.4 establishes the start of the sequence in the range from 34,091 to 34,005 cal BP at 68,3% probability. Fig. 37 shows the multiple plots of the calibrated data composing the sequence and the graph of Fig. 38 the calibrated sequence is reported.

In these circumstances, to exactly fix in time the radiocarbon sequence, it would be necessary to use an independent and external time-scale, as the ice-core timescale. The ^{10}Be isotope can be detected in the ice cores has a cosmogenic origin and its production is modulated by the solar activity and the intensity of the earth's geomagnetic field, exactly as ^{14}C. The result is that, these two isotopes' production co-vary globally in the same way. But while ^{14}C enters the carbon cycle, ^{10}Be is mainly removed from the atmosphere by precipitation and spread on the earth's surface. Ice-cores layers can provide, similarly to tree-rings, a sequence of ^{10}Be concentrations over time.[43]

Thanks to the common signal and nature of the isotopes, ^{14}C in the tree-rings and ^{10}Be in the ice-core layers, these two time-scales can be synchronized providing a reliable method to exactly fix in time radiocarbon tree-ring sequences.[44]

The Furadouro site chronology does not have a sufficient extension to enable this kind of procedure at the moment, but the climatic and environmental information extrapolated from the sub-fossil trees can be used to better define and tight the likely living time range.

To characterise the climate conditions and then the growth conditions during the Glacial period when the trees grew, the mean ring width (MRW) and the mean ring width of the first 50 years ($MRW_{(50)}$) were taken into consideration, together with the main characteristics of the site, i.e., proximity to the sea and type of soil, for comparison.

A site of living pines on the southern Baltic coast can be used as a possible recent comparison pine site. There the living *Pinus sylvestris* L. stand at the southern Baltic coast is characterised by forms of fluvial, coastal and aeolian environment, i.e., the pines are growing on a podzol developed on aeolian dunes. The trees were divided in 3 groups and show a MRW of 1,93, 1,83 and 1,03 mm according to a decreasing degree of pedogenesis of the podzol.[45]

The Furadouro site chronology has a MRW of 1,75 mm with maxima peaks beyond 5,00 and 6,00 mm and the mean ring width of the first 50 years ($MRW_{(50)}$) there is 1,90 mm. This value gives a hint of the potential growth rate and of the growth conditions during the juvenile phase of the trees, when the influence of competition for light and nutrients is still low compared to the following adult phase when the wood growth slows down and the ring-width decreases.

The mean annual air temperature (MAAT) at the site described in Cedro et al. (2022)[45] is ~ 8,6° C and the mean annual precipitation equals to 564 mm.

These values roughly agree with those reconstructed in Gracìa-Amorena et al. (2007)[35] using a taxonomic approach of botanical macro remains' species found *in situ*.

Moreover, one of the few Iberian Peninsula paleoclimate reconstructions of the last Glacial period, in the range between 33,000 to 35,000 cal BP, reports MAAT from 12 to 14° C.[46] The analysed data of that study come from the lake Padul in the southern interior area of Spain, the climate of which, nowadays, is classified, according to Köppen classification, as "Cs", i.e., continental climate with dry summer season, similarly to what we suspect for the climate in Furadouro from the sub-fossil trees. Nowadays the mean annual temperature in Padul is ~ 13° C and a little bit milder in Furadouro ~ 15° C (climate-data.org).

It is reasonable to suppose, that the climate conditions at the two sites, even at that time, could be quite similar.

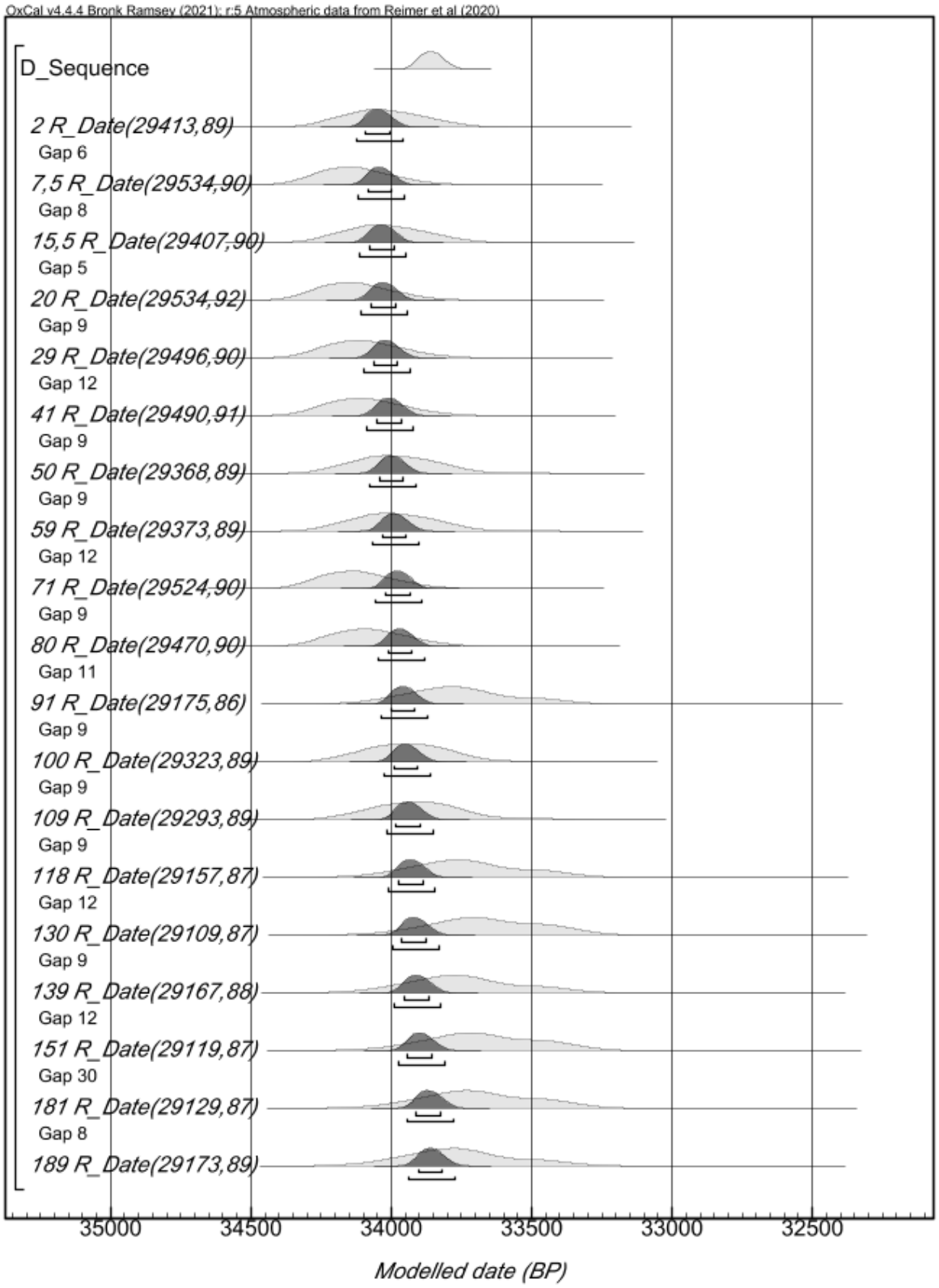

Figure 37 *Multiple plots of the sequence's calibrated ages using Oxcal 4.4. and Intcal20. From the left to the right: the number of the ring to which the date refers; in brackets the radiocarbon age value and the relative error*

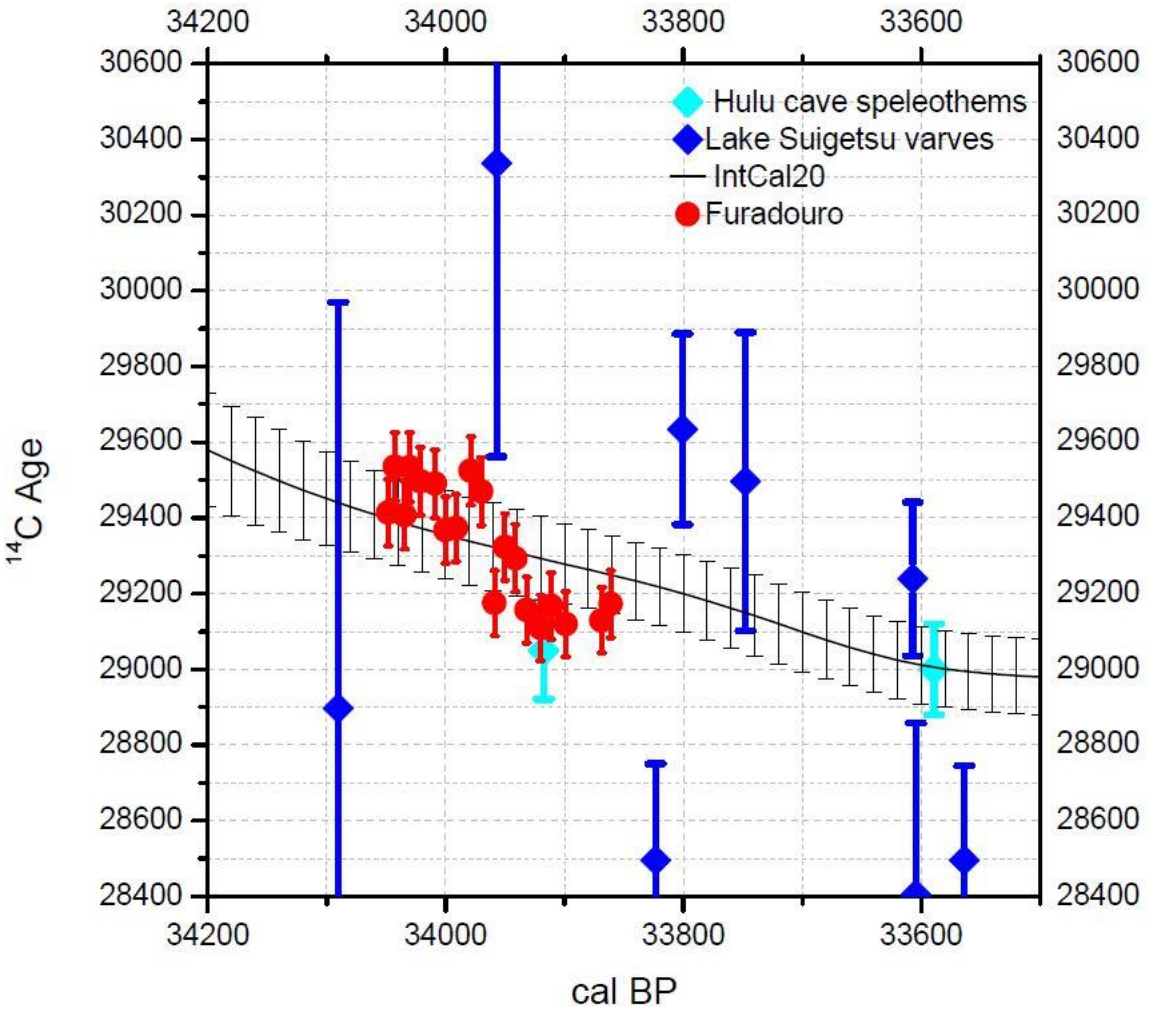

Fig. 38 *The Furadouro sequence (red dots and error bars) positioned with Ring n.1 at 34,048 cal BP, the middle of the calibrated range. In the graph all available data in this time period from Hulu Cave speleothems and Lake Suigetsu are shown (blue and light blue data)*

The information gained from tree-ring widths and ecological analysis, statistics and available climate reconstructions allow to hypothesize that the Glacial forest of Furadouro developed under favourable climate conditions in a protected and poorly disturbed environment.

It is widely accepted that the last glaciation was characterised by numerous and very rapid climate fluctuations, known as Dansgaard-Oeschger (DO) events,[47] that is likely caused by changes in the Atlantic Meridional Overturning Circulation (AMOC), which governs the heat transport toward the high latitudes. These changes lead to the differentiation of warmer and colder periods named Greenland Interstadial (GI) and Greenland Stadials (GS), respectively.

The fluctuations in the $\delta\ ^{18}O$ ($^{18}O/^{16}O$), commonly used as temperature indicator and especially detected in ice-cores and speleothems, are used to identify such events.[48-50]

In Fig. 39 we show the $\delta\ ^{18}O$ (‰) curve from NGRIP2 ice-core[51] and the Furadouro ^{14}C-sequence in a likely position given by the calibration with IntCal20.

At ~ 33,700 b2k there is evidence of an inversion of the $\delta\ ^{18}O$-curve, i.e., $\delta\ ^{18}O$ lower values indicate an increase in temperature in Greenland lasting for more than 500 years, which has been recognized as the onset of GI-6.[50]

The obvious offset between the radiocarbon time scale (Intcal20) and the Greenland ice-core chronology GICC05 was found and best quantified by Adolphi et al. (2018).[50] Following the transfer function proposed there, the shift at 34,000 cal BP is ca. 250 years and at a probability of 68,3 %, it can reach an upper limit of 644 and a lower limit of -24 years. Within that age range the position of the Furadouro sequence at the onset of the warm period GI-6 is possible, which would explain the suitable conditions for trees' sprouting and the favourable tree-growth within a relatively short time of some decades and the subsequent end of the warmer period and the continuous deterioration of the climate conditions that led to a uniform decline of the trees. Moreover, the development of the forest at Furadouro in the warm period GI-6, would also explain the detected frequent forest fires as the greater amount of heat that warmed the air could trigger instability and storms formation with associated lightnings that started the fires.

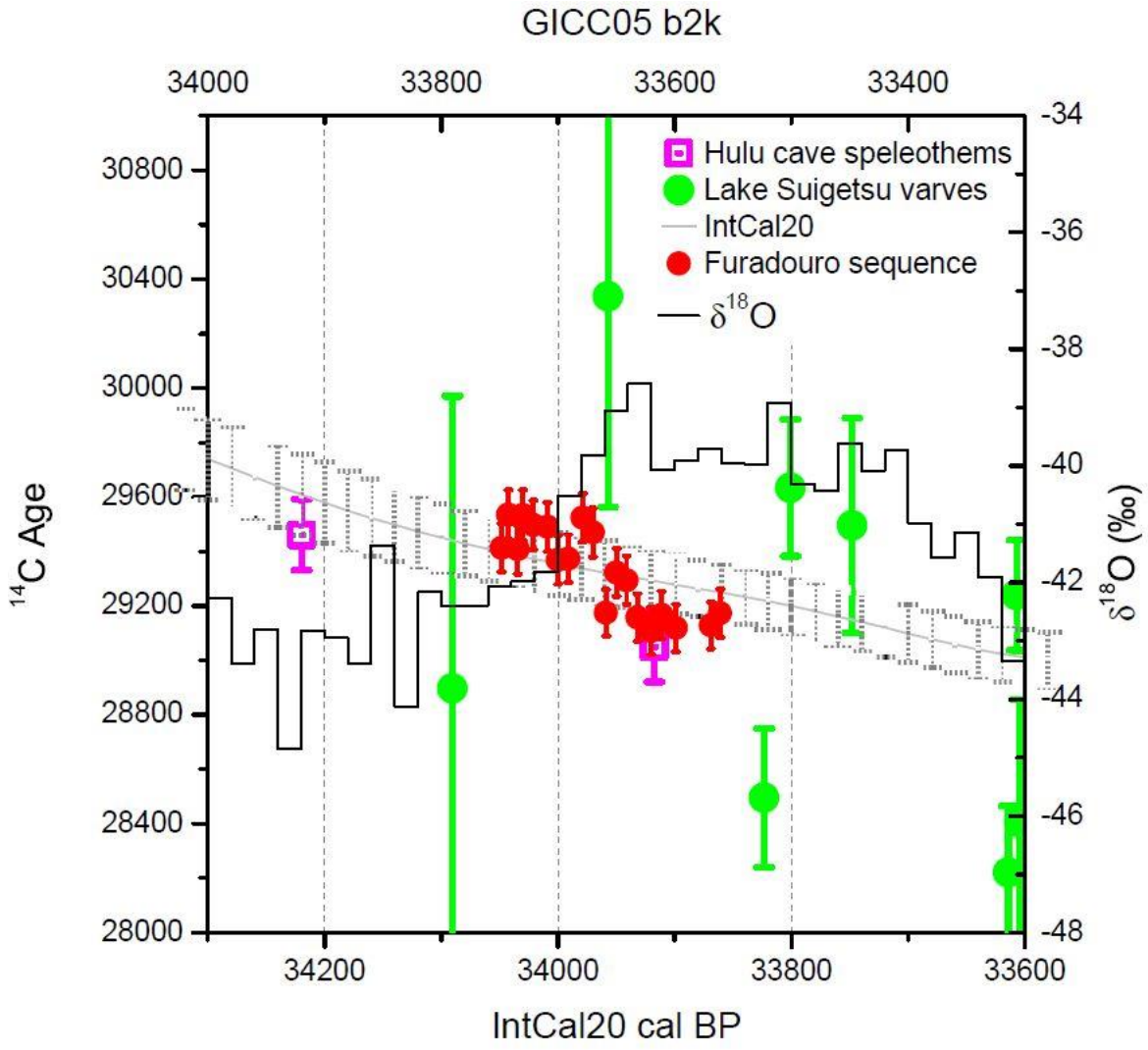

Fig. 39 *The Furadouro sequence positioned according to Intcal20 calibration to 34,048 cal BP for the start ring. The datasets of Hulu cave speleothems and lake Suigetsu varves are shown for comparison with the high-precision and high-resolution data characterising the tree-ring sequence. The δ ^{18}O values from NGRIP2 ice-core (Andersen et al. 2004[515] is plotted on the GICC05 scale shifted 50 years from Intcal20 time scale, since the latter refers to 1950 AD as present, while the GICC05 scale refers to 2000 AD. Moreover, the GICC05 timescale is shifted 270 years following the transfer function of (Adolphi et al., 2018)[504] The δ ^{18}O has been shifted within the uncertainty of the transfer function positioning the onset of the warmer period at the start of the tree-ring sequence.*

CHAPTER 4

Conclusions and future outlook

The major goal of this study was to contribute to the improvement of the radiocarbon dating, especially for archaeological findings dating back to the upper Pleistocene, prior to the tree-ring based calibration at 14,226 years BP.

More reliable and accurate calibrated dates are the results of improvements of the radiocarbon calibration curve, which can be achieved through the development of new high- precision and high-resolution radiocarbon data sequences describing the real fluctuations of the atmospheric radiocarbon concentration in the past.

This project shows that the dendrochronological analysis on sub-fossil trees of glacial time combined with the most suitable cellulose extraction protocol and the AMS (Accelerator Mass Spectrometer) measurements are suitable tools to build new 'floating' tree-ring chronologies, which can be incorporated into the calibration curve to better define its real structure, when independently dated in the future. To fix the 'floating' chronologies independently in time, the common signal variations of the cosmogenic isotopes ^{14}C in the tree-rings and ^{10}Be in the Greenland ice cores can be used, as the production of both isotopes is modulated similarly by the solar activity and the strength of the geomagnetic field. So far, in the case of the Furadouro pine chronology this comparison hampers due to the short length of the tree-ring chronology that can be overcome by new fieldwork in the near future. However, this thesis represents a valuable contribution to the radiocarbon calibration in the period around 29,000 years BP by providing new tree-ring based, high resolution and high precision radiocarbon data that allow insight in the ^{14}C-variability at that time.

A key goal within the experimental and methods section of this Ph.D. project was to assess the most suitable pretreatment method to extract cellulose deprived of any contamination to obtain reliable radiocarbon dates from glacial sub-fossil trees that is the basic prerequisite for high precision ^{14}C-dates. Considering the obtained results from the tests done on the basis of cellulose yield and radiocarbon age, both BABAB and ABA-B protocols result suitable methods to pretreat glacial sub-fossil trees. Although both methods gave reasonable results on well-preserved subfossil wood samples, the ABA-B method consistently showed too young ages in the pine samples from Furadouro,

especially in the case of poor wood preservation. Therefore, the BABAB protocol is recommended for samples with poor preservation, even if this requires larger sample quantities.

High precision AMS measurements on the uncontaminated extracted cellulose on the pine tree-ring sequence of Furadouro result in ages of around 29,000 BP. Dendrochronological analysis of the trees from Furadouro led to a robust 220 years-long pine tree-ring width chronology. By the analysis of trees' growth, we found that the trees grew in favourable conditions comparable to the Holocene. The study of the germination and death phases of the trees was related to the changing environmental and climatic conditions: two main germination phases are detectable within the first 60 years and the dieback phases of the trees seem to be linked to a progressive worsening of the growth conditions and to severe forest fires, that could be reconstructed by fire-scars and other fire indicators in the wood of the pines.

The growth conditions appear to have been stable and favourable, without strong biotic or abiotic limiting factors, with the exception of forest fires. According to the fire records of our pine trees the forest fires probably did not only occur locally at individual sites, but affected larger areas of the lagoonal pine forest.

Based on the established tree-ring chronology we created a ^{14}C series in sub-decadal resolution for the entire period. At the moment, this Furadouro radiocarbon sequence is too short to be absolute fixed in time by the GICC05 time scale, using comparisons of the trees' ^{14}C-series to the ^{10}Be fluctuations in the ice core. A univocal match is therefore not possible yet.

Combining the rough dating of the trees by comparison with the existing calibration curve IntCal20 with the findings from the growth analyses of the trees, which indicate good growth conditions, and compare this with the climate proxies from the ice cores, we can conclude that the trees must have grown in a warm period of the glacial period, i.e., a Greenland interstadial, most likely at the beginning of Greenland Interstadial 6 (GI-6).

Anyway, this represents one of the possible interpretations of the data, it remains the need to exactly fix this sequence independently in time by comparisons of the fluctuations of $\Delta^{14}C$ of the trees and $\Delta^{10}Be$ of the ice that would allow the incorporation of the new floating tree-ring chronology into International Calibration series (IntCal).

Therefore, it is essential to extend the sequence by new sub-fossil pine trees by future fieldworks in the study area and in the neighbouring areas with similar dynamism of the coastal environment, that continuously uncover sediments of the Glacial.

It is very likely, that due to the minimal estimated length of the Interstadial GI-6 of 500 years, there is a good chance that more trees could be still preserved embedded in the sediments and therefore a further extension of the tree-ring chronology is feasible.

Improving the radiocarbon calibration curve in this period would have great significance, as it would result in more precision and accuracy of calibrated radiocarbon dates, providing better absolute ages to interpret archaeological findings and to study Human Evolution.

References

1 H. M. Granja and G. Soares de Carvalho', *Terra nova*, 1995.

2 H. M. Granja, Thomas A. M. De Groot And Ana L. Costa, Sedimentology, 2008, 55, 1203–1226.

3 B. F Atwater, A. R Nelson, J.J Clague, G. A Carver, D. K. Yamaguchi, P.T. Bobrowsky, J. Bourgeois, M. E. Darienzo, W.C. Grant, E. Hemphill-Haley, H.M. Kelsey, G.C. Jacoby, S.P. Nishenko, S.P. Palmer, C. D. Peterson and M. A. Reinhart, *Earthquake Spectra*, 1995, 11, 1-18.

4 F. H. Schweingruber, *Microscopic Wood Anatomy*, Eidgenössiche Forschungsantalt für Wald, Schnee und Landchaft, Birmensdorf, 1990.

5 F. H. Schweingruber, *Tree Rings - Basics and Applications of Dendrochronology*, Springer Dordrecht, 1988.

6 Spurk, M., Friedrich, M., Hofmann, J., Remmele, S., Frenzel, B., Leuschner, H., & Kromer, B., *Radiocarbon*, 40(3), 1107-1116, 1998.

7 A. Buras, M. Wilmking, *Dendrochronologia*, 2015, *34*, *29–30*.

8 M. G. L. Baillie and J. Pilcher, *tree-ring bulletin*, 1973, 33.

9 A. M. Fowlera, M. C. Bridge, *Dendrochronologia*, 2017, 42, 51–55

10 M. Bernabei M, 2022, *Dendrochronologia*, 76, 126025.

11 J. H. Speer, *Fundamentals of Tree-Ring Research*, University of Arizona Press, 2010

12 H. Fritts, *Tree rings and climate*, Academic Press, 1976

13 D. Bowman1, R. J.W. Brienen, E. Gloor, O. L. Phillips and L.D. Prior, *Trends in Plant Science*, 2012, 1–7

14 P. F. Sullivan, R. Pattison, A.H. Brownlee, S. Cahoon and T. Hollingsworth, *Environmental research letter*, 2016, 11

15 S. Cercatillo, M. Friedrich, B. Kromer, D. Paleček, S. Talamo, *New Journal of Chemistry*, 2021, 45, 8936-8941

16 M. Spurk, *Dendrochronologia*, 1997, 15, 51–72.

17 W. Oberhuber, M. Stumböck and W. Kofler, *Trees*, 1998, 13, 19–27.

18 W. Oberhuber and W. Kofler, *Plant Ecology*, 2000, 146, 231–240.

19 J. Oleksyn, M. G. Tjoelker and P. B. Reich, 1998, *Silva Fennica*, 32, 129–140.

20 J. Hofmann, 1997, *Veröffentlichungen des Brandenburgischen Landesmuseums für Ur- und Frühgeschichte* 31, 169-224.

21 M. Bembenek, D. F. Giefing, T. Jelonek, Z. Karaszewski, R. Kruszyk, A. Tomczak, M. Woszczyk, P.S. Mederski, *Baltic foresty*, 2015, 21, 279-284

22 J. E. Keeley, *Annals of Forest Science*, 2012, 69:445–453

23 E. Błońska, B. Bednarz, M. Kacprzyk, W. Piaszczyk and J. Lasota, *Forest Ecosystems*, 2020, 7:28

24 M. Manton , C. Ruffner , G. Kibirkštis, G. Brazaitis, V. Marozas, R. Pukien, E. Makrickiene and P. Angelstam, *land*, 2022, 11, 260

26 N. Gaudio1, P. Balandier, S. Perret and C. Ginisty, *Forestry An International Journal of Forest Research*, 2011, 84

27 B. Romero and A. Ganteaume, *plants*, 2021, 10, 2164

28 J.G.A. Lageard, P.A. Thomas, F.M. Chambers, *Palaeogeography, Palaeoclimatology, Palaeoecology*, 2000, 164, 87–99

29 M. Génova, P. Ortega, E. Sadornil, *iForest*, 2022, 15: 171-178.

30 M. Adámek, V. Hadincová, J. Wild, *Forest Ecology and Management*, 2016, 380, 285–295

31 M. Zadina, L. Purina, A. Pobiarzens, J. Katrevics, J. Jansons and A. Jansons, 2014

32 O. Zackrisson, 1980, *in Gen. Tech. Rep.*, 120-125.

33 R.D. Laven, P.N. Omi, J.G. Wyant, and A.S. Pinkerton, 1980, *in Fire History Workshop*, 46-49.

34 S. Hood, A. Sala, E. K. Heyerdahl and M. Boutin, *Ecology*, 2015, 1846–1855

35 A. Bär,S. T. Michaletz,S. Mayr, *New Phytologist*, 2019, 223, 1728-1741

35I. García-Amorena, F. Gómez Manzaneque, J.M. Rubiales, H.M. Granja, G. Soares de Carvalho and C. Morla, *Palaeogeography, Palaeoclimatology, Palaeoecology*, 2007, 254, 448–461

36 K. G. Miller, W. J. Schmelz, J. V. Browning, R. E. Kopp, G. S. Mountain and J. D. Wright, *Oceanography*, 2020, 33, 2

37 K. Lambecka, H. Roubya, A. Purcella, Y. Sunc and M. Sambridgea, *PNAS*, 2014, 111, 15296 - 15303.

38 H. M. Granja, *Geologie en Mijnbouw*, 1998, **77**, 233 - 245.

39 J. Cabral, *Journal of Iberian Geology*, 2012, 38, 71 - 84.

40 F. A. Roig, C. Le-Quesne, J. A. Boninsegna, K. R. Briffa, A. Lara, H. Gruddk, P. D. Jones and C. Villagràn, *Letters to Nature*, 2001, 410, 567-570

41 P. J. Reimer, W. E. N. Austin, E. Bard, A. Bayliss, P. G. Blackwell, C. Bronk Ramsey, M. Butzin, H. Cheng, R. L. Edwards, M. Friedrich, P. M. Grootes, T. P. Guilderson, I. Hajdas, T. J. Heaton, A. G. Hogg, K. A. Hughen, B. Kromer, S. W. Manning, R. Muscheler, J. G. Palmer, C. Pearson, J. van der Plicht, R. W. Reimer, D. A. Richards, E. M. Scott, J. R. Southon, C. S. M. Turney, L. Wacker, F. Adolphi, U. Büntgen, M. Capano, S. M. Fahrni, A. Fogtmann-Schulz, R. Friedrich, P. Köhler, S. Kudsk, F. Miyake, J. Olsen, F. Reinig, M. Sakamoto, A. Sookdeo, S. Talamo, *Radiocarbon*, 2020, 62, 725-57.

42 R. Muscheler, F. Adolphi, T.J. Heaton, C. B. Ramsey, A. Svensson, J. van der Plicht, P. J Reimer, *Radiocarbon*, 2020, 62, 4, 1079–1094

43 J. Masarik and J. Beer, *Journal of Geophysical Research Atmospheres*, 2009, 114

44 F. Adolphi, R. Muscheler, M. Friedrich, D. Güttler, L. Wacker, S. Talamo, B. Kromer, *Quaternary Science Reviews*, 2017, 170, 98-108

45 A. Cedro, B. Cedro and M. Podlasinski, F*orests*, 2022, 13, 470

46 M. Rodrigo-Gamiz, A. García-Alix, G. Jimenez-Moreno, M. J. Ramos-Roman, J. Camuera J. L. Toney, D. Sachse, R. S. Anderson, J. S. Sinninghe Damst, *Quaternary Science Reviews*, 2022, 281, 107434

47 W. Dansgaard, S. J. Johnsen, H.B. Clausen, D. Dahl-Jensen, N. S. Gundestrup, C. U. Hammer, C. S. Hvldberg, J.P. Steffensen, A. E. Svelnbjomsdottlr t, J. Jouzel t & G. Bond, *Letters to Nature*, 1993, 364

48 E. C. Corrick, R. N. Drysdale, J. C. Hellstrom, E. Capron, S. O. Rasmussen, X. Zhang, D. Fleitmann, I. Couchoud, E. Wolff, *Science*, 2020, 369, 963–969

49 A. Svensson, K. K. Andersen, M. Bigler, H. B. Clausen, D. Dahl-Jensen, S. M. Davies, S. J. Johnsen, R. Muscheler, F. Parrenin, S. O. Rasmussen, 2008, 4, 47-57

50 F. Adolphi, C. Bronk Ramsey, T. Erhardt, R. L. Edwards, H. Cheng, C. S. M. Turney, A. Cooper, A. Svensson, S. O. Rasmussen, H. Fischer and R. Muscheler, *Climate of the Past*, 2018

51 K. K. Andersen, N. Azuma, N. Caillon and J. Chappellaz, *Nature*, 2004